Annual Report 2005

of the chair of Prof. Dr. Winfried Petry

Physik Department E13

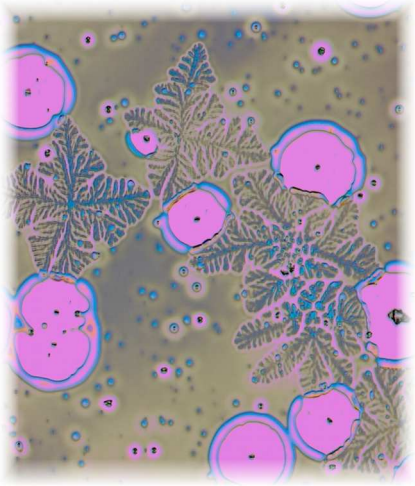

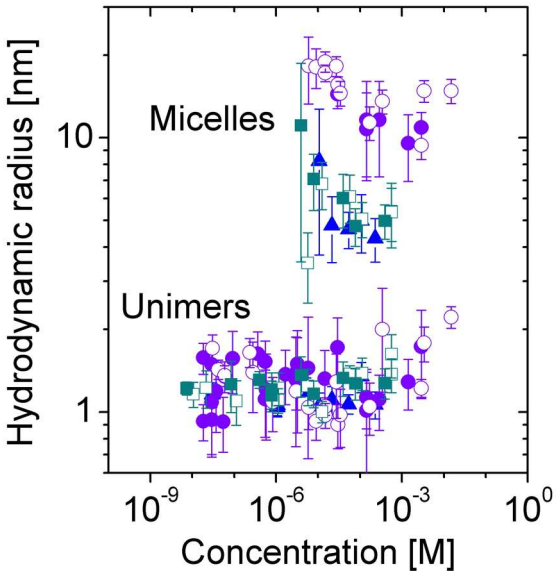

Technische Universität München

Prof. Dr. Winfried Petry
Lehrstuhl für Experimentalphysik IV
Physik Department E13

Prof. Petry is currently the scientific director of the
Research Reactor Heinz Maier-Leibnitz.
The chair is therefore headed by
Prof. Dr. Andreas Meyer

Physik Department E13
Technische Universität München
James-Franck-Straße
D-85748 Garching

Secretary: Elke Fehsenfeld

Tel.: +49 (0)89 289 12452
Fax: +49 (0)89 289 12473

E-mail: ameyer@ph.tum.de
efehsen@ph.tum.de
http://www.e13.physik.tu-muenchen.de

Cover:

In 2005, two instruments have been purchased: An instrument for fluorescence correlation spectroscopy (FCS) as well as an optical microscope, both equipped with heating stages.

FCS is a modern tool for the investigation of the phase behavior and dynamics of soft matter. By monitoring the diffusion time of fluorescent molecules through the detection volume (which is as small as $1 \mu m^3$), FCS allows measurements of diffusion coefficients. Only small sample amounts are necessary, and the measuring times are as short as seconds. Thus, FCS complements the 'classical' techniques of photon correlation spectroscopy (PCS) and small-angle scattering (SAS). We use FCS for the investigation of the aggregation behavior of amphiphilic copolymers in solution and have been able to characterize the unimer-to-micelle transition taking place at very low concentrations which are not easily accessible with PCS and SAS [1]. Our measurements on amphiphilic poly(2-oxazoline) copolymers of different architectures (di- and triblock copolymers as well as random copolymers) have shown that the micellar hydrodynamic radius depends strongly on the polymeric architecture (right figure).

The optical microscope is dedicated to investigations of thin crystalline block copolymer films. Quenching the films rapidly below their melting temperature allows us to follow the crystallization in situ (left figure) and to prepare well-characterized samples for grazing-incidence diffraction and small-angle scattering measurements of the crystalline and the mesoscopic order.

1. T. B. Bonné, K. Lüdtke, R. Jordan, P. Štěpánek and C. M. Papadakis, Coll. Polym. Sci. 282, 833 (2004).

Preamble

The last year was again a very successful year for our institute. In particular, there were two major developments: The group of Prof. Christine Papadakis is now established in full. Together with the group of PD Peter Müller-Buschbaum, she is achieving a large part of the institute's research activities, which are reflected in this report in the chapter on polymers. Another most intriguing event for E13 was the start of the routine operation of our neutron time-of-flight spectrometer ToF-ToF at the neutron source Heinz Maier-Leibnitz (FRM-II) in July. With the highest neutron flux on the sample, an excellent energy resolution and an outstanding signal-to-noise ratio, ToF-ToF outperforms any other spectrometer of its kind. You may find some results of the first successful experiments in this report.

For a long time, the study of the liquid to glass transition is a focus of the institute's research. This field has received a particular acknowledgment last November, when Prof. Wolfgang Götze (T37) was announced as the winner of the Max Planck medal of the Deutsche Physikalische Gesellschaft. About twenty years ago, Wolfgang Götze and coworkers formulated their mode coupling theory. MCT represents an exceptional contribution to the understanding of the dynamics of viscous liquids. Its predictions initiated numerous experiments as well as the development of new experimental techniques. Over the last decade, E13 participated with eight dissertations and two habilitations with ingenious dynamic light and quasielastic neutron scattering experiments in the stringent tests of MCT. Currently, we apply MCT to simple liquids and to more complex, multi-component systems.

With Estelle Bauer, Tune Bodén, Ronald Gebhardt, Florian Kargl, Edith Maurer and Suresh Mavila Chathoth a large group of thesis students finished their dissertation in 2005. With Mottakin Abul Kashem, Charles Darko, Andreas Meier-Koll, Ian Perlich, Sebastian Stolz and Fan Yang the next “wave” already started their Ph.D. work on structure and dynamics of polymers as well as of liquid metals and silicates.

This annual report highlights the engaged and fruitful scientific research of E13. Moreover, in 2005 our institute was again very committed to teaching and to the organization of international workshops and the Edgar Lüscher lecture series.

Andreas Meyer March 2005

Contents

1 Instrumentation

Progress at the Neutron Source Heinz-Maier-Leibnitz (FRM II)

Winfried Petry[1] and Jürgen Neuhaus[1]

[1] Heinz Maier–Leibnitz Forschungsneutronenquelle, FRMII, Technische Universität München, Garching

The outstanding event of the past year certainly was the beginning of the routine operation of FRM II. After having completed the nuclear commissioning in 2004, the Bavarian regulator gave the permission for routine operation of the FRM II on April 22. On Tuesday, May 2, FRM II reached its nominal power of 20 MW, and the first neutrons were delivered to the users. All together, FRM II operated in 2005 for 3 full cycles, each of which lasted for 52 days.

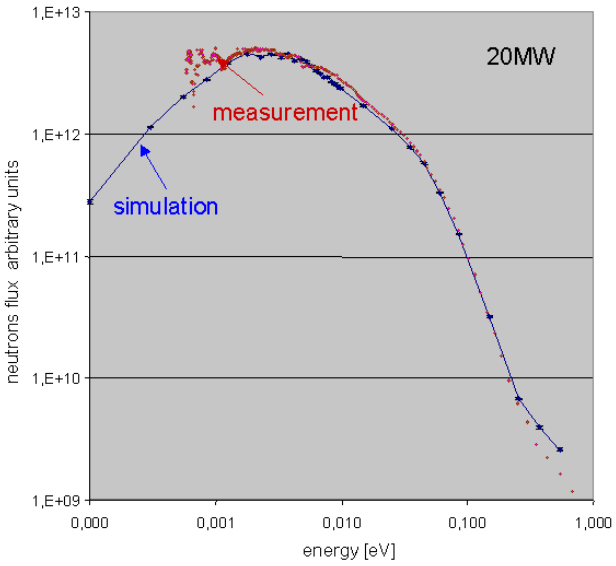

Figure 1.1:
Measured and calculated neutron flux coming from the cold source seen through a pin hole geometry at the exit of beam hole SR4.[2]

The neutron fluxes at the instruments are fulfilling more than our expectations. The neutron beams which come from the cold source through the neutron guides to the positions at the instruments have been characterized in great detail. Some of them are the most intense ones world wide. Table 1 summarizes the intensities measured at the end of selected guides. Total flux measurements were performed by gold foil activation, spectral fluxes were determined by a time of flight spectrometer. More details are reported in Ref.[1]. These measurements have been accompanied by extended Monte Carlo simulations of the neutron flux. As a typical example for the agreement now a days achievable between simulation and measurements the spectral neutron flux of the cold source is shown in figure 1.1 as seen by a pin hole geometry in front of beam hole SR4 [2]. The FRM II cold source is undermoderated, i.e. moderation of the thermal neutrons to D_2 temperature is not complete in order to have higher fluxes and a broader spectral distribution. Of course the spectral width usable at an instrument depends on the curvature of the particular neutron guide. As an example the spectral distribution at the time of flight spectrometer ToF-ToF is shown in figure 1.2.

Beam profile at sample position

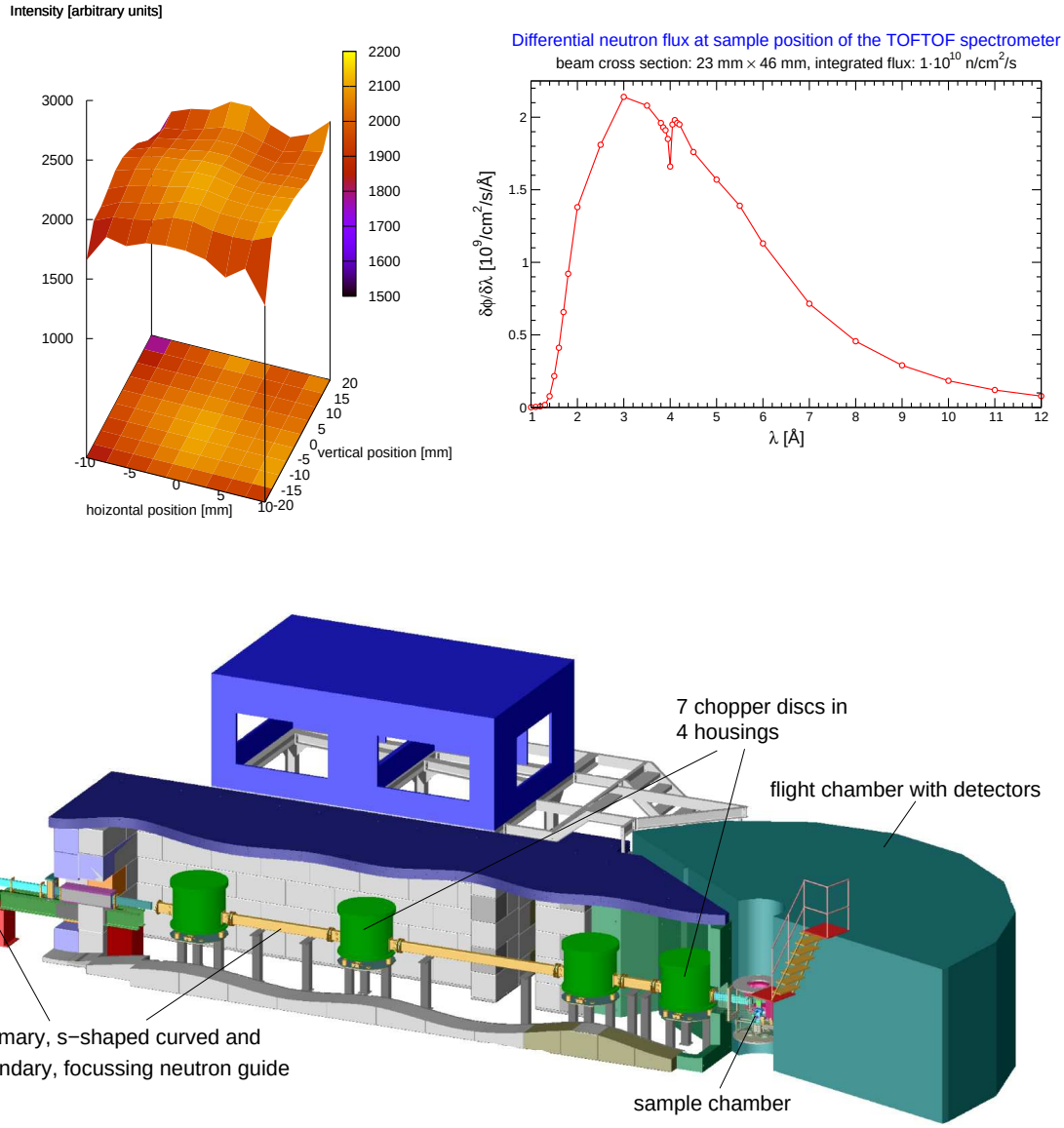

Figure 1.2: Spectral flux at the sample position of the time of flight spectrometer ToF-ToF. For this measurement the chopper system has been at rest with all slits in open position.[3]

Characteristic fluxes at end positions of neutron guides			
NL1:	int. = 9.8 x	10^9 n/cm2/s	extrapolated to 20MW
NL2a:	int. = 1.0 x	10^{10} n/cm2/s	measured at 20MW at sample position
NL2b:	int. = 1.8 x	10^9 n/cm2/s	extrapolated to 20MW
NL3b	int. = 6.8 x	10^9 n/cm2/s	measured at 20MW
NL4:	int. = 7.0 x	10^9 n/cm2/s	extrapolated to 20MW
NL6a:	int. = 4.9 x	10^9 n/cm2/s	extrapolated to 20MW

Table 1: Integral neutron fluxes measured at neutron guide end positions.

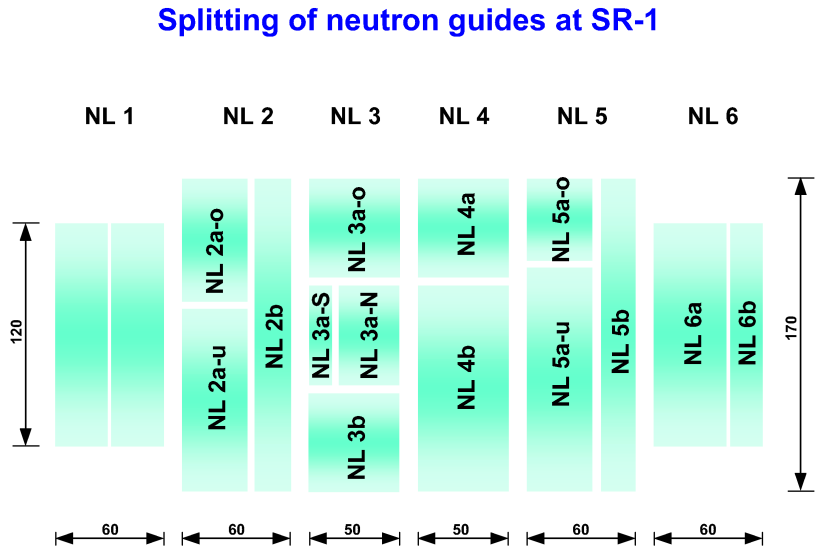

Figure 1.3: The six large neutron guides facing the cold source via beam hole SR1 are segmented in smaller portions thereby delivering a maximum number of instruments with optimised beam cross section, spectral width and divergence.

By the end of 2005, 14 beam hole instruments are operational. We expect 5 further instruments to start routine operation in 2006. Table 2 summarizes the actual status of the instrumentation for FRM II, including the irradiation facilities. Table 3 summarizes the thermal fluxes and demonstrates the suppression of unwanted epithermal and fast neutrons for theses irradiation positions [4]. Despite of the many instruments foreseen for the neutron guide hall, almost all of them are at end positions of guides. Figures 1.3 and 1.4 give an idea, how the neutron beams have been split to reach that goal.

Irradiation Facilities		Operator	Status
rapid pneumatic irradiation system	t_{trans} ~ 250 ms	TUM chemistry	project
pneumatic rabbit system	t_{trans} ~ 5-10 s	TUM FRM II	routine operation
hydraulic rabbit system	t_{trans} > 10 s	TUM FRM II	routine operation
large volume irradiation		TUM FRM II	routine operation
irradiation position in control rod	$\Phi_{schnell}$	TUM FRM II	test operation
silicon doping	∅ 20 cm, length 50 cm	TUM FRM II	routine operation
Radio- and Tomography			
with cold neutrons ANTARES		TUM physics	routine operation
with fast neutrons NECTAR	MeV neutrons	TUM chemistry	test operation
Diffractometer			
materials diffractometer STRESSSPEC		Hahn Meitner Institut	routine operation
powder diffractometer SPODI		TU Darmstadt/LMU Munich	routine operation
thermal single crystal diffraktometer RESI		Uni Augsburg/LMU Munich	routine operation
hot single crystal diffractometer HEIDI		RWTH Aachen	routine operation
beam for neutron optics MIRA		TUM physics	routine operation
reflectometer for biological samples REFSANS		GKSS/LMU Munich	routine summer 2006
reflectometer for hard matter n-REX+		MPI Stuttgart	routine summer 2006
small angle scattering KWS 2		JCNS	routine March 2007
small angle scattering KWS 1		JCNS	routine autumn 2007
small angle scattering KWS 3		JCNS	routine autumn 2007
small angle scattering SANS-1		TUM physics/GKSS	routine end 2008
Spectrometer			
conventional spin echo NSE		JCNS	routine end 2006
resonance spin echo RESEDA		TUM physics	routine summer 2006
backscattering SPHERES		JCNS	routine autumn 2006
time-of-flight TOF-TOF		TUM physics	routine operation
diffuse & inelastic DNS		JCNS	routine March 2007
cold three axis PANDA		TU Dresden	routine operation
thermal three axis PUMA		Uni Göttingen	routine operation
polarised three axis TRISP		MPI Stuttgart	routine operation
Fundamental physics			
cold beam for nuclear physics MEPHISTO		TUM physics	routine operation
prompt gamma analyse PGAA		Uni Cologne/TUM chemistry	routine end 2006
Positron source			
NEPOMUC		Uni Bundeswehr/TUM physics	routine operation & extension
Clinical tumor therapy			
MEDAPP	MeV neutrons	TUM FRM II	routine end 2006
Projects			
acceleration of fission fragments MAFF		LMU/TUM physics	project
ultra cold neutrons UCN		TUM physics	project
bio diffractometer		TUM FRM II	project
high intensity reflectometer MARIA,		JCNS	project
thermal time-of-flight TOPAS		JCNS	project
GKSS outstation, 2 instruments		GKSS	project

Table 2: Actual status of the instrumentation

Rabbit irradiation system (RPA) for irradiation up to 10^{17} n/cm²

Position	Φ_{th} ($cm^{-2}s^{-1}$)	Φ_{epi} ($cm^{-2}s^{-1}$)	Φ_{fast} ($cm^{-2}s^{-1}$)
RPA-1	3.6×10^{13}	6.7×10^{9}	2.0×10^{9}
RPA-2	1.5×10^{13}	3.2×10^{9}	4.1×10^{8}
RPA-3	4.8×10^{13}	7.6×10^{8}	7.2×10^{7}
RPA-4	7.3×10^{13}	2.4×10^{10}	5.6×10^{10}
RPA-5	3.9×10^{13}	1.2×10^{10}	5.9×10^{9}
RPA-6	7.1×10^{13}	1.2×10^{9}	1.5×10^{8}

Capsule irradiation system (KBA) for irradiation from 10^{17} n/cm² to ca. 5×10^{19} n/cm²

Position	Φ_{th} ($cm^{-2}s^{-1}$)	Φ_{epi} ($cm^{-2}s^{-1}$)	Φ_{fast} ($cm^{-2}s^{-1}$)
KBA 1-1	1.3×10^{14}	2.6×10^{11}	3.9×10^{11}
KBA 1-2	9.3×10^{13}	9.9×10^{10}	2.0×10^{11}
KBA 2-1	1.1×10^{14}	7.5×10^{10}	2.1×10^{11}
KBA 2-2	7.7×10^{13}	3.9×10^{10}	1.0×10^{11}

Short term irradiations with small volume up to 5×10^{16} n/cm²

Position	Φ_{th} ($cm^{-2}s^{-1}$)	Φ_{epi} ($cm^{-2}s^{-1}$)	Φ_{fast} ($cm^{-2}s^{-1}$)
SDA-1	1.2×10^{13}	1.0×10^{9}	1.5×10^{10}

Table 3: Neutron uxes at irradiation positions[4].

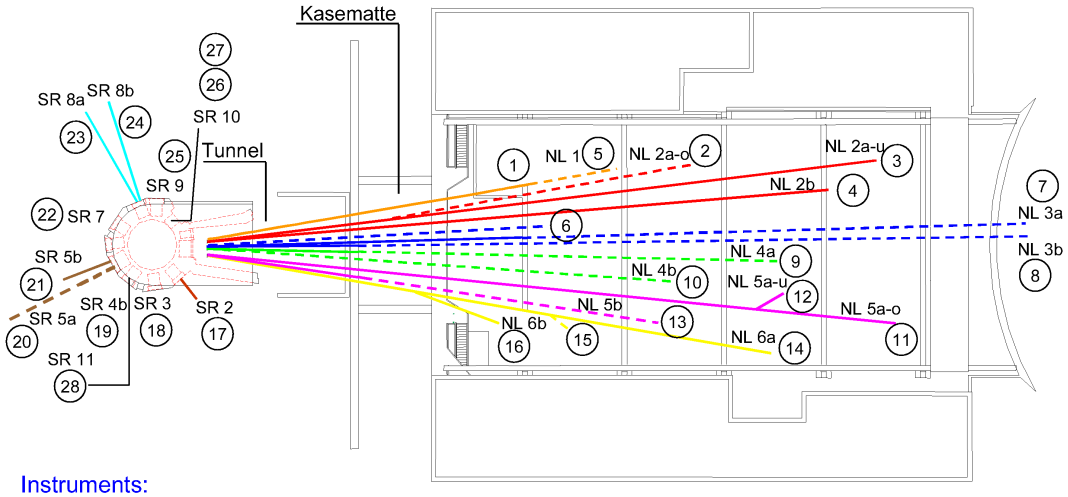

Instruments:

1. n-REX+	5. Mephisto	9. SANS-1	13. MARIA	17. PANDA	21. TRISP	25. HEIDI
2. NSE	6. KWS-3	10. PGAA	14. SPHERE	18. STRESS-SPEC	22. PUMA	26. MEDAPP
3. TOF TOF	7. KWS-2	11. RESEDA	15. DNS	19. ANTARES	23. SPODI	27. NECTAR
4. REFSANS	8. KWS-1	12. NOSPEC	16. MIRA	20. TOPAS	24. RESI	28. NEPOMUC

Figure 1.4: Splitting of the cold guides to the instruments.

278 proposals were submitted in two proposal rounds in 2005. Overbooking of the beam time is a factor of 2 on average. About 40 % of the beam request came from research groups outside of Germany.

[1] K. Zeitelhack, C. Schanzer, A. Kastenmüller, A. Röhrmoser, C. Daniel, J. Franke, E. Gutsmiedl, V. Kudryashov, D. Maier, D. Rathe, W. Petry, T. Schöffel, K. Schreckenbach, A. Urban, U. Wildgruber, Nuclean Instruments & Methods B, in print (2006)

[2] A. Röhrmoser, Annual Report Neutron Source Heinz Maier-Leibnitz (FRM II), 2005

[3] T. Unruh et al, see next contribution

[4] www.frm2.tum.de/kn/industry/irradiations.html

Time–of–Flight Spectrometer ToF-ToF in Routine Operation

Tobias Unruh[1], Andreas Meyer, Jürgen Neuhaus[1], Winfried Petry[1]

[1] Heinz Maier–Leibnitz Forschungsneutronenquelle, FRMII, Technische Universität München, Garching

Since summer 2005 the time–of– ight spectrometer ToF-ToF is in routine operation and rst international research groups could bene t from the world class performance of the instrument, which will be presented and illustrated by experimental examples in this article.

The ToF-ToF spectrometer is a chopper disc time–of– ight spectrometer and is positioned in the neutron guide hall of the FRM–II more than 60 m away from the reactor core. All the instruments in the neutron guide hall, including the ToF-ToF spectrometer, are powered with neutrons from the cold source of the reactor operating with D_2O at 25 K. The remote position of the spectrometer in combination with an elaborate shielding concept and the s–shaped curved primary neutron guide which acts as a neutron velocity lter, results in an excellent signal to background ratio (see below). The primary spectrometer is equipped with a system of 7 high speed carbon ber chopper discs and a focussing secondary neutron guide with supermirrors (m=3.6) which reduces the cross section of the primary beam from 44 mm (height) x 100 mm (width) to 23 mm x 47 mm. Including the divergency of 0.6° neutrons the beam size at sample position is about 35 mm x 60 mm. It can be reduced in width and height with an automated double slit system 18 cm in front of the sample. The primary beam monitor, a calibrated ssion chamber, is positioned directly behind this slit system.

The sample chamber is accessible from the top or optionally via a small door from the side. Standard sample environments currently available are cryostats with or without ^{3}He inserts and ^{3}He/^{4}He–dilution inserts as well as a high temperature furnace and a chamber for biological samples with good control for moderate temperatures. For special purposes a goniometer with xyz-table, rotation and two 2° Euler cradles is available. A radial oscillating collimator inside the sample chamber reduces the background intensity produced by neutrons not scattered by the sample but e.g. by the aluminium housing of a cryostat.

605 of the 1006 sites of the detector bank are currently equipped with squeezed ^{3}He detectors. The detectors are arranged in 4 raws at 400 mm distance from the sample covering angles from -15° to 140° and oriented tangentially to the Debye–Scherrer cones. The active detector length is 40 cm. With 10 bar gas pressure the detecors are very ef cient even for thermal neutrons. This

is important for the inelastic part of spectra and when using short incident wavelengths which are available at particular high intensity already starting from 1.5 Å (cf. Fig. 1.5).

The overall performance of the ToF-ToF spectrometer is characterized by good energy resolution at very low background and high neutron flux.

Fig. 1.5 shows the white beam neutron flux at sample position. The sharp cut-off towards wavelengths below 1.4 Å is due to the filtering property of the s–shaped curved neutron guide which

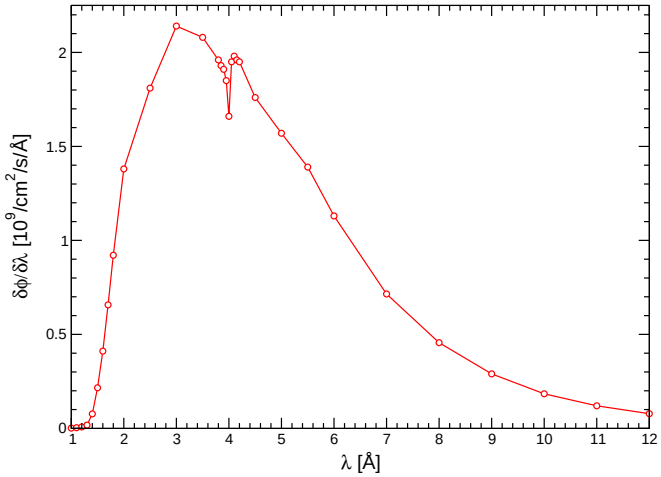

Figure 1.5: Differential neutron flux at sample position of the ToF-ToF spectrometer; clearly seen is the Bragg–edge of the Al windows

was designed to have a critical wavelength of 1.38 Å. In contrast to a simple curved neutron guide, the s–shape virtually eliminates all background from fast neutrons leaking through the choppers and produces a symmetric profile of the primary beam. A particular high intensity of 10^{10} n/cm^2/s — particle flux integrated over spectral distribution — is measured at sample the position.

The energy resolution of the spectrometer fits very well the theoretically expected values according to [1]. The instrumental line width ΔE (FWHM) can be expressed as:

$$\Delta E = \frac{h^3}{m_n^2 e} \frac{1}{\lambda_f^3} L_{sd} L_{pm} \sqrt{A^2 + B^2 + C^2}$$

$$A = t_m \left(L_{pm} + L_{ms} + \frac{\lambda_f^3 L_{sd}}{\lambda_i^3} \right)$$

$$B = t_p \left(L_{ms} + \frac{\lambda_f^3 L_{sd}}{\lambda_i^3} \right)$$

$$C = L_{pm} m_n \lambda_f \Delta L_d / h$$

with h: Planck's constant, m_n: neutron mass, e: elementary charge, λ_i: wavelength of the incident and scattered λ_f neutrons, respectively and using the instrument parameters given in Table 4.

For example an incident neutron wavelength of $\lambda_i = 5.4$ Å in combination with choppers rotating at 12000 rpm yields an accessible wavenumber range at zero energy transfer of $\sigma = 0.2 \ldots 2.2$ Å^{-1} and an energy resolution of 51 μeV (FWHM) at 90° scattering angle. For this configuration a hollow

parameter	description	value / range	unit
L_{pm}	distance between rst and last chopper	10	m
L_{sd}	distance between sample and detector	4	m
L_{ms}	distance between last chopper and sample	1.4	m
t_p	opening time of st chopper pair	$a_p/180°/\omega_c$	s
t_m	opening time of last chopper pair	$a_m/180°/\omega_c$	s
ω_c	rotation frequency of choppers	10–367	1/s
a_p	opening angle rst chopper pair	13.82 or 6.91	degree
a_m	opening angle last chopper pair	5.0 or 2.5	degree
L_d	length of other ight path uncertainties	$\pm$ 0.005 ¡ 0.05	m

Table 4: Some instrument parameters

cylindrical vanadium standard with a diameter of 23 mm, a vanadium wall thickness of 0.88 mm (' 10 % scatterer) and a height of 40 mm gave a count rate of 2900 cps summed over all 605 detectors (frame overlap ratio: 3).

In order to provide rotation speeds of the chopper discs of 600 mm diameter of up to 22000 rpm it was necessary to develop a new concept on the basis carbon ber reinforced plastics. Magnetic bearings and a fast positioning control systems assure a phase stability of the disc rotation better than 0.05%. Changing the incident wavelength of the spectrometer or switching the slit type of the rst or last chopper pair does not take longer than 10 s. To change the chopper speed by 1000 rpm will take about 2 min. These quick con guration changes are also supported by the full remote control of the spectrometer, which means that all devices can be programmed by the user directly via a python script in the control program.

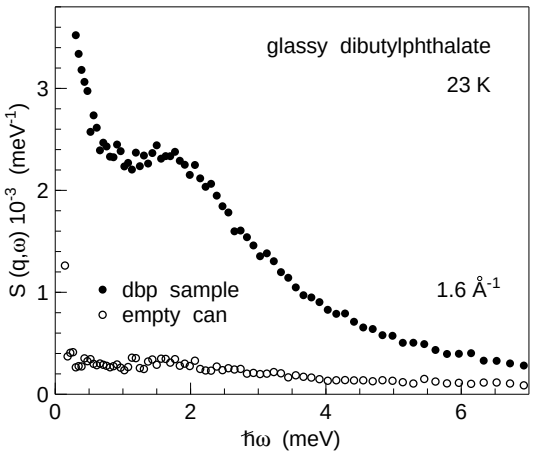

Figure 1.6: Inelastic neutron scattering on glassy dibutylphthalate at 23 K

The experiment on glassy dibutylphthalate ($C_{16}H_{22}O_4$) demonstrates the mentioned exceptional signal to noise ratio of ToF-ToF. As compared to an ideal Debye solid, disordered solids feature an enhanced scattering intensity at a few meV — the so called Boson peak. In dibutylphthalate this peak is located around 2 meV. With an experimental setup similar to that described for the vanadium standard and a hollow cylindrical $C_{16}H_{22}O_4$ sample with 0.1 mm wall thickness the Boson peak can be resolved on the neutron energy gain side even at 23 K (Fig. 1.6). The signal to noise ratio ($S(q;\omega = 0)$ of the $C_{16}H_{22}O_4$ sample to $S(q;\omega = 5$ meV) of the aluminum empty can)

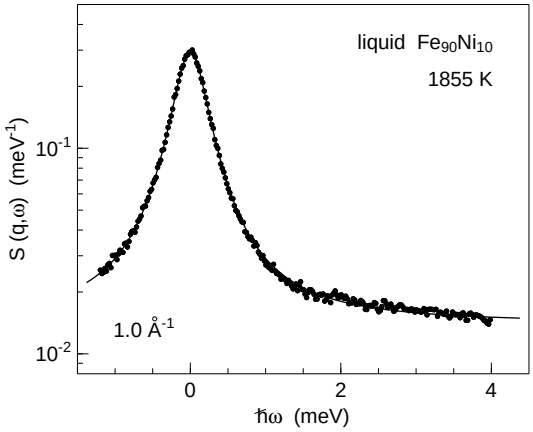

Figure 1.7: Quasielastic neutron scattering on a $Fe_{90}Ni_{10}$ melt at 1855 K

is better than [5].

Time critical experiments benefit from the high neutron flux such as high temperature experiments limited by evaporation and/or interdiffusion between sample and sample holder. Figure 1.7 shows the quasielastic signal of liquid $Fe_{90}Ni_{10}$ at 1855 K measured in an alumina can that provides a hollow cylindrical sample geometry with 1.2 mm sample wall thickness. Measuring time was one hour. Interestingly with . . Δ^{-9} m^2/s the resulting self diffusion coefficient of Nickel is slightly smaller than in dense packed pure liquid Nickel [2] or Ni rich NiAl alloys [3].

[1] R. E. Lechner, Technical report, KEK reports 90-25 (1991)

[2] S. Mavila Chathoth, A. Meyer, H. Schober, F. Juranyi, Appl. Phys. Lett. **85**, 4881 (2004)

[3] S. K. Das, J. Horbach, M. M. Koza, S. Mavila Chathoth, A. Meyer, Appl. Phys. Lett. **86**, 011918 (2005)

2 Polymers

Polymers offer additional characteristics in material science as compared to metals and ceramics. Research comprehends bulk, solutions and gels as well as thin film and surface structures.

In 2005, a new instrument for studies of the dynamics of polymeric systems was purchased: A fluorescence correlation spectrometer equipped with a heating and cooling sample cell and the possibility for two-color cross correlation experiments will allow us to continue our studies of polymer solutions and gels.

Another highlight were first high-resolution grazing-incidence small angle x-ray scattering experiments at the HASYLAB providing a combination of GISAXS, with an extremely high collimated and focussed x-ray beam. Due to the unique combination of a special x-ray beam and the surface sensitive scattering technique GISAXS a structural investigation becomes accessible by scattering.

2.1 Structures of solutions, gels and in the bulk

Aggregation behavior of amphiphilic copolymers in aqueous solution

T. B. Bonné, R. Ivanova, K. Lüdtke[1], R. Jordan[1], C. M. Papadakis

[1] Lehrstuhl für Makromolekulare Stoffe, Department Chemie, TU München

Poly(2-oxazoline) copolymers are very versatile candidates for studies of the aggregation behavior of amphiphilic copolymers in aqueous solution, since their hydrophobicity can be controlled by the addition of various side groups to the same polymer backbone (fig. 2.1). We have studied aqueous solutions of diblock, triblock and random copolymers consisting of hydrophilic poly(2-methyl-2-oxazoline) and of hydrophobic poly(2-nonyl-2-oxazoline) with the focus on the critical micelle concentration (CMC) and the micellar size. Tracer diffusion measurements were carried out with fluorescence correlation spectroscopy (FCS) and the identical, fluorescence-labeled polymers and allowed us to cover ta concentration range of $^{-9}$ $^{-2}$M.

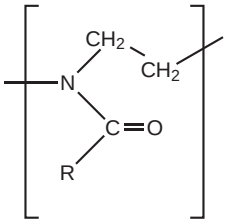

Figure 2.1:
Structure of the oxazoline monomer. Chosing methyl or nonyl as the side group R leads to hydrophilic or hydrophobic monomers PMOx and PNOx, respectively.

Tracer diffusion measurements on two similar diblock copolymer solutions show a change of behavior near concentrations of $^{-5}$ M, which we identify as the critical micelle concentration (CMC). Only above this critical micellar concentration, micelles are formed (fig. 2.2).

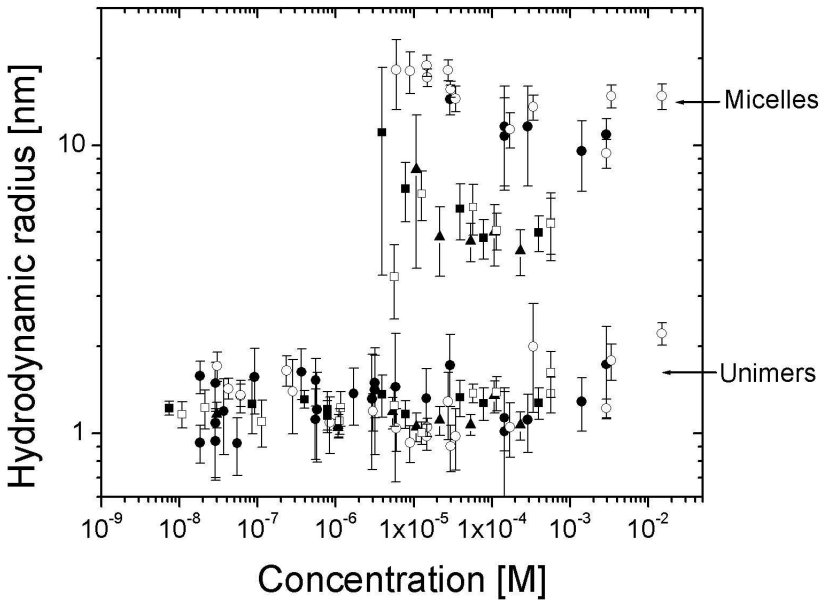

Figure 2.2:
Hydrodynamic radii of unimers and micelles in aqueous solutions of P[(NOx)$_{10}$-b-(MOx)$_{32}$] and (±) P[(NOx)$_7$-b-(MOx)$_{40}$] diblock copolymers, (¢) P[(MOx)$_{20}$-b-(NOx)$_7$-b-(MOx)$_{14}$] and (¥) P[(MOx)$_{30}$-b-(NOx)$_7$-b-(MOx)$_{26}$] triblock copolymers, and (N) P[(MOx)$_{40}$-r-(NOx)$_6$] random copolymers in dependence on the total polymer concentration.

The micelles formed by the triblock copolymers P[(MOx)$_{20}$-b-(NOx)$_7$-b-(MOx)$_{14}$] and P[(MOx)$_{30}$-b-(NOx)$_7$-b-(MOx)$_{26}$] are smaller than the ones formed by the diblock copolymers described above. The micellar hydrodynamic radii are roughly half of the ones of the diblock copolymers, which can be understood by the requirement that the triblock copolymers have two junction points at the surface of the micellar core, whereas the hydrophobic blocks of the diblock copolymers stretch into the center of the micellar core.

Also random copolymers P[(MOx)$_{40}$-r-(NOx)$_6$] form micelles above a critical micelle concentration of » 10^{-5} M. Their hydrodynamic radius is smaller than the ones of both di- and triblock copolymers. This is probably due to the structure of the aggregates, which are not expected to be of the core-shell type.

FCS is thus ideally suited to investigate the micelle formation in amphiphilic copolymer systems.

This project was funded by DFG (Pa 771/2-1) and by EU (Marie Curie Grant).

[1] T. B. Bonné, K. Lüdtke, R. Jordan, P. Štěpánek and C. M. Papadakis Coll. Polym. Sci. 282, 833 (2004).

Multicompartment hydrogels from lipophilic-hydrophilic-fluorophilic triblock copolymers

R. Ivanova, T. B. Bonné, T. Komenda[1], K. Lüdtke[1], R. Jordan[1], K. Mortensen[2], P.K. Pranzas[3], C. M. Papadakis

[1] Lehrstuhl für Makromolekulare Stoffe, Department Chemie, TU München
[2] Danish Polymer Centre, Risø National Laboratory, Roskilde, Denmark
[3] Institut für Werkstoffforschung, GKSS-Forschungszentrum, Geesthacht

Amphiphilic copolymers find numerous applications, e.g. for drug delivery, as gel formers or as nanoreactors. Poly(2-oxazoline) block copolymers constitute a very versatile system [1,2]: The amphiphilicity can be controlled by the choice of side groups (Fig. 2.3), and in aqueous solution, unimers, micelles or micellar hydrogels are formed, depending on the block copolymer architecture [3]. Micellar hydrogels with chemically different types of micelles may be achieved by using triblock copolymers with blocks containing lipophilic, hydrophilic and fluorophilic side groups. Here, the presence of a fluorophilic moiety increases strongly the degree of segregation, and multicompartment gels may be formed even at low degrees of polymerization.

We have used small-angle neutron scattering with contrast matching to study the structures of poly(2-oxazoline)-based micellar gels with the focus on the question whether the two end blocks indeed form separate micelles. In order to uniquely interpret the (complex) scattering curves of the micellar gels formed by concentrated solutions of the (P(NOx_{12}-*b*-MOx_{64}-*b*-FOx_9)) triblock copolymers (Fig. 2.3), the sizes and shapes of the micelles formed by P(MOx_{30}-*b*-NOx_6) and P(MOx_6-*b*-FOx_{40}) diblock copolymers were investigated as well, namely in aqueous solutions of lower concentration. Furthermore, we verified that aqueous solutions containing both diblock copolymers do not form mixed micelles.

We found that, upon dissolution in water at room temperature, P(MOx_{30}-*b*-NOx_6) diblock copolymers form large aggregates in addition to the expected spherical core-shell micelles. These aggregates - which are presumably due to the strong association via the nonyl side chains of the lipophilic blocks in the bulk state - dissolve upon annealing the solutions at elevated temperatures, and only spherical (equilibrium) micelles remain (Fig. 2.4). In contrast, P(MOx_6-*b*-FOx_{40}) diblock copolymers do not form spherical, but slightly elongated micelles (Fig. 2.4). This is possibly due to the steric demands of the fluorophilic side chains forcing the polymer backbones to stretch.

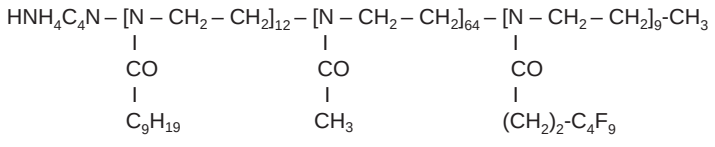

Figure 2.3:
A poly(2-oxazoline) triblock copolymer with a lipophilic, a hydrophilic and a fluorophilic block.

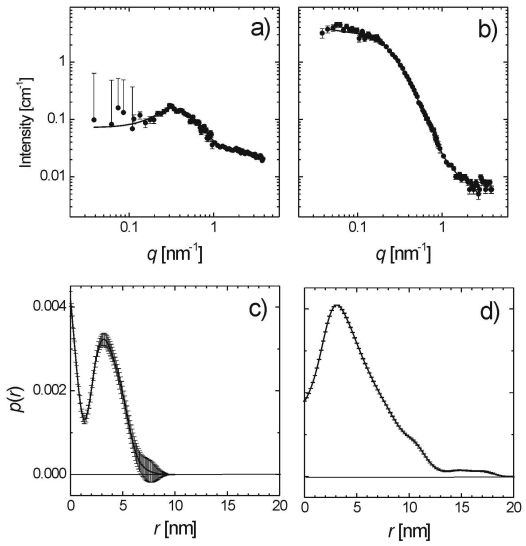

Figure 2.4:
SANS intensity profiles together with the pair distribution functions of (a,c) P(MOx_{30}-*b*-NOx_6) and (b,d) P(MOx_6-*b*-FOx_{40}) diblock copolymers. The SANS curves were obtained from D_2O/H_2O solutions with the MOx-blocks being contrast-matched, i.e. only the micellar core is visible. The pair distribution functions were determined following the method of Glatter [4].

The P(NOx_{12}-*b*-MOx_{64}-*b*-FOx_9) triblock copolymers form gels above polymer concentrations of 10 wt-%. Their scattering can be described by a coexistence of spherical, lipophilic and elongated, fluorophilic micellar cores, which are linked by the hydrophilic blocks (Fig. 2.5). Thus, the system forms a multicompartment gel.

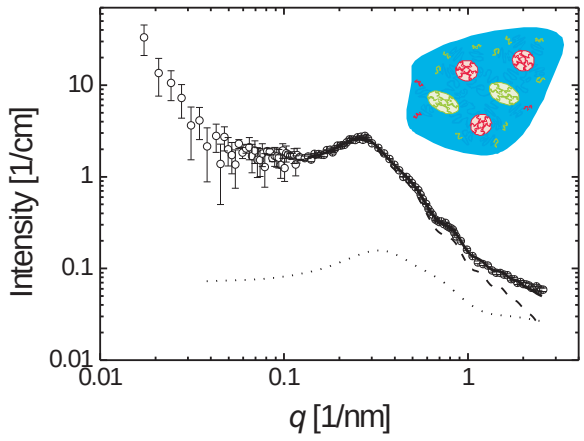

Figure 2.5:
SANS intensity profile of a hydrogel of (P(NOx_{12}-*b*-MOx_{64}-*b*-FOx_9)) having a polymer concentration of 20 wt-%. (±) experimental data, dotted line: fitting curve of P(MOx_{30}-*b*-NOx_6) (spherical micelles), dashed line: fitting curve of P(MOx_6-*b*-FOx_{40}) (elongated micelles). Solid line: weighted sum of the two fitting curves. Inset: Schematic representation of the structure of the multicompartment hydrogel.

This project was financially supported by DFG (Pa 771/2-1).

[1] R. Jordan, K. Martin, H. J. Rädler, K. K. Unger, Macromolecules **38**, 8858 (2001)
[2] T. Komenda, R. Jordan, Polymer Preprints **44**, 986 (2003).
[3] T.B. Bonné, K. Lüdtke, R. Jordan, P. Štěpánek, C.M. Papadakis, Coll. Polym. Sci. **282**, 833 (2004).
[4] O. Glatter, J. Appl. Cryst. **10**, 425 (1977) and **13**, 577 (1980).

Influence of the morphology on the slow dynamics in diblock copolymer melts

C.M. Papadakis, F. Rittig[1]

[1] BASF AG GKP/P, Ludwigshafen

Diblock copolymers in the melt form a variety of ordered morphologies besides the disordered state, e.g. the lamellar, the gyroid, the hexagonal and the body-centered cubic structure. Diblock copolymer melts constitute thus an ideal model system for studying the influence of the structure on the single-chain as well as on the collective dynamics.

A number of analogies between the dynamics of ordered block copolymer melts and other systems may be drawn, e.g. with the smectic phase in liquid crystals, lyotropic lipid or surfactant systems. However, investigations on solvated low molar mass components may suffer from the finite permeability of the surfactant layers to the water and from hydration effects. Block copolymer systems, in constrast, are one-component systems, which facilitates the assignment of the dynamic processes. Another interesting aspect of block copolymer melts is the fact that diffusion proceeds in structures formed by self-organization, in contrast to host-guest system like nanoporous solids.

We have studied the relationship between the block copolymer morphology and the translational and collective dynamics using a series of poly((ethylene propylene)-*b*-(dimethylsiloxane)) (P(EP-*b*-DMS)) diblock copolymers. This system has the advantage that the dynamics are accessible in a large temperature range. Dynamic light scattering (DLS) allowed us to detect a number of (slow) dynamic processes. The combination with pulsed field gradient (PFG) NMR proved to be useful because the latter technique monitors the long-range molecular displacements and thus helps to decide which of the processes observed are due to long-range self-diffusion.

With all three samples, we could in this way identify the isotropic chain diffusion in the disordered state (Fig. 2.6 a-c). Furthermore, due to the polymers' high degradation temperature, we were able to characterize the so-called ultraslow cluster mode in detail. It is present in the DLS curves with a significant amplitude even at temperatures as high as 300°C, i.e. more than 50 K above the order-to-disorder transition (ODT) temperature. This is in contradiction to the previous speculation that it is related to the onset of microphase separation above the ODT temperature [2].

In the ordered state, we found that the mechanism of chain diffusion depends strongly on the morphology: In the lamellar and the hexagonal state, the thermodynamic repulsion between the two blocks leads to predominantly two- or one-dimensional copolymer diffusion along the interfaces, respectively (Fig. 2.6 a,b). The cubic micellar state appears qualitatively different, because copolymer diffusion along the interfaces does not correspond to long-range diffusion (Fig. 2.6 c).

An additional, fast dynamic process observed in our DLS experiments in the lamellar state, had previously been related to the undulations of the lamellar interfaces [3]. A fast process in the hexagonal state could also be attributed to undulations of the cylinders.

In the body-centered cubic state, the self-diffusion of copolymers proceeds in two ways: The chains can diffuse through the matrix where they only experience the friction of the matrix block (in our case PDMS). In addition, they can diffuse from micelle to micelle, which is an activated process leading to a strong temperature dependence (Fig. 2.6 c). This assignment is corroborated by the good agreement of the reduced diffusivities with data from the literature on chemically different systems [1].

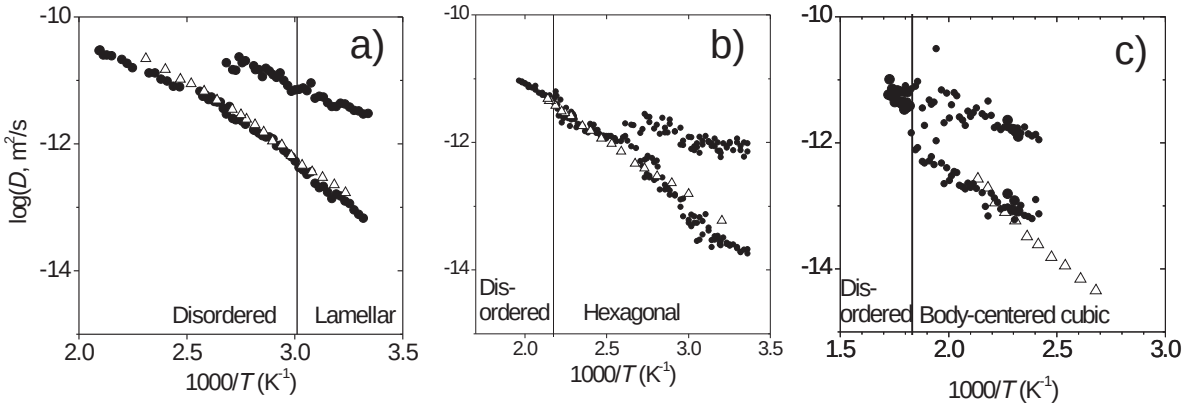

Figure 2.6:
Results from various P(EP-*b*-DMS) diblock copolymers: Arrhenius diagrams of the (apparent) diffusivities from DLS ( ) and from PFG NMR (·) of the lamellar (a), the hexagonal (b) and the body-centered cubic sample (c). The vertical lines denote the ODTs.

Our work has shown that systematic studies on the same sample system in different morphologies, minimizing the variation of other properties like the degree of entanglement, are mandatory to gain a conclusive image.

This work was funded by DFG within the SFB 294 'Moleküle in Wechselwirkung mit Grenzflächen' at the University of Leipzig (Projects D4 and G4).

[1] C.M. Papadakis, F. Rittig, J. Phys. Cond. Matter **17**, R551 (2005).
[2] S.M. Chitanvis, Phys. Rev. E **57**, 1921 (1998).
[3] P. Štěpánek, F. Nallet, K. Almdal, Macromolecules **34**, 1090 (2001).

Investigation of polymeric foams on the nanometric scale by USAXS

C.C. Egger [1], V. Schädler [1], S.V. Roth [2], P. Müller-Buschbaum

[1] ISIS-BASF, Strasbourg (France)
[2] HASYLAB, Hamburg

We report the study of polymeric foams with very low density (200 g/L) and pores in the range of 100 to 500 nanometres by ultra small angle x-ray scattering (USAXS). The given foams have first been characterised using standard techniques such as scanning electronic microscopy to access morphological features, mercury intrusion to access overall pore volume and pore sizes greater than 100 nm, or nitrogen sorption for pores smaller than 100 nm. Highly porous materials such

as aerogels (pore volume 99%) exhibiting pores in the range of a few nanometres to 50 nm have been fully characterised by N2 sorption and SAXS [1]. A critical comparison between SAXS, N2 adsorption and Hg penetration is available on inorganic porous particles with pore radii ranging from 2.0 to 20 nm [2]. Polyurethane-type foams have already been investigated by SAXS, and their fractal nature revealed [3,4]. However, the characterisation of the foams produced in our laboratory is even more challenging, owing to the larger pores formed, from 100 to 500 nanometres, preventing in most cases the use of N2 sorption or SAXS. Mercury intrusion, the principle of which is to force into the pores a non-wetting liquid -mercury- by applying pressure, and then to work out the intruded porous volume, also finds its limitations here due to the fragility of such polymeric foams, with pore volumes estimated around 85 %. Indeed, such a technique generates high stress in the materials, stress that polymeric foams cannot always sustain, causing the collapse of the structure upon measurement. Consequently, USAXS was thought of as an independent alternative technique to sorption/intrusion means. The utility and real impact of USAXS for the characterisation of heterogeneous systems has been well established since the early 1990's [5].

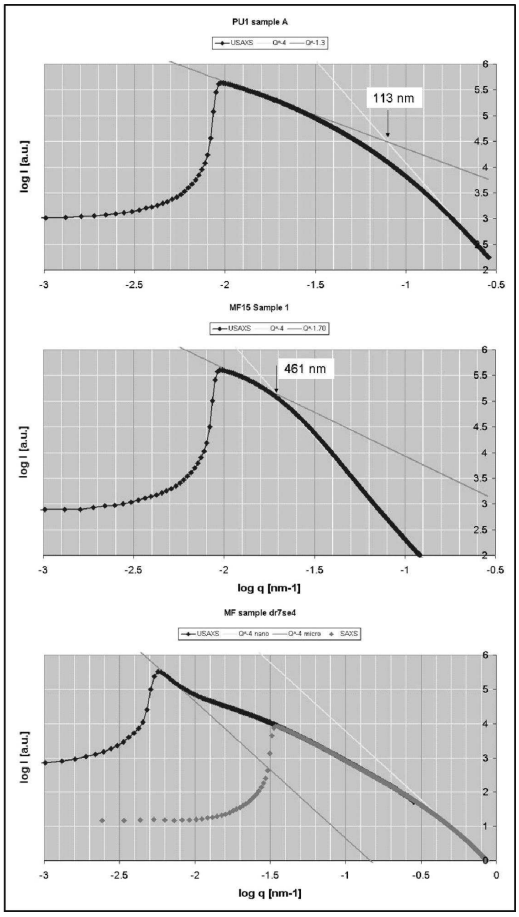

Figure 2.7:
USAXS curves measured at BW4 beamline of three specimens: -top- highly porous polyurethane foam, -middle- dense melamine formaldehyde resin, -bottom- low-density MF foam; here the beam stop was vertically off-centred to enlarge the q-range to smaller q-values (USAXS resolution $d_{max} > \mu m$)

The USAXS experiments were performed at the BW4 USAX beamline of the DORIS III ring storage at HASYLAB/DESY, Hamburg. The sample-to-detector distance was 12.71 m, the beam size 400 £ 400 μm^2 and the wavelength 0.138 nm. The data were taken using a two-dimensional MAR CCD (MAR research) with a pixel size of 79.1 μm and a total number of 2048 £ 2048 pixels.

Three characteristic samples have been chosen for this study: (i) a polyurethane (PU) foam (estimated density 0.190 g/L) which cannot be characterised neither by nitrogen adsorption due to a lack of reproducibility in the data (multilayer condensation takes place), nor by mercury intrusion, due to the fragility of the framework collapsing upon measurement, (ii) a high density melamine formaldehyde (MF) resin (density calculated from mercury data: 675 g/L), showing monodisperse pores centred about 550 nm (Hg intrusion), studied here as a reference, (iii) a low-density melamine formaldehyde foam (density calculated from mercury data: 275 g/L) exhibiting two well-defined pore sizes from Hg penetration, at 260 nm and 2.3 mm. The USAXS curves of the three samples are gathered in figure 2.7 below. The standard MF specimen -middle curve- clearly shows the Porod regime at high $logq$ values following a power law of -4 (light gray fit), characteristic of a smooth surface, whereas the low $logq$ region characteristic of a mass fractal has dimensionality of -1.7 (gray fit). At the intersection of the fitting curves, qR =4.5, and therefore the radius R of the pores is calculated to be 461 nm. Although when compared to the mercury data, the pore diameter from USAXS is 40% overestimated, the order of magnitude of both techniques (USAXS and Hg) are comparable. The PU foam -top curve- exhibits a similar behaviour with data shifted to higher $logq$ values, and a pore radius of 113 nm is found. This result cannot be compared against Hg data (structure collapse) but a pore diameter around 132 § 88 nm can be estimated using the reference of the high density MF sample. As for the third specimen, the low-density MF foam, two Porod regimes are found (from USXAS and SAXS data), one in the -0.5 to 0 $logq$ region and the other one in the -2.3 to -2 log q region. It correlates very well with the mercury intrusion data, showing two pore sizes (nm and mm). The lack of correlation between these two regimes is characteristic of a non-fractal structure.

Preliminary USAXS studies show good qualitative agreements, when possible, with sorption or intrusion data. More work regarding the relevance on the dilute phase condition is necessary, and trials to fit the scattering curves using a global unified equation could be carried out. Discrepancies between pore sizes could also be investigated further. The fractal character of the specimens 1 and 2 could also be checked by carrying out complementary SAXS measurements.

[1] (a) D. W. Schäfer and K. D. Keefer, Phys. Rev. Let., 56(20), 2199 (1986); (b) J. C. Dore and A. N. North, Mineralogical Society series 4, 1367-3920, 11, (1993)

[2] A. M. Brenner, B. D. Adkins, S. Spooner, B. H. Davis, J. Non-Cryst. Solids, 185, 73 (1995)

[3] G. L. Wilkes, S. Abouzahr, D. Radovich, J. Cellular Plastics, 248, (July/August 1983)

[4] H. J. M. Grünbauer, J. C. W. Folmer, J. App. Polym. Sci., 54, 935 (1994)

[5] A. N. North, J. C. Dore, A. R. Mackie, A. M. Howe, J. Harries, Nuclear Inst. Methods in Phys. Res., B47, 283 (1990)

Microscopic structures of adhesive polymer films as investigated by USAXS

E. Maurer, M. Ruckpaul [1], D. Wulff [1], N. Willenbacher [2], P. Müller-Buschbaum

[1] BASF, Ludwigshafen
[2] Karlsruhe

Pressure sensitive adhesives (PSA) are based on polymers. They adhere by simply applying pressure to a huge variety of materials. In many PSA applications a controlled release of the adhesive bond is desired. One of the most prominent examples in daily life are stick-on notes, making use of the ability to undergo several cycles of bonding and detaching. Scientifically, the quality of adhesion is quantified in the so called tack test [1]. A probe punch, like a flat-ended cylinder, is pressed with a defined force onto a PSA film. After maintaining the force for a controlled time the punch is withdrawn from the surface with a fixed velocity (see figure 2.8 a). During the process the force needed to sustain the constant retraction velocity is probed as a function of the film-punch distance. Usually, the resulting curves show characteristic features such as a maximum force followed by a force plateau. PSA debonding during the tack test was in detail analysed by optical microscopy through a transparent substrate [2]. In early debonding stages macroscopic cavities appear locally, introduced into the former homogenous film by tensile stress [3]. With proceeding tension they grow in number and size until the former contact area is almost completely covered. Finally, the polymeric material located at the partition walls separating cavities is elongated in direction of tension. Thereby numerous fibrils are formed. Thus investigations based on optical microscopy yield a detailed overview of the evolving structures during retraction.

Nevertheless, investigations by conventional microscopy are restricted towards small length scales by the optical resolution limit. In order to overcome this limit we applied in-situ ultra small angle x-ray scattering (USAXS) during the tack test [4, 5]. As a PSA model system, we investigated films (thickness 30 μm) of a statistical copolymer of 80 % 2-ethyl hexylacrylate (EHA) and 20 % methyl methacrylate (MMA).

The USAXS experiments were performed at HASYLAB beamline BW4 operating a two-dimensional position sensitive detector. The direct beam (diameter approximately 400 μm) was shadowed by a beam stop. Using a wavelength of 0.138 nm and a sample detector distance of 13.0 m structures between 25 nm and 400 nm were resolvable. The PSA film was placed parallel to the incident beam shadowing only a small part of the beam. While film and beam remained solidly attached, the punch was retracted in the direction perpendicular to both film surface and incoming beam (see figure 2.8 b). Former scattering experiments were dedicated to a detailed study of debonding stages after the force maximum [4-6]. As in the presented investigations we concentrated on early debonding stages, retraction was stopped after a punch-film-distance 12.5 μm. At this debonding stage, no bubbles are macroscopically present. Microscopic structures present in this stage could therefore be interpreted as precursors of the later nucleation of macroscopic bubbles. We further addressed the influence of the probe material. A typical scattering pattern is presented in figure 2.8 c. It contains beside the USAXS signal also diffuse scattering from the PSA surface. Focussing on the USAXS signal we restrict ourselves to horizontal cuts out of the 2D intensity map through the direct beam position and parallel to the PSA film surface $q_z = 0$.

In figure 2.8 d the resulting curves are displayed for several punch materials. Partly, the cuts show well pronounced, multiple fringes. A further eye-catching feature is the asymmetry of the curves with respect to the horizontal momentum transfers [4, 5]. Qualitatively, the use of glass punches

with low roughness strongly favours the presence of a microscopic substructure, as indicated by modulated scattering signals. The length scales have been determined as 167-189 nm. Moreover a microscopic, but compared to glass punches relatively small structuring (80 nm) was detected for plexiglass. If metallic punches were used, only weak deviations from a homogeneous decay ware visible in the scattering signal. For copper punches structures with 107 nm in size were resolved.

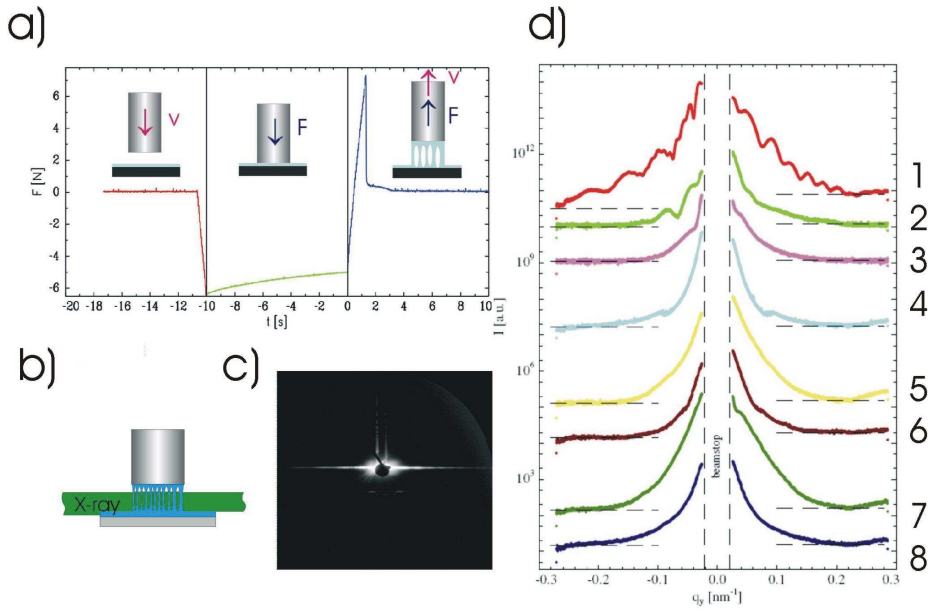

Abbildung 2.8:
a) In the tack test a punch is pressed onto a PSA film, the contact is maintained for a fixed period and later the punch is retracted again. The force F is recorded as a function of time t. b) In-situ to the tack test the debonding zone under the punch is investigated by ultra small angle scattering. The X-ray beam is aligned parallel to the adhesive surface. c) Typical two-dimensional scattering pattern showing horizontal streaks from a transmission (USAXS) scattering and diffuse scattering from the adhesive surface. d) Horizontal USAXS cuts displaying intensity versus horizontal momentum transfer q_y for different punch materials (1: polished glass, 2: glass with roughness 3 μm, 3: glass with roughness 15 μm, 4: Plexiglas, 5: brass, 6: copper, 7: aluminium, 8: stainless steel). The resolution is limited to large structures by the presence of the beamstop.

This work was financially supported by the BMBF (grant 03CO333).

[1] A. Zosel, Coll.Polym. Sci 263, 541 (1985)

[2] H. Lakrout, P. Sergot, C. Creton, J. Adhesion 69, 307 (1999)

[3] C. Creton, H. Lakrout, J. Polymer Sci, Polym. Phys 38, 965 (2000)

[4] P. Müller-Buschbaum, T. Ittner, W. Petry, Europhys. Lett. 66, 513 (2004)

[5] E. Maurer, S. Loi, D. Wulff, N. Willenbacher, P. Müller-Buschbaum, Physica B 357, 144 (2005)

[6] E. Maurer, S. Loi, P. Müller-Buschbaum, in Adhesion's current Research and Applications, Wiley-VCH, 421,(2005)

Self supported particle track etched polycarbonate membranes as templates for cylindrical polypyrrole nanotubes and nanowires

N. Hermsdorf [1], M. Stamm [1], S. Förster [2], S. Cunis [3], S. S. Funari [3], R. Gehrke [3], P. Müller-Buschbaum

[1] Institut für Polymerforschung, Dresden
[2] Universität Hamburg, Institut für Physikalische Chemie, Hamburg
[3] HASYLAB, Hamburg

In previous work, particle track etched polymer membranes (nanoPTM) have been shown to offer exciting possibilities as separation media when the pores are left open and as the basis for many different types of sensors when the pores are filled [1]. Filling was performed with, for example, metals or conductive polymers. The template synthesis of nanoscale materials by filling the porosity of nanoPTM is a method now successfully used [2]. This method provides the possibility to fabricate nanowires and nanotubes made out of polymers with a high aspect ratio. Because previous work was focused on the track etching process, nanoporous track etched polycarbonate membranes can be prepared with high reproducibility [3, 4]. These nanoPTM have a well-controlled pore size in the range of 20-150 nm and a nearly perfect cylindrical pore shape. Consequently, their use as templates leads to the synthesis of shape-controlled nanomaterials with a well-defined size. In literature commonly sizes and size distributions of NanoPTM and nanomaterial were determined from real space techniques such as transmission electron microscopy (TEM) and scanning electron microscopy (SEM). As a consequence, the statistical relevance of the obtained parameters is limited, because local techniques enable the determination of relevant structural parameters (mean pore size and pore shape) based on a restricted number of pores or nanowires only. Moreover numbers estimated from surface probes can yield misleading results in case the pore shape deviates from a simple cylinder and the diameter at the surface differs from the one inside the film.

Within this investigation both problems are overcome by applying a scattering technique [5]. The accessible q-range is extended by a combination of SAXS and USAXS data. SAXS measurements based on synchrotron radiation were performed at the A2 beamline with a wavelength 0.15 nm. For USAXS measurements with synchrotron radiation the BW4 beamline was used and a wavelength 0.138 nm was selected. During the scattering measurements, the sample is placed vertically in a special sample holder allowing to tilt the sample with respect to the X-ray beam. In a first experimental configuration, an angle of 30^o between pores/nanotubes and X-ray beam was chosen which resulted in an anisotropic scattering pattern. In a second experimental configuration, X-ray beam and pores/nanotubes were aligned parallel to each other and a nearly isotropic intensity distribution was detected. Background scattering of the set-up was recorded before and after the measurement of the samples to enable a later correction of the recorded intensities.

The nanoPTM were made from 21 μm thick polycarbonate films. A large regime of nominal pore sizes from 5 to 150 nm as determined by SEM and pore density up to 109 pores/cm^2 is investigated. Depending on the pore diameter either nanotubes or nanowires are produced. For comparison, with each ion beam irradiated, etched and filled sample an equally prepared, but non-irradiated one was measured. These additional measurements were used as a reference in order to receive the scattering contribution of the pores or nanotube/-wires from the difference between them. The effect of pore density and pore size on the scattering data is displayed in figure 2.9.

Figure 2.9 a compares virgin (unfilled) polycarbonate membranes PC80 with pore densities of 10^7;10^8;10^9 pores/cm^2. The samples were measured for 6 £ 30 minutes each. With decreasing pore densities per surface area the scattered intensity decreases. As a consequence a reduced statistics results but no significant change in the curve shape. Thus the pore shape and size are unaffected by a change in the pore density [6].

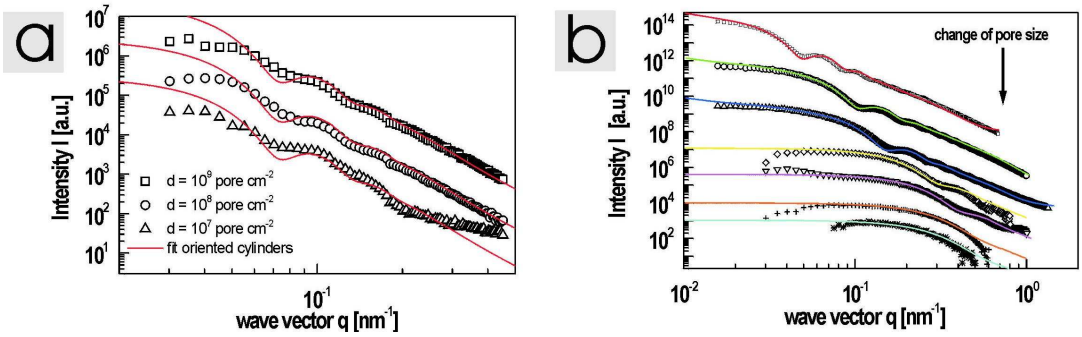

Figure 2.9:
a) Influence of pore density: Scattering data of the PC virgin membranes PC80, from the bottom to the top the pore density increases 10^7 (triangles), 10^8 (circles), 10^9 pores/cm^2 (squares). The fits to the data (red lines) assumes oriented cylinders. b) Influence of pore diameter: Scattering data of the PC virgin membranes PC5, PC10, PC15, PC20, PC50, PC75 and PC150 (from bottom to top), the pore diameters extracted from the fits to the data (solid lines) are respectively 17, 17, 21, 28, 54, 78 and 162 nm. Data and fits are successively shifted on the intensity axis for clarity. For more details see reference [6].

Figure 2.9 b compares several virgin membranes with a nominal pore diameter ranging from 5 to 150 nm. All curves show well pronounced modulations of the intensity, resulting from the presence of monodisperse pores. The first peak in the scattering data shifts towards smaller q-values with increasing pore size. The peak and the minimum position correspond to the real size of the pores. Due to the accessible q-range of the SAXS experiment of 0.6 nm^{-1} only pores with diameters larger than 20 nm were well resolved. To detect structures smaller than 20 nm it would have been necessary to increase the q-range, which was not performed due to the limited synchrotron beam time. From fits to the experimental data, the relevant parameters such as pore diameter and pore density are determined. A density profile of oriented cylinders is used for the unfilled membranes. The good agreement between calculated and measured data confirms the underlying model. The comparison with the numbers determined by SEM shows deviations. In general, with SEM the pore diameter was underestimated, which might result from the necessary sample pre-treatment to enable SEM or from the fact that SEM probes the pure surface information only. In contrast our scanning force microscopy data compare well within the experimental error (few nanometers) with the results obtained by fitting the scattering data and are therefore not listed separately [7]. The standard deviation for pore size σ_R for all samples was 0.13 [6]

[1] Schönenberger, C., van der Zande, B.M.I., Fokkink, L.G.J., Henny, M., Schmid, C., Kruger, M., Bachtold, A., Huber, R., Birk, H., Staufer, U.; J. Phys. Chem. B 1997, 101, 5497

[2] Piraux, L., Dubois, S., Demoustier-Champange, S.; Nucl. Instrum. Meth. B 1997,131 357

[3] Demoustier-Champange, S., Duchet, J., Legras, R.; Synthetic Metals 1999, 101, 20

[4] Jerome, C., Demoustier-Champagne, S., Legras, R., Jerome, R.; Chemistry-A Eurp. J. 2000, 6, 3089

[5] Förster, S., Timmann, A., Konrad, M., Schellbach, C., Meyer, A., Funari, S.S., Mulvaney, P., Knott, R.; J. Phys. Chem. B 2005, 109, 1347

[6] Hermsdorf, N., Stamm, M., Fster, S., Cunis, S., Funari, S.S., Gehrke, R., Müller-Buschbaum, P.; Langmuir 2005, 21, 11987

[7] Müller-Buschbaum, P.; J. Phys. Condens. Matter 2003, 15, R1549

2.2 Polymer thin film and surface structures

The scattering cross-section of lamellar block copolymer films in the distorted-wave Born approximation

C.M. Papadakis, P. Busch[1], M. Rauscher[2], D.-M. Smilgies[3], D. Posselt[4]

[1] Materials Science and Chemical Engineering, Cornell University, Ithaca NY, USA
[2] MPI für Metallforschung, Stuttgart und Institut für Theoretische und Angewandte Physik, Universität , Stuttgart
[3] Cornell High-Energy Synchrotron Source (CHESS), Cornell University, USA
[4] IMFUFA (Department of Mathematics and Physics), Roskilde University, Denmark

Organic, layered structures are used for a number of purposes, such as photonic crystals. In thin, supported films, symmetric diblock copolymers spontaneously form layered structures under certain conditions [1]. Grazing-incidence small-angle X-ray scattering is a convenient tool to study the lamellar structures formed in such films. Even though the X-ray contrast between the blocks is relatively weak, the use of incident angles α_i slightly above the critical angle of total external reflection of the polymer film, α_{cP}, enables one to investigate the internal film structures with high spatial (up to 1000 Å) and temporal resolution (a few seconds, Ref. 2).

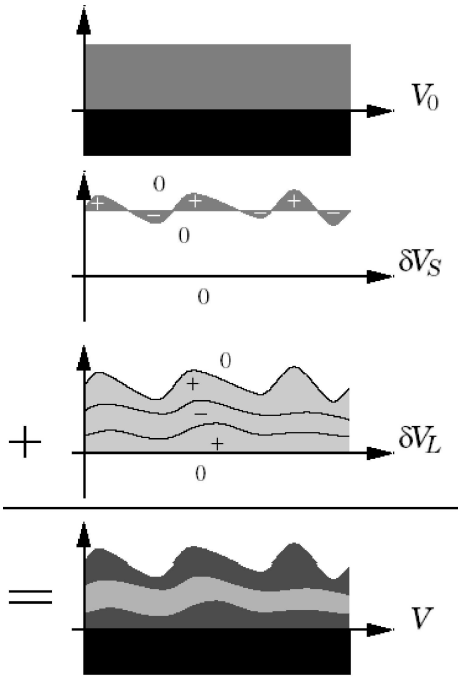

Figure 2.10:
Schematic drawing of the contributions to the sample potential V of a polymer film with lamellae parallel to the substrate: The sum of the potentials of a homogeneous, flat film, V_0, and the perturbation due to a rough film surface, δV_S gives a homogenous rough film. The potential δV_L represents the lamellar structure in the film with rough interfaces. The shades of grey represent different values of the potentials, the darker the higher. Note that the amplitudes of the roughnesses are exaggerated.

For scattering obtained with incident or exit angles close to α_{cP}, a purely kinematic theory such as the Born approximation is not adequate, and rather the distorted-wave Born approximation (DWBA) has to used [3]. The potential describing the sample is split up into (i) the scattering from a homogeneous film with ideal planar interfaces and (ii) the scattering from the internal, lamellar structure (Fig. 2.10). Dynamic effects such as total external reflection, refraction at the film surface and reflections from the substrate are included. We have taken into account the roughness of both the lamellar interfaces and the film surface and have assumed them to be small compared to the lamellar thickness with Gaussian distributions. The lamellar interfaces are furthermore assumed to be perfectly correlated. The in-plane structure of the lamellae (dependent on $q_{||}$) and the information about the stacking of the lamellae (dependent on q_z) factorize, as expected.

We have compared the calculated scattering cross-section with experimental data from poly(styrene-*b*-butadiene) (P(S-*b*-B)) films on Si wafers. 2D images of such films show intensity maxima at $q_{||}$ (Fig. 2.11 a). The intensity profiles along q_z from 2D images, taken at several incident angles, show that the positions of these maxima vary in a well-defined way with α_i (Fig. 2.11 b). They are reproduced by our calculations (Fig. 2.11 c), and we find that the cross-terms involving both scattering and reflection at the substrate surface are essential to describe the experimentally obtained intensity profiles correctly [3]. Thus, GISAXS combined with a quantitative analysis in the framework of the DWBA is a powerful tool to investigate nanostructured polymer films.

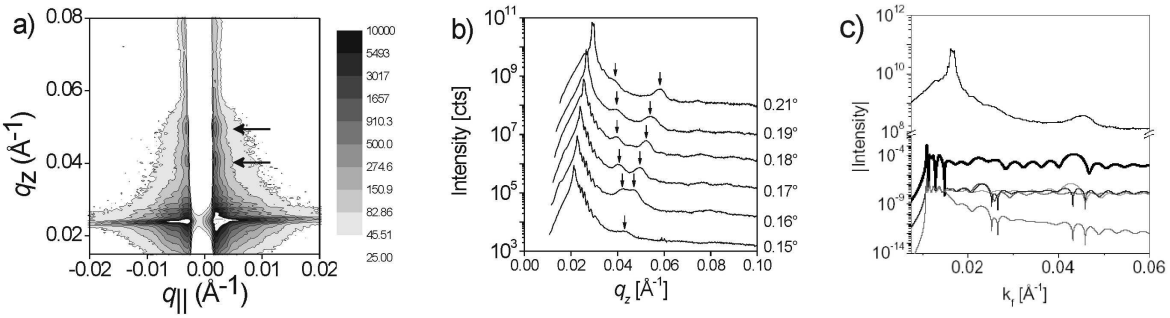

Figure 2.11:
(a) GISAXS map of a lamellar P(S-*b*-B) film with a lamellar thickness of 197 Å and a film thickness of 1570 Å. α_i . °, measuring time 10 sec. The vertical white stripe is due to the beam stop. (b) Integrated intensities over a stripe between $q_{||}$. and +0.005Å^{-1} for the α_i-values given in the right. (c) Comparison of the experimentally obtained intensity profile at α_i . ° (upper line) with the calculated profile (thick line). The experimental profile contains a peak at The lower, thin lines represent the different parts of the calculated profile of the diffuse scattering. As some of them are negative, they cancel each other except at k_f . Å^{-1}. (k_f is the wave vector of the scattered radiation.)

This work was funded by DFG (PA 771/1-1) and by NATO within a Collaborative Linkage Grant (PST.CLG.978046).

[1] P. Busch, D. Posselt, D.-M. Smilgies, B. Rheinländer, F. Kremer, C.M. Papadakis, Macromolecules **36**, 8717 (2003).

[2] D.-M. Smilgies, P. Busch, C.M. Papadakis, D. Posselt, Synchr. Rad. News **15**, 35 (2002).

[3] P. Busch, M. Rauscher, D.-M. Smilgies, D. Posselt, C.M. Papadakis, J. Appl. Cryst., under review.

Transient states during vapor treatment of thin diblock copolymer films: An in-situ GISAXS study

C.M. Papadakis, D. Posselt[1], D.-M. Smilgies[2]

[1] IMFUFA (Department of Mathematics and Physics), Roskilde University, Denmark

[2] Cornell High-Energy Synchrotron Source (CHESS), Cornell University, USA

Diblock copolymers in thin film geometry spontanously self-organize into mesoscopically ordered structures. In order to understand their response to changes in the environment, in-situ and real-time scattering methods are of great value.

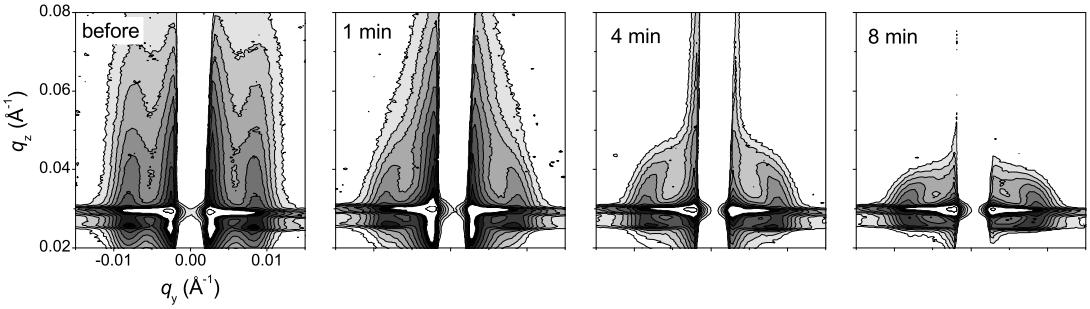

Figure 2.12:
2D GISAXS images of a P(S-*b*-B) diblock copolymer film in the dry state and during vapor treatment with toluene [2]. Initial lamellar thickness 839 Å, incident angle 0.20°.

We have performed time-resolved grazing-incidence small angle X-ray scattering (GISAXS) measurements on thin films of lamellar poly(styrene-*b*-butadiene) (P(S-*b*-B)) diblock copolymers forming lamellae with the lamellar interfaces being initially parallel or perpendicular to the substrate surface [1]. The films were prepared by spin-coating onto Si wafers. We followed their structural changes during treatment with toluene vapor, a good solvent for both blocks. At D-line (CHESS, Cornell University), the measuring times were as short as 10 s, allowing investigations of the structural changes during early stages of film swelling.

We have found that the response to toluene vapor is very different for the two initial lamellar orientations. Films with the perpendicular orientation showed elongated Bragg rods in the dry state (Fig. 2.12). They reacted at once to the vapor treatment, and continuous swelling of the film occurred on the time scale of minutes, which gave rise to the shortening of the Bragg rods along the film normal, q_z. Tilting of lamellar stacks was observed as well, as evidenced from the appearance

of a partial ring of high intensity. However, during drying, the perpendicular orientation was recovered [2].

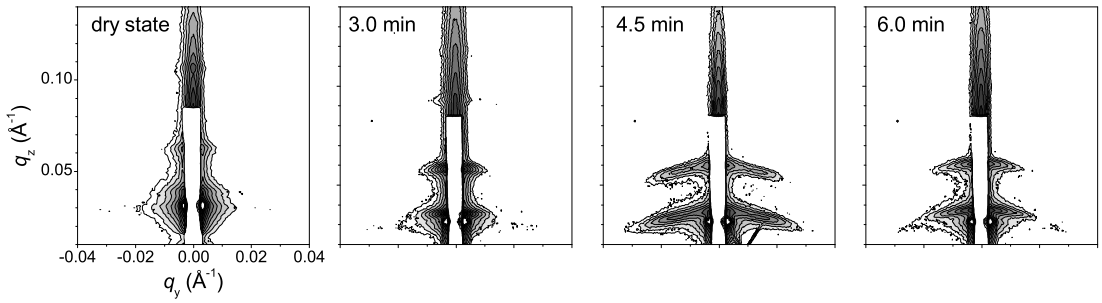

Figure 2.13:
Same as Fig. 2.12, but initial lamellar thickness 189 Å, incident angle 0.22°. The intensity maxima along the film normal q_z are due to the parallel lamellar orientation.

In films with the initially parallel orientation, intensity maxima are observed along the film normal (Fig. 2.12). Their positions are consistent with the ones predicted by DWBA theory for the bulk lamellar thickness [3]. During treament with toluene vapor, the peaks move towards smaller q_z-values, i.e. the lamellae swell. During the first three minutes, the peaks remain only weakly extended along q_y, i.e. the lamellar interfaces remain flat. Afterwards, the peaks start to widen along q_y, which is attributed to undulations of the lamellar interfaces. These undulations, however, diminish again after a few more minutes in the vapor, and the initial lamellar thickness is recovered - even though the film is still in the vapor. These observations point to an instability during the swelling process of the film with initially parallel lamellae.

This work was funded by DFG (PA 771/1-1) and by NATO within a Collaborative Linkage Grant (PST.CLG.978046).

[1] P. Busch, D. Posselt, D.-M. Smilgies, B. Rheinländer, F. Kremer, C.M. Papadakis, Macromolecules **36**, 8717 (2003).

[2] D.-M. Smilgies, P. Busch, C.M. Papadakis, D. Posselt, Synchr. Rad. News **15**, 35 (2002).

[3] P. Busch, M. Rauscher, D.-M. Smilgies, D. Posselt, C.M. Papadakis, J. Appl. Cryst., under review.

Perpendicular lamellae in thin films of high molar mass poly(styrene-*b*-butadiene) diblock copolymers

C.M. Papadakis, P. Michelberger, C. Darko, E. Metwalli, S.V. Roth[1]

[1] Hasylab at DESY, Hamburg

Because of their ability to self-organize laterally on the submicrometer scale, diblock copolymer thin films are good candidates for various applications, such as the formation of nanoporous films. We have found that, under certain conditions, lateral structures are formed spontaneously in thin films of symmetric poly(styrene-*b*-butadiene) (P(S-*b*-B)) diblock copolymers [1,2]. In thin films of a high molar mass copolymer (183 kg/mol) having a bulk lamellar thickness of 839 Å, the lamellar interfaces are perpendicular to the film surface, leading to a meandering lamellar surface texture [1]. This purely perpendicular orientation is only found for film thicknesses below 2300 Å [2]. For a higher film thickness (7400 Å), several lamellar orientations have been found to coexist with the perpendicular orientation, i.e. the bulk limit with randomly oriented lamellar domains is approached. The aim of the present project is to investigate at which film thicknesses P(S-*b*-B) films of high molar mass start to approach the bulk behavior.

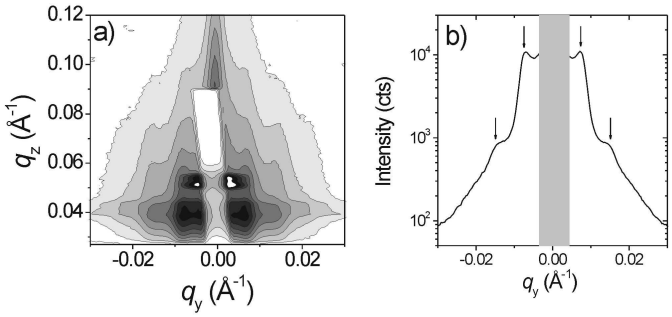

Figure 2.14:
(a) 2D GISAXS map of a thin film of P(S-*b*-B) having 183 kg/mol, a bulk lamellar thickness of 839 Åand a film thickness of 3700 Å. The incident angle was 0.35°. The light stripe in the center is due to the rod-like beam stop. (b) Intensity profile along q_y taken at the q_z-value of the Yoneda peak of the polymer film (0.043 Å^{-1}). The arrows denote the positions of the Bragg peaks expected from the bulk lamellar thickness. The grey rectangle marks the position of the beam stop.

In P(S-*b*-B) films of lower molar mass (13.9-54.5 kg/mol), the lamellae have previously been found to be parallel to the film surface [1,2]. In order to better define the transition between the parallel and the perpendicular orientation, we have here investigated the lamellar orientation of a copolymer with an intermediate molar mass as well (148 kg/mol).

The copolymer films were spin-coated from toluene solution on cleaned Si wafers with a native SiO_x layer and were heat treated under vacuum at 150°C for a few hours. The lamellar orientation was monitored using GISAXS at BW4 (Hasylab, DESY). The lateral structures were further characterized from the intensity profiles along q_y taken at the q_z-value of the Yoneda peak of the polymer film.

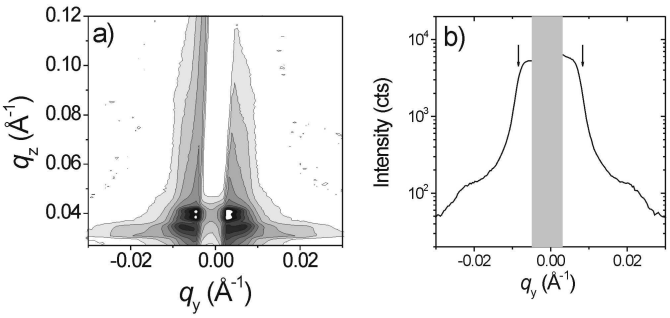

Figure 2.15:
(a) 2D GISAXS map of a thin film of P(S-*b*-B) having 148 kg/mol, a bulk lamellar thickness of 752 Å and a film thickness of 3300 Å. The incident angle was 0.24°. The light region in the center is due to the rod-like beam stop. (b) Intensity profile along q_y taken at the q_z-value of the Yoneda peak of the polymer film. The incident angle was 0.24°.The arrows denote the positions of the Bragg rods expected from the bulk lamellar thickness.

The 2D GISAXS image of a film with a molar mass of 183 kg/mol and a film thickness of 3700 Å shows straight Bragg rods at the q_y-positions expected from the lamellar thickness known from bulk studies (Fig. 2.14 a). No signs of scattering from differently oriented lamellae are present, and we conclude that the purely perpendicular orientation is maintained for this film thickness. The presence of second-order Bragg peaks (Fig. 2.14 b) indicates a high degree of correlation between the lamellar interfaces.

The 2D GISAXS map of a thin film from a P(S-*b*-B) sample of intermediate molar mass (148 kg/mol) and a film thickness of 3300 Å also shows scattering at finite q_y-values (Fig. 2.15 a). However, no distinct peaks are revealed in the intensity profile along q_y (Fig. 2.15 b). This can be understood from the AFM image (not shown) which reveals that instead of long, meandering lamellae, short ellipsoid-like structures are present.

We have thus identified the limits of the perpendicular lamellar orientation for high molar mass P(S-*b*-B) films: For the highest molar mass sample (183 kg/mol), the purely perpendicular lamellar orientation, i.e. laterally structured films, is maintained for film thicknesses as thick as four times the bulk lamellar thickness. The bulk behavior is approached only for higher film thicknesses (7400 Å, Ref. 2). For an intermediate molar mass, the lateral structure consists of short ellipsoids rather than long, meandering lamellae.

This work was funded by DFG (PA 771/1-1) and by NATO within a Collaborative Linkage Grant (PST.CLG.978046).

[1] P. Busch, D. Posselt, D.-M. Smilgies, B. Rheinländer, F. Kremer, C.M. Papadakis, Macromolecules **36**, 8717 (2003).

[2] P. Busch, D. Posselt, D.-M. Smilgies, M. Rauscher, and C.M. Papadakis, in preparation.

Thin films of crystallizable, lamellar diblock copolymers

C. Darko, I. Botiz[1], G. Reiter[1], D.W. Breiby[2], S.V. Roth[3], C.M. Papadakis

[1] Institut de Chimie de Surfaces et Interfaces, CNRS, Mulhouse, France
[2] Danish Polymer Centre, Risø National Laboratory, Roskilde, Denmark
[3] Hasylab at DESY, Hamburg

Diblock copolymers with one crystallizable block can exhibit considerable morphological richness, arising from the two forces which can drive structure development [1]: (i) microphase separation between unlike blocks, which favors the formation of mesoscopic domains (e.g. lamellae), and (ii) crystallization of one block, which favors the formation of alternating armorphous and crystalline layers with the thickness of the latter depending on the degree of chain folding. Another parameter determining structure formation are the mechanical properties of the amorphous block: When the non-crystallizing block is glassy during crystallization, the microphase-separated structure is usually retained, and crystallization proceeds in a confined environment [2]. In contrast, when crystallization takes place above the glass transition temperature of the amorphous block, the two driving forces mentioned above compete, and the resulting mesoscopic structure can differ considerably from that established by microphase separation alone.

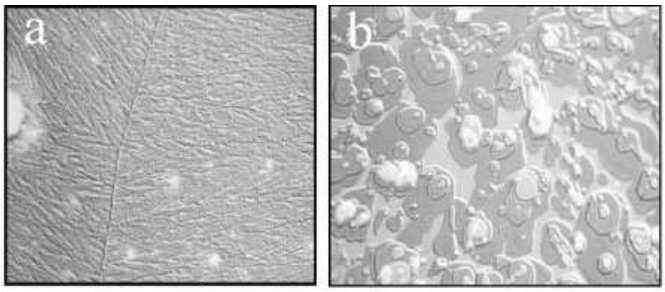

Figure 2.16:
Optical micrographs of thin P(S-*b*-EO) films (Θ μm^2), crystallized at (a) 40°C, and (b) 50°C.

The thin film geometry allows studies of the interplay of microphase separation, crystallization and glass formation, especially of the orientation of the crystallites and of the mesoscopic lamellae with respect to the film surface. We are studying the influence of the crystallization kinetics on the structures by combining grazing-incidence small-angle and wide-angle X-ray scattering (GISAXS and GIWAXS). In this way, we obtain information on the structures of crystallized block copolymer films on a large range of length scales.

The system chosen is lamellae-forming poly(styrene-*b*-(ethylene oxide)) (P(S-*b*-EO)) diblock copolymers with the blocks having molar masses of 3000 g/mol. Samples were prepared by spin-coating from toluene solution onto Si wafers. The crystal growth was monitored in the optical microscope until the entire film was crystallized (Fig. 2.16). It is seen that variation of the crystallization temperature, T_c, has a large effect on the large scale surface topography [3].

GIWAXS and GISAXS experiments were carried out at beamlines BW2 and BW4 at Hasylab. The GIWAXS reciprocal space map of a P(S-*b*-EO) film crystallized at 40°C shows a number of reflections (Fig. 2.17 a). Comparison with the PEO unit cell known from the bulk [4] shows that all reflections can be indexed such that the c-axis and thus the crystal stems are parallel to the film normal. The 2D GISAXS map (Fig. 2.17 b) gives insight into the lamellar orientation.

The peak near q_z = 0.1 Å^{-1} is located at the position expected from a DWBA model for parallel lamellae of thickness 15 nm [5], i.e. the lamellae are parallel to the film surface. The chain stems are thus perpendicular to the lamellar interfaces. The Future work will focus on the influence of the crystallization temperature on the microphase-separated structure in the thin film geometry.

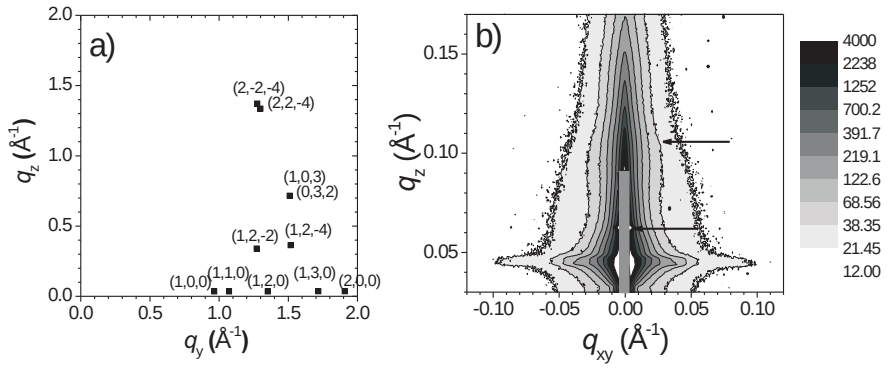

Figure 2.17:
(a) Reflections observed in the GIWAXS experiment as a function of q_{xy} and q_z from a thin film of lamellar P(S-*b*-EO) crystallized at 40°C. The indexing has been made for a crystal orientation with the chain stems parallel to the surface normal. (b) 2D GISAXS map from the same sample, measured at an incident angle α_i = 0.39°. The grey rectangle marks the rod-like beamstop. The lower and the upper arrows indicate the specularly reflected beam and the Bragg peak due to the lamellar structure with a lamellar thickness of 15 nm, respectively.

This project was financially supported by DFG (PA 771/3-2).

[1] I. W. Hamley, Adv. Polym. Sci. **148**, 113 (1999)

[2] L. Zhu, S. Z. D. Cheng, B. H. Calhoun, Q. Ge, R. P. Quirk, E. L. Thomas, B. S. Hsiao, F.-J. Yeh, B. Lotz, J. Am. Chem. Soc. **122**, 5957 (2000)

[3] G. Reiter, L. Vidal, Eur. Phys. J. E **12**, 497 (2003)

[4] Y. Takahashi and H. Takadoro, Macromolecules **6**, 672 (1978)

[5] P. Busch, M. Rauscher, D.-M. Smilgies, D. Posselt, C.M. Papadakis, J. Appl. Cryst., under review.

Structural investigations of recombinant spider silk protein films using grazing-incidence small-angle x-ray scattering

E. Metwalli, U. Slotta[1], T. Scheibel[1], C. M. Papadakis

[1] Lehrstuhl für Biotechnologie, Department Chemie, TU München

Spider silk protein films have a number of potential applications, such as scaffolds for the immobilization of enzymes and as wound dressings [1,2]. Various structural motifs of the spider silk protein including β-sheet, β-turn, α-helix, and spacers play an important role for the overall

physical properties of the protein film [3]. The goal of our work is to investigate the structural and conformational changes of recombinant spider silk protein films which occur upon chemical treatment.

Cloning strategies have recently been used to produce large quantities of recombinant silk-like proteins which closely resemble the natural ones but with the additional possibility to vary the sequence of amino acids [4]. We have used the synthetic spider silk protein derived from the garden spider's (Araneous diadematus) dragline silk protein ADF-4 [4]. The protein films were deposited from hexafluoroisopropanol solutions either by casting or by spin coating onto UV-cleaned transparent quartz plates and silicon wafers. Subsequently, the films were chemically treated with either potassium phosphate or methanol. The protein films before and after the chemical treatments were analyzed using circular dichroism (CD) and grazing-incidence small-angle X-ray scattering (GISAXS). The CD measurements obtained from the as-cast immobilized film reveal that the proteins are rich in α-helices [5]. In contrast, the CD spectrum of the chemically treated film is characteristic of a β-sheet rich structure. The conformational changes of the protein film from α-helix to β-sheet rich structure is paralleled by the transition from water-soluble to water-insoluble film.

We have investigated the protein film structure using GISAXS at beamline BW4 of HASYLAB/DESY. At an incidence angle of 0.39°, a two-dimensional distribution image is obtained using a 2D CCD camera. Figure 2.18 shows the 2D images of protein films cast from 10 % solution onto silicon wafer before and after treatment with methanol.

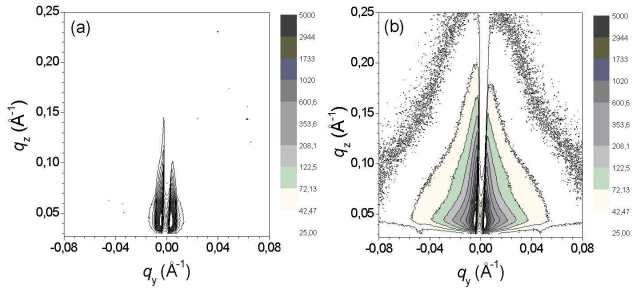

Figure 2.18:
GISAXS images from thin films of spider silk protein on silicon wafers cast from 10 % solution; a) before, b) after treatment with methanol. The vertical stripe in the middle of image is due to the beam stop.

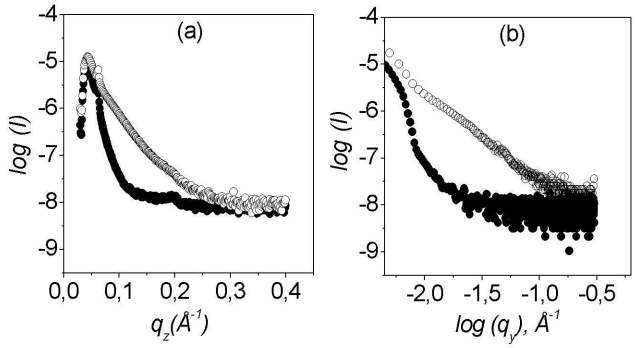

Figure 2.19:
The intensity profiles (a) along q_z, and (b) along q_y for protein films before (²) and after (±) the treatment with methanol.

The images indicate a clear structural variation upon treatment with the scattering being much more significant after the treatment. The structural information along the film normal and in the film plane (Figure 2.19) are obtained by slicing the images in the vertical and horizontal directions, respectively.

These results will be further analyzed in order to extract detailed structural information and to relate to the known conformational changes obtained by CD measurements. In general, we conclude that the structural transformations in the spider silk upon chemical treatment are quite significant. In the future, surface coating chemistry will be used instead of solution treatment to control the conformation perturbation.

This project has been financially supported by the DFG within the SFB 563 'Bioorganic functional systems on solids' (TP A10).

[1] B. Panilaitis et al., Biomaterials **24**, 3079 (2003).
[2] G.G. Altman et al., Biomaterials **24**, 401 (2003).
[3] T. Scheibel, Micro. Cell Fact. **3**, 14 (2004).
[4] D. Huemmerich et al., Biochemistry **43**, 13604 (2004).
[5] D. Huemmerich, U. Slotta, T. Scheibel, Appl. Phys. A, in press (2005).

High-resolution grazing incidence small angle x-ray scattering: Investigation of micrometer sized structured polymer films

P. Müller-Buschbaum, E. Bauer, V. Körstgens, J. Wiedersich [1], S.V. Roth [2], R. Gehrke [2]

[1] TU München, LS Physik Weihenstephan, Freising
[2] HASYLAB, Hamburg

The structure of polymer surfaces and thin polymeric films at the mesoscopic scale is of interest, both for application and basic research [1]. As the size of many technological devices decreases, the natural length scales of many typical polymers such as the radius of gyration, the persistence length, or the domain size in block copolymers, match the feature size and thus the materials are expected to display a new behaviour [2, 3]. On the other hand, the tendency towards spontaneous structure formation may stabilize or even generate morphological features of larger size [4, 5]. As a consequence, the range of interesting polymeric structures starts on the molecular level and extends up to several micrometers. With the ongoing improvement of sample preparation techniques, these structures may extend to macroscopic surface areas of several tens of square centimetres [6]. Along this line of enlarged structured surface areas, very local spatial probes such as atomic force microscopy (AFM) and transmission electron microscopy (TEM) are of less statistical significance. With AFM and TEM only a few exemplary spots of the surface can be probed. The resulting low statistics include the danger of being mislead by an artificial local structure as for example caused by defects. The use of a strongly averaging experimental technique such as scattering is therefore very advantageous [7].

One particular strength of GISAXS is the probing of small sized structures such as micro-phase separation structures in copolymer films. Such molecular structures are easily detected with a relaxed resolution [7]. Following the same principles as in the transmission geometry (SAXS to USAXS) larger length scales may be addressed by an increase in the sample detector distance. In accordance to the transmission this sometimes yields a change in the used abbreviation from GISAX to GIUSAXS (or x-ray reflection ultra small-angle scattering in pioneering work [8]). Highly collimated x-ray beams enable the extension of GISAXS experiments into the high-resolution regime. By making use of the absence of any beamstop, the resolution can be optimised to the

detector pixel size as demonstrated in this investigation. With the ongoing development towards high-resolution set-ups large sized surface structures such as phase separation structures in polymer blend films are improvingly determinable. In addition, this development enables the overlap with optical techniques combined with the very high sensitivity of the grazing incidence geometry. However, the high demand on collimation requires the use of high flux sources of large scale facilities such as special synchrotron radiation beamlines.

The model system used consists of blend films of polystyrene (PS) and poly-n-butylacrylate (PnBA) with molecular weights M_w= 207 k (M_w/M_n= 1.02) and M_w= 260 k (M_w/M_n= 3.78), respectively. Both components were blended in toluene solution at different weight ratios of PS:PnBA= 0.1:9.9 to 9:1 and prepared from solution casting onto pre-cleaned silicon (100) substrates. Varying the solution concentration as well as the amount of solution deposited on the solid support enables the installation of different polymer film thicknesses. The smooth drying process in a special designed sample chamber at ambient conditions results in polymer blend films with marked surface structures due to phase separation (the polymer-polymer interaction parameter of PS and PnBA is 0.162 at 20 ^{o}C). The grazing incidence small angle x-ray scattering (GISAXS) measurements were performed at the BW4 USAX beamline of the DORIS III storage ring at HASYLAB/DESY in Hamburg. The selected wavelength was 0.138 nm. The scattered intensity was recorded with a two dimensional detector which consists of a 2048 £ 2048 pixel array. Due to the sample-detector distance of 12.9 m a high resolution was achieved. The beam divergence in and out of the plane of reflection was set by two entrance cross-slits. At one fixed angle of incident the two-dimensional intensity distribution can be cut in several vertical and horizontal slices with respect to the sample surface. Vertical slices contain mainly scattering information from structures perpendicular to the sample surface, whereas horizontal slices contain only scattering contributions with an in-plane information.

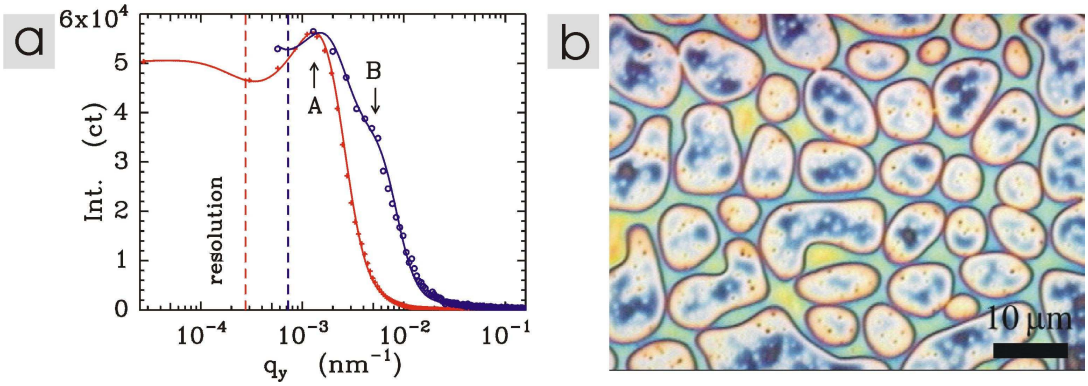

Figure 2.20:
a) Example of blend film sample measured under two different experimental resolution conditions: high resolution set-up (blue open circles) and ultra-high resolution (red crosses). The corresponding resolution limits are marked by vertical lines and the most prominent in-plane length of 4.8 mm is marked by an arrow 'A'. The solid lines are fits based on a model described in the text. b) Corresponding optical micrograph. [9]

In figure 2.20 a GISAXS data measured with the high resolution set-up (blue open circles) are compared with an ultra-high resolution set-up (red crosses). This further increase in resolution marks the actual technical limit with the currently available settings at the BW4 beamline. A further drastic optimisation of the slit settings and the focussing conditions together with a 2

dimensional detector with 78 μm pixel size only are the base of this improvement [9]. The nominal resolution is $\cdot \; q_y \quad . \quad \Theta \quad ^{-4}$ nm^{-1} corresponding to 22 μm maximum real space length. This maximum accessible lateral length scale of this ultra-high resolution set-up has been confirmed by the means of Monte-Carlo ray tracing simulation of the beamline BW4 [10].

The structure shown in figure 2.20 b is close to the resolution limit of the high resolution set-up and easily detected with the improved resolution. The peak in the intensity (marked with A) corresponds to a most prominent in-plane length of 4.8 μm. It should be noted, that without fitting the data with a simple model, just from the position of the peak in the high resolution set up (blue open circles in figure 2.20 a) a smaller length would be determined, due to the influence of the resolution function. Only in case of a clear separation of the resolution peak and the structural peak, such as measured with the ultra-high resolution set-up for this particular example, the peak position directly gives access to the most prominent in-plane length via a simple Bragg-like analysis and without applying a model fit [9].

[1] Fedynyshyn T H, Editor (2002) Advances in Resist Technology and Processing XIX Proceedings of SPIE Vol. 4690

[2] Findenegg G H, Herminghaus S (1997) Curr. Opin. Coll. Int. Sci. 2: 301

[3] Russell T P (2002) Science 297: 964

[4] Geoghegan M, Krausch G (2003) Prog. Polym. Sci. 28: 261

[5] Ryan AJ (2002) Nature Materials 1: 8

[6] Müller-Buschbaum P, Bauer E, Wunnicke O, Stamm M (2005) J. Phys. Condens. Matter 17: S363

[7] Müller-Buschbaum P (2003) Anal. Bioanal. Chem. 376: 3

[8] Müller-Buschbaum P, Casagrande M, Gutmann J, Kuhlmann T, Stamm M, Cunis S, von Krosigk G, Lode U, Gehrke R (1998) Europhys. Lett. 42: 517

[9] Müller-Buschbaum P, at press

[10] Roth SV in preparation

Rearrangement of polymer blend nano-structures by dewetting upon a thick polyimid film

E. Bauer, P. Müller-Buschbaum

The wetting behaviour of thin polymer films is of major interest in technical applications like dielectrics or coatings, as well as in fundamental science [1]. To address transport properties as a function of the substrate we studied the decay of a web-like polymer structure instead of homogeneous films. In more detail, a polymer blend was used in this study to focus on the movement on substrates such as bare silicon, polymer films and polymer brushes. Polymer films with controlled thickness corresponding to the web-like state [2] can be prepared by the spin-coating technique.

In general, different substrates such as silicon wafers, polyimid films and polystyrene brushes are compared, whereas in the present investigation we focus on the polyimid substrates only. These polyimid substrates are prepared on Si (100) wafers which are coated with a polyimid film (PI, PI2611, HD Microsystems). Substrate cleaning was applied before spin-coating the PI film. The spin-coating conditions were optimised to yield PI films with a continuous thickness of 100 nm after heat treatment (different steps up to T = 400 ^{o}C). The investigated polymer blend consists of 10 % polystyrene (PS, with a molecular weight of M_W=27500 g/mol and a narrow weight

distribution M_W /M_N = 1.04) and 90 % brominated polystyrene (PBr_xS, x= 1.09 with a molecular weight of M_W=144600 g/mol and a narrow weight distribution M_W /M_N = 1.04). A toluene based solution was spin-coated upon the PI films. Since the concentration of the blend in toluene is small ($<$1 mg/ml), no homogeneous film can develop, and instead a web-like structure is installed.

At the final preparation step the samples were exposed to toluene vapour for fixed times. A series with different exposure times was performed for each substrate to obtain the different dewetting stages, starting with the web-like structure and ending-up with droplets on the PI surface. Due to the initially prepared concentrations of the blend solution and due to mass conservation, the resulting structures are well below the optical resolution limit. As a consequence, the resulting structures were probed by atomic force microscope (AFM) and by grazing incidence small-angle x-ray scattering (GISAXS) [3]. The GISAXS measurements were performed at the beamline BW4 of HASYLAB/DESY, Hamburg. The wavelength of the incident x-ray beam was 0.138 nm. The samples were placed horizontally in the GISAXS sample chamber at 12.77 m distance from the two-dimensional (2D) MAR CCD (pixel size 79.1 μm, total number of pixels 2048 x 2048). The flight path, including the sample chamber, was evacuated to reduce air scattering. An incident angle of α_i= 0.535 ^{o} above the critical angle of the substrate materials PI, SiOx and Si was selected. The selected α_i yields a compromise between separation of the important scattering features, namely the specular and the Yoneda peak, on the detector and a reasonably high intensity in the Yoneda range. From the 2D intensity distribution typical vertical and horizontal cuts were performed instead of handling the full 2D information. For the position of the horizontal cuts the critical angle of PS (α_c = 0.138 ^{o}) was chosen to probe the structures created by the polymer. Both, the Si substrate as well as the PI film are not effected by annealing under vapour. Compared to the evolving polymeric structures, the PI film and Si are flat.

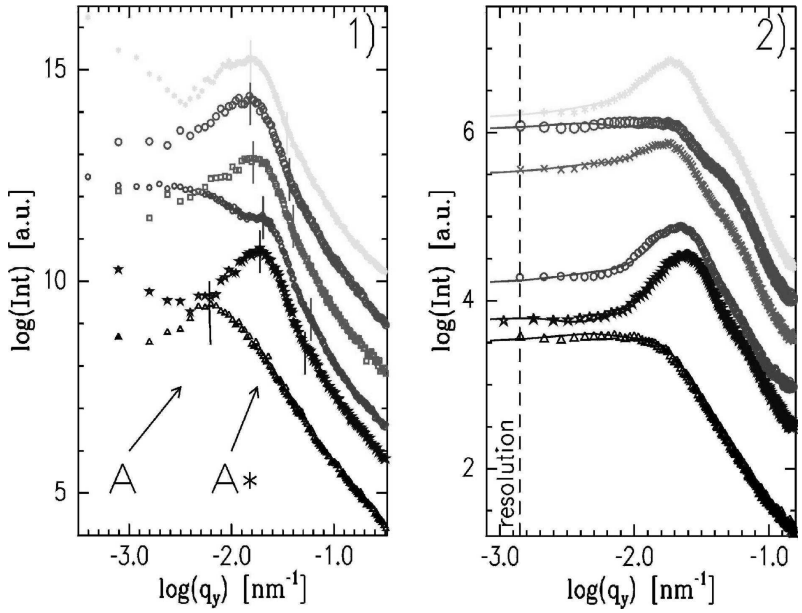

Figure 2.21:
1) PSD-curves calculated from AFM data and 2) horizontal cuts at the critical angle of PS of the GISAXS measurements (symbols) displayed with fitting curves (lines). From bottom to top the vapor exposure time increases from 0 to 38 hours. In each graph the data are shifted vertically for clarity. The broken lines denote the resolution limit of the GISAXS measurements and A and A* together with short vertical lines mark dominant length scales of the PSD-curves respectively. [5]

In general, within this investigation it was observed that the different substrates change the wetting behaviour of the blend film with respect to the kinetics as well as to the equilibrium structure. Time constants as well as final states differ as a function of the substrate. However, all samples show patterns which are attributed to a typical dewetting scenario, starting with the web-like structure, with rims decaying into islands and finally drops after several hours of vapour exposure. Nevertheless, contact angles as well as time scales differ for the decaying process. As an example in figure 2.21 AFM and GISAXS data related to blend structures on PI films are compared in reciprocal space. The AFM data were 2D-Fourier transformed, and the resulting power spectral density functions are displayed after radial averaging. From bottom to top the exposure times increase and equal exposure times are displayed in the same colour. In general, a good agreement between the out-of plane data and the data calculated from the AFM measurements is observed. It has to be noted, that both techniques, GISAXS and AFM strongly differ in the probed surface area (more than a factor of 100), which results in a higher statistical relevance of the GISAXS data [3]. Thus from the good agreement between both we can conclude that the AFM measurements have been representative for the present surface structure and no further internal dominant in-plane structures are present. Therefore the peaks in the displayed data have to be identified with different types of surface features: web-rims and holes, islands with defined size and distance and finally drop diameters and distances.

From the detailed analysis of these lateral lengths, the transported mass is obtained, gaining an insight into the substrate dependence of transport processes [4, 5]. To control transport processes, energetic as well as entropic properties can be varied. A deep understanding taking into account both effects to predict the final states has to be achieved.

This work was financially supported by the DFG in the framework of the SPP 1164 ”Nano- and Microfluidics” (Mu1487/2).

[1] F. Brochard-Wyart, C. Redon, C. Sykes; C.R.Acad.Sci.Ser.2 19, 314 (1992)

[2] T.G. Stange, R. Mathew, D.F. Evans, W.A. Hendrickson; Langmuir 8, 920 (1992)

[3] P. Müller-Buschbaum; Anal. Bioanal. Chem. (2003) 376, 3

[4] P. Müller-Buschbaum; Eur. Phys. J. 12, 443 (2003)

[5] E. Bauer, P. Müller-Buschbaum; to be published

Movement of liquid fronts: Influence of substrate softness

R. Hengstler, E. Bauer, P. Müller-Buschbaum, P. Truman [1], P. Uhlmann [1], M. Stamm [1]

[1] Institut für Polymerforschung, Dresden

Microscopic and nanoscopic flow was investigated on different types of solid supports and with different purposes. One sort of experiments was performed with the aim to investigate the influence of selected boundary conditions on the movement of liquid fronts to reach a deeper understanding of the influence of the selected boundaries on flow at different lengths scales. The second kind of experiments was devoted to the investigation of flow on a microscopic scale on surfaces with gradually changing boundary conditions. These experiments were performed to design an experimental set-up to be able to investigate the movement of liquids and liquid mixtures on surfaces with confinements and variable boundaries. For both sorts of experiments new experimental

tools were developed and both sorts of experiments illuminated the liquid flow on polymer brushes from different points of view giving a complementary picture from the ongoing phenomena.

Non-equilibrium conditions were introduced by the presence of a source or drain of the liquid. Different simple liquids, i.e. solvents such as toluene, ethanol or water and mixtures of those were used to investigate flow on polymer brush surfaces with constant and gradually changing properties. For reference reasons and for adjusting proper and reproducible experimental conditions for the flow, experiments were performed on silicon (Si) substrates covered with a native oxide layer of approximately 1 nm thickness in addition.

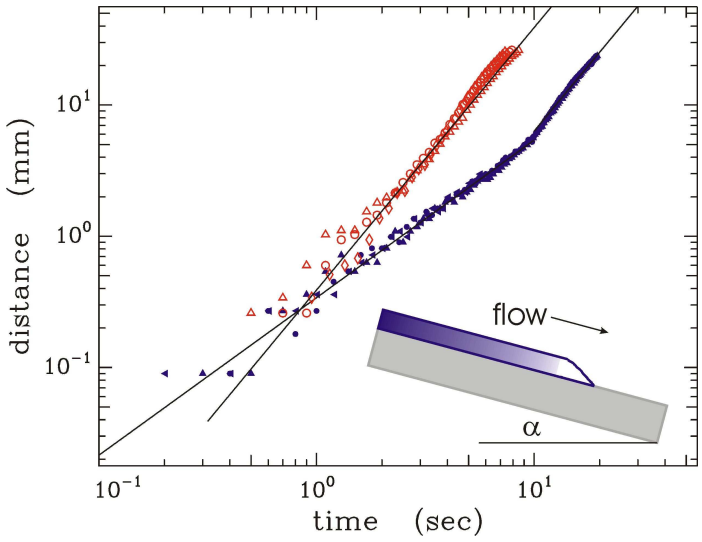

Figure 2.22:
Double logarithmic plot of the distance the toluene in the finger had moved as a function of time. Data were extracted from optical micrographs cut from several real time observation (squares, circles, triangle) of flow on bare Si-SiOx (open symbols) and a grafted PS brush (filled symbols). The solid lines show the power law behaviour and the inserted sketch depicts the experimental geometry.

Experimentally, the flow was observed in real and reciprocal space gaining complementary information. The use of the new flow cell to investigate the movement of solvents at surfaces functionalised with polymer brushes has started. Additionally real space methods (optical and fluorescence microscopy with video system, imaging ellipsometry, IR microscopy) were used to track the movement, anisotropy, composition and thickness of the liquid front in real time. Reciprocal space methods, namely scanning subμ-GISAXS [1] were applied to detect the internal arrangement of the liquid during flow. These type of experiments were very limited in number because they are restricted to synchrotron radiation at one special beamline at the ESRF.

To focus on microscopic flow, a large amount of liquid (volume > 100 μl) was deposited on the solid support. It turned out that flow was introduced by the concept of applying an incline with a higher experimental reproducibility than by successively adding liquid by a micro-syringe. Thus the liquid of choice was deposited on the incline and the forced movement was controlled by the angle of the inclination of the solid support.

Although a liquid rim was deposited on the incline, the liquid front moves non parallel. Irrespective of the special surface chemistry, a liquid finger was developed and most of the liquid volume

flows in this finger downhill. Following the work of Thiele and co-workers the transversal instability of driven advancing and receding contact lines gives rise to front instabilities [2, 3]. From the optical real time observation the movement of this liquid finger was analysed as a function of time. Figure 2.22 shows the distance the toluene had moved as a function of time. Two types of different substrates were compared: The reference bare Si-SiOx (open symbols) and the grafted PS brush (filled symbols) [4].

As visible in figure 2.22 the flow on bare Si-SiOx is quicker as compared to the PS brush. Whereas on the rigid Si surface a power law with an exponent of 2 describes the behaviour in the entire observed time regime, on the soft PS brush this exponent is only valid for the late stages. At the early stages a slower flow with an exponent of 1.2 was fitted to the data. Possibly, the brush has an additional mechanism for energy dissipation, which reduces the velocity of the flowing toluene. In addition, on the brush a very thin precursor film might be present on top of which the macroscopic amount of fluid flows. Along this line, in the first slowed down regime, this precursor film has to be installed.

Investigations on more complicated substrate structures such as channeled substrates and binary brushes are currently in progress.

This work was financially supported by the DFG in the framework of the SPP 1164 "Nano- and Microfluidics" (Mu1487/2).

[1] Müller-Buschbaum P, Roth SV, Burghammer M, Bauer E, Pfister S, David C, Riekel C; Physica B 357, 148 (2005)

[2] Thiele U, Neuffer K, Bestehorn M, Pomeau Y, Velarde GM; Colloids Surf. A (2002) 206, 87-104

[3] Thiele U, Knobloch E; Phys.Fluids (2003) 15, 892-907

[4] Ionov L, Houbenov N, Sidorenko A, Stamm M, Luzinov I, Minko; Langmuir (2004) 20, 9916-9919.

Characterization of conjugated polymer thin films for organic opto-electronics by GISAXS measurements

K. Matoy [1], F. Muller [2], K. Stubenrauch [1], G. Fritz [2], R. Resel [1], P. Müller-Buschbaum

[1] TU Graz, Graz (Austria)

[2] Karl Franzens Universität, Graz (Austria)

Thin films of conjugated polymers attract considerable interest from theoretical and practical points of view due to their industrial applications and the study of fundamental problems in interface science. In order to enhance specific properties and performances, the alignment of the polymer chains relative to a substrate with a thickness from one monolayer (few nanometers) to some microns is needed.

The structure and the inter-chain order (crystalline, semi-crystalline or amorphous structures) within a polymer thin film strongly depend on the film growth, i.e. on the preparation [1, 2]. In order to achieve the optimal design of the films, the link between morphology of the polymers, nature of the substrate and preparation techniques on the local structure and interactions needs to be understood at the fundamental level. This structure-property relationship of thin films made of polymers for organic electronics or optical sensors is not well understood: weak long range order

which hampers a detailed structural characterization, low ionic density, small scattering volume, and in plane geometries have to be considered.

The films need to be located on a solid support which is several orders of magnitude thicker. As a consequence, common small angle x-ray scattering (SAXS) measurements are impossible. The technique which allows and leads to interpretative results is grazing incidence small angle x-ray scattering (GISAXS) [3].

In the present work, we focus on two types of thin films. The first system was based on the semi-crystalline poly[(9, 9-dioctylfluorenyl-2, 7-diyl)-co-(bitiophene)] copolymer (F8T2), adsorbed on a poly(imide) (PI) layer. Thin films with different F8T2 concentrations have been prepared with or without rubbing of the PI layer (the rubbing should induce alignment of the F8T2 chains). The second system was based on poly(norbornene-dicarboxylic acid-dimethylester)-co-(norbornene-dicarboxylic acid) copolymer synthesized via the ROMP technique. Two copolymers with block lengths of 100-100 and 175-75 have been studied. For both systems, the solid support was silicon substrate.

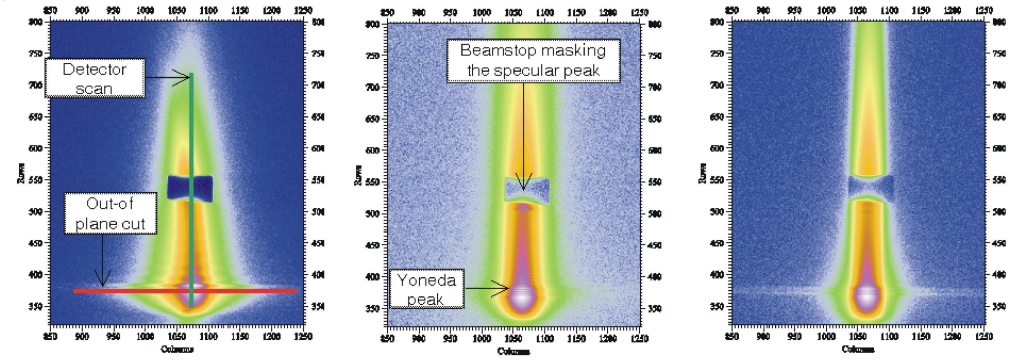

Figure 2.23:
Two dimensional detector pictures as measured for: (left) rubbed-PI, (middle) F8T2, (right) F8T2/rubbed-PI. Shown are raw data without correction for background or detector efficiency.

The GISAXS measurements were performed at the A2 beamline of the DORIS III storage ring at HASYLAB/DESY. For further information of the A2 beamline see [4]. The wavelength was fixed at 0.15 nm and the angle of incidence was set to about 1.6 for all measurements. The two-dimensional MARCCD detector (2048 £ 2048 pixel) was located at 1070 mm behind the sample. In order to reduce the background, the sample-detector path was under vacuum.

We started the experiments by the characterization of the F8T2-PI system. In order to characterize the system, it has been investigated step by step, i.e. PI and rubbed PI on silicon, F8T2 on silicon and so on. In general, two orientations were investigated: parallel and perpendicular to the rubbing direction. The data are still under treatment. Nevertheless, we can already give primary conclusions. Rubbed PI, F8T2, and F8T2-PI films exhibit strong correlations along the vertical detector direction (so called detector scan), as shown in the figure 2.23 by the horizontal fringes between the Yoneda peak and the specular peak. An out-of-plane vertical cut (corresponding to intensity versus q_z at q_y = 0 in the reciprocal space, which is similar to the vertical line in figure 2.23, left) has been performed to determine the correlation length of each film (not shown). No horizontal correlations have been seen for these films (figure 2.23, out-of plane cut on the Yoneda peak, horizontal line, left). This indicates that the films are homogeneous parallel to the surface.

For comparison a second model system, the corresponding asymmetric copolymer (175/25), was investigated. The result corresponds to the scattering of domains randomly oriented on the surface. The symmetric copolymer has been found to have a more pronounced preferred orientation parallel to the surface (result not shown). These results are currently cross-checked with the results obtained by SAXS in solutions and on free standing films.

[1] R. Resel et al., Thin Solid Films 305, 232 (1997)

[2] R. Resel et al., J. Mater. Res. 15, 934 (2000)

[3] P. Müller-Buschbaum et al., Phys. Chem. Chem. Phys. 1, 3857 (1999)

[4] http://www-hasylab.desy.de

Highly ordered biopolymeric nanostructures build from thin Casein films as investigated by GISAXS

P. Müller-Buschbaum, E. Maurer, R. Gebhardt, E. Bauer, W. Doster

Nanostructured polymer surfaces are of strong interest with respect to several applications. Frequently lithographic pattern techniques are utilized. One alternative way to prepare isotropic nanostructures is based on the destabilization of extremely thin initially homogeneous films. Due to mass conservation, both major dewetting processes spinodal decomposition or nucleation and growth, give rise to an increase of the most prominent in-plane length scale with increasing thickness of the initial film. Detailed different routes for the preparation of nanostructured films based on synthetic polymers were established [1]. Within the present investigation, possibilities of expanding these preparation routes towards biopolymers are focused.

As a prominent biopolymer we select casein. Representing about 80 % of milk proteins casein is easily available. The conformation of caseins is much like that of denatured globular proteins. The high number of proline residues in caseins causes particular bending of the protein chain and inhibits the formation of close-packed, ordered secondary structures. Caseins contain no disulfide bonds and are conjugated proteins, most with phosphate group(s) esterified to serine residues. The lack of tertiary structure ensures a certain comparability to synthetic diblock copolymers. The principal casein fractions are alpha(s1)- and alpha(s2)-caseins, beta-casein, and kappa-casein.

Without a tertiary structure there is considerable exposure of hydrophobic residues. This results in strong association reactions of the caseins and renders them insoluble in water. The casein proteins arrange with calcium phosphate into a super-structure known as the casein micelle. Beside the numerous x-ray and neutron scattering experiments [2 and references therein] the micelle substructure is still under debate and different models are discussed in literature. However, with respect to the creation of orders biopolymer nanostructures, the micelle structure itself, given by the size and the distance between micelles, is of primary interest. Due to the typical size of micelles on the order of 100 nm, these experiments addressing the mesoscopic structure require a high resolution. To probe nanostructured films grazing incidence small angle x-ray scattering (GISAXS) offers an opportunity to address large scale structures [3]. In principle, with the present set-ups available at the BW4 USAXS beamline of the DORIS III storage ring at HASYLAB/DESY in Hamburg lengths up to more than 10 micrometers are accessible. This resembles a sufficient resolution to account for highly ordered structures resulting from casein micelles.

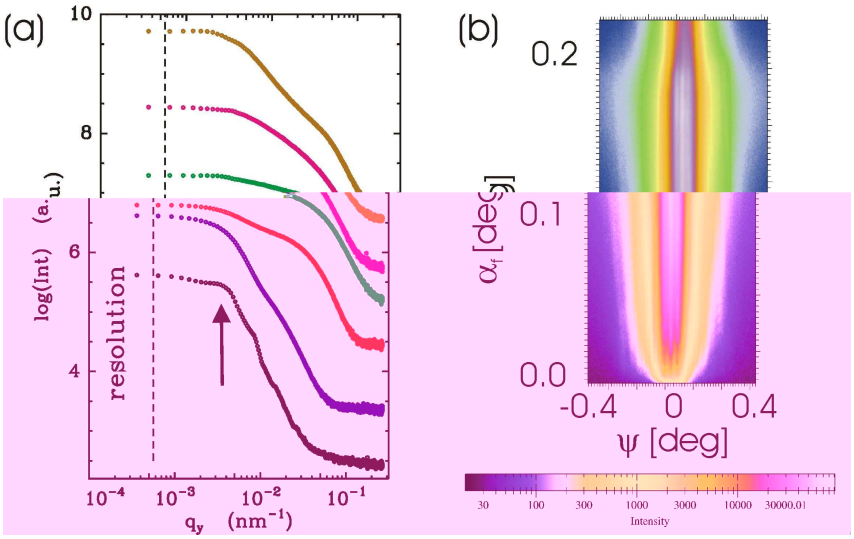

Figure 2.24:
a) Double logarithmic plot of GISAXS cuts (dots) from samples at pH=8.1 with different concentrations used for the spin-coating. From the bottom to the top the concentration increases from 0.32 to 100 g/l in exponential steps. The arrow marks a position of a well pronounced lateral structure. The dashed line indicates the resolution limit. All curves are shifted along the y-axis for clarity. [6] b) 2D intensity zooming in the region of the Yoneda peak from samples at a fixed concentration of 0.32 g/l used for the spin-coating. The intensity is displayed on a logarithmic scale with the given alternating color scale bars.

Extracted casein micelles of a desired concentration were dissolved in purified water. The pH of the solution was adjusted to 8.1. Within a dilution series purified water was added to change the concentration used for the film preparation. Whereas previous investigations showed the rather large polydispersity of the casein micelles in solution and in thin films [4, 5], to enable the creation of ordered structures a reduction of the polydispersity was achieved by centrifuging of the solutions. Casein films were prepared by spin-coating onto pre-cleaned glass slides. The cleaning was performed in base baths yielding a defined surface chemistry. The samples were freshly prepared in advance of the scattering experiment. Dry films were investigated. The GISAXS experiment was performed at a fixed wavelength of 0.138 nm and a sample-detector distance of 12.9 m allow for a high resolution. To check for possible radiation damage, the total counting time was split into smaller slots and the resulting signals were compared. Within the presented concentration and pH range no signature of radiation damage was detected. The scattered intensity was recorded with a two dimensional detector which consists of a 2048 Θ2048 pixel array. At the fixed angle of incidence 0.5174^o the major signals, namely the specular and the Yoneda peak are well separated and enable an easy detection of the GISAXS signal from the 2d intensity distribution via a horizontal cut. The horizontal slice contains only scattering contributions with an in-plane information. Because the flat glass surface gives no contribution with a marked intensity distribution to the diffuse scattering, the probed signal originated from the casein film. In case of c 100 g/l we assume bulk like films.

Figure 2.24 shows the influence of film thickness (concentration of the solution used for the spin-coating) on the resulting scattering pattern. In figure 2.24a from the bottom to the top the concentration increases from 0.32 to 100 g/l at a fixed pH=8.1. In figure 1b the 2D intensity region of the

Yoneda peak for the casein films at $c = 0.32$ g/l is shown to emphasize on the presence of a highly orders surface structure [6]. Clearly in addition to the central intense Yoneda peak, two additional strong peaks located left and right to the central line are visible. In the double logarithmic presentation these maxima collapse into the peak marked with the arrow in figure 2.24a. Moreover, the presence of higher order peaks at larger q_y-values, indicating well defined order, are visible in the logarithmic intensity. At higher concentration the ordering seems to be less pronounced. However, all GISAXS cuts exhibit clear indications of long ranged order. A detailed analysis of the type of structural order is in progress.

[1] P. Müller-Buschbaum, E. Bauer, O. Wunnicke, M. Stamm; J. Phys. Condens. Matter 17, S363 (2005)

[2] C. Holt, C.G. de Kruif, R. Tuinier, P.A. Timmins; Coll. Surf. A (2003) 213, 275

[3] P. Müller-Buschbaum, M. Casagrande, J. Gutmann, T. Kuhlmann, M. Stamm, S. Cunis, G. von Krosigk, U. Lode, R. Gehrke; Europhys. Lett. (1998) 42, 517

[4] R. Gebhardt, W, Doster, U. Kulozik; Brazilian Journal of Medical and Biological Research 38, 1209 (2005)

[5] P. Müller-Buschbaum, R. Gebhardt, E. Maurer, E. Bauer, R. Gehrke, W. Doster; to be published

[6] P. Müller-Buschbaum, R. Gebhardt, E. Maurer, E. Bauer, S.V. Roth, R. Gehrke, W. Doster; to be published

Fast swelling kinetics of thin polystyrene films

P. Müller-Buschbaum, E. Bauer, E. Maurer, R.Cubitt [1]

[1] ILL, Grenoble (France)

In typical applications polymer coatings are subjected to a surrounding atmosphere. The permeability of the polymer-atmosphere interface with respect to small molecules yields an incorporation of molecules from this atmosphere inside the thin polymer film below the glass transition temperature. As a consequence, the polymer film swells with increasing amount of molecules added [1, 2]. Depending on the vapor pressure of the solvent atmosphere and the wetability of the interfaces (substrate-film and film-atmosphere) different morphological scenarios arise as demonstrated in self-consistent field calculations. While these equilibrium structures are well predictable and probed in several experiments, the underlying kinetic evolution driven by the transport of the solvent molecules across the film-atmosphere interface is neither predicted theoretically nor experimentally fully probed [3]. The early stages of this kinetic evolution are focussing within this investigation. For simplicity a homopolymer film is investigated, to rule out more complex phenomena such as phase separation in blend films and micro-phase separation in block copolymer films. Consequently, the general phenomena such as mass uptake and swelling are directly probed. The use of neutron scattering allows for the determination of film thickness, roughness and PSd volume fraction in-situ to the swelling kinetic.

The scattering experiments were carried out at the D17 reflectometer of ILL, Grenoble, in time-of-flight (TOF) mode. TOF allowed for a specular and off-specular reflectivity experiment, in which neutrons with a broad range of wavelength were used simultaneously and registered as a function of their respective times of flight.

The as prepared, dry PSd films were mounted in an own-made vapor chamber. Before starting the swelling experiment, each individual film was measured with a high resolution D17 set-up, yielding the total film thickness, surface roughness (σ_{PSd}= 1.1 nm) and scattering length density ($\rho_{PSd} = 5.96 \cdot 10^{-6}$ Å^{-2}). The vapor chamber was thermostated to 30^o C. The injection of 4 ml protonated toluene marked the start (time t= 0 s) of the kinetic. By installing a relaxed resolution of the D17 (increased projected sector opening of the chopper system and slit opening optimized to a complete illumination of the 70×70 mm^2 surface area) an extremely high time resolution of only 30 s between to successive measurements was reached. The probed q_z range between 0.08 and 0.58 nm^{-1} was optimized to cover the critical edges of protonated (toluene) and deuterated (PSd) substances, thereby allowing for the detection of 3 full fringes of the reflectivity curve of the dry film and nearly four order of magnitude in reflectivity. The swelling experiments were repeated to optimize the time resolution necessary to probe the initial stages and the fast swelling as well as to ensure reproducibility of the reported results. After the ending of the fast swelling (1 hour), the counting time was increased to 600 s to follow the successive slow swelling with improved statistics. After 385 min the kinetic investigation was stopped, because with respect to the fast as well as slow swelling kinetics equilibrium was reached. The vapor chamber was rapidly opened and thus the swollen PSd film quenched to ambient conditions. On significantly larger storage times a second process, the destruction of the highly swollen PSd/toluene film by dewetting would occur. However, after 385 min the quenched PSd film remained homogenous, as neutron reflectivity and optical microscopy have proven. With respect to film thickness and scattering length density the treated films are indistinguishable from the as prepared, dry ones.

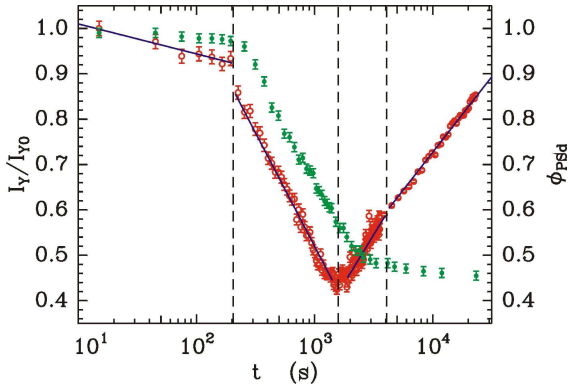

Figure 2.25:
Normalized off-specular intensity I_Y/I_{Y0} (circles) and PSd volume fraction ϕ_{PSd} (dots) as a function of exposure time t: To emphasize on different regimes in the kinetics solid lines with different slopes are fitted to the data. The four regimes are marked by dashed lines.

A more detailed investigation of the time evolution of the swelling induced roughness is accessible from the off-specular reflectivity recorded simultaneously with the specular reflectivity. Because off-specular intensities are significantly less as compared to specular ones, a detailed analysis of intensity as a function of lateral wavevector component q_x is impossible. The necessary improvement of statistics is achieved by an integration of off-specular intensities. To maintain the very high time resolution of the scattering experiment, integration is performed in q-space rather than in the time domain. The Yoneda peak intensity is summed.

When the dry PSd film is exposed to the toluene vapor four different regimes are identified: In the first regime, characterizing the initial stages, the toluene molecules enter into the porous struc-

ture of the polymer and diffuse into all accessible volume (so called mass uptake). As a consequence the PSd volume fraction ϕ_{PSd} is reduced to 0.99 right for the first accessible data point (see fig. 2.25). The total film thickness remains basically unchanged (slight increase of 0.8 nm) because the solvent molecules fill only the available free volume. Accordingly, the normalized off-specular intensity I_Y/I_{Y0} decays slightly, perhaps due to the installation of a thin and smooth toluene layer on top of the PSd surface. However, because PSd is soluble in toluene, there is a strong attractive interaction between both, and the net interaction between the polymer segments is repulsive. As a result, the coiled PSd chains start to swell as soon as they are in contact with the toluene molecules. Due to the fast swelling (second regime) of the PSd film the film thickness increases rapidly, accompanied by a strong decrease of ϕ_{PSd} and I_Y/I_{Y0}. Upon further incorporation of toluene molecules the polymer starts to go into the solvent quite comparable to the early stage of a solution process. Calculated from the fitted scattering length densities, the third regime with the characteristic increase in I_Y/I_{Y0} starts at a PSd volume fraction of approximately 0.56. Due to successive slow swelling the concentration ratio between PSd and toluene is reversed ($\phi_{PSd} < 0.5$). Film thickness and surface roughness of the 'solution' increase. A further roughening of the swollen film at constant film thickness marks the finale stages (fourth regime). At the end of the investigated kinetic the PSd volume fraction has decayed to 0.45. The surface roughness remains smaller as compared to the value of the initial dry film, due to the reduced surface tension of the PSd/toluene 'solution' as compared to pure PSd.

This work was financially supported by the DFG (Mu1487/4).

[1] E. Pitard, J.-P. Bouchaud *Eur. Phys. J. E* **5**, (2001) 133.

[2] A. Singh, M. Mukherjee *Macromolecules* **3**6, (2003) 8728.

[3] D. G. Bucknall, J. S. Higgins, S. A. Butler *J. Polym. Sci. Part B Polym. Phys.* **4**2, (2004) 3267.

[4] P. Müller-Buschbaum, E. Bauer, E. Maurer, R. Cubitt *Physica B* at press

Structural analysis of triblock / diblock copolymer blend films: A comparative study of films obtained by spin-coating and solution casting

V. Körstgens, N. Hermsdorf [1], P. Müller-Buschbaum

[1] Henkel, Düsseldorf

Triblock copolymers are known to adopt nano-separated structures in case of immiscibility of the individual blocks. For the triblock copolymer styrene-isoprene-styrene of different block length highly ordered structures like lamellae, spheres or cylinders have been found. The different morphologies have a great impact on the mechanical properties of these materials [1, 2]. The system under investigation is a blend of styrene-b-isoprene-b-styrene (SIS) triblock copolymer with styrene-b-isoprene-(SI) diblock copolymer. Additional a naphtenic oil and an antioxidant are added components of the mixture. Such a composition may serve as the basis of a model adhesive compound [3]. In that case tackifying components like resins have to be added to introduce tackiness. The pure blend system is close to be non-sticky. The diblock content of the SIS/SI blend is 25 %. The styrene content of the blend is 16 % by weight.

Polymer films were prepared from toluene solution. Glass slides cleaned in an acidic bath were used as substrates. Films were prepared by two different procedures: On the one hand the spin-coating technique was applied and on the other hand films were solution-cast and dried. The

spin-coating technique is an advanced method to obtain homogeneous thin films. The solution-cast method resembles more the way films are obtained in industrial applications, but the preparation of thin homogeneous films is limited. For the solution-cast films polymer blend solution was poured onto the glass slide, until it was fully covered. After evaporation of toluene, films with a thickness of approximately 100 μm remained. These dry films were not fully homogeneous in height, rather they showed some uprisings at the edges of the glass slide due to edge effects. In order to prevent scattering of the incident beam at these uprisings, a small part of the film at one edge of the sample was carefully manually removed using a scalpel. In comparison to the solution-cast films, films obtained with spin-coating technique are markedly thinner and more homogeneous in height.

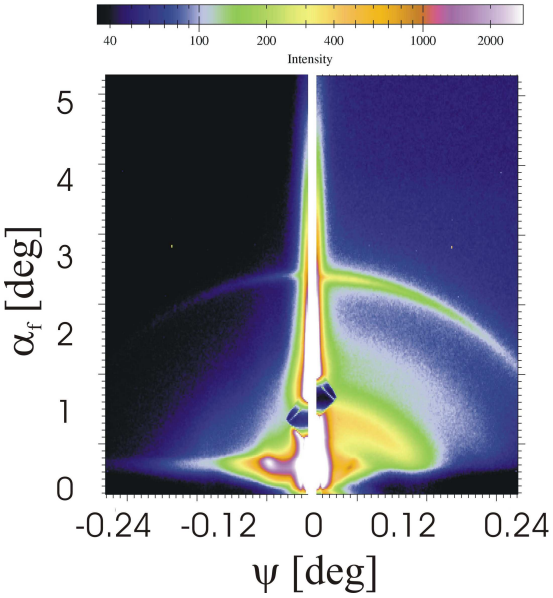

Figure 2.26:
Typical two-dimensional GISAXS scattering pattern measured at BW4: left half displays the scattering probed at the thin spin-coated film and right half the corresponding scattering from the thick solution-cast film. The different positions of the beamstop not have to be mixed with different incident angles, they just result from a minimization of the strong intensity in the central vertical detector lines (to emphasize on the weak diffuse scattering). The colour coding was chosen to emphasize on the features in the diffuse scattering (blue=low and purple=high intensity).

Grazing incidence small angle scattering (GISAXS) has been chosen as it is a non-destructive probe allowing scattering with statistical information not only on the surface illuminated, but also on the bulk sample [4]. The GISAXS measurements were performed at the beamline BW4 of the HASYLAB/DESY in Hamburg. The selected wavelength was 0.138 nm. The beam was focused to the size of 76 $\times$ 40 μm by using an assembly of refractive beryllium lenses. The samples were placed horizontally in the GISAXS sample chamber at 1.114 m distance from the 2D-detector (MARCCD, 2048 $\times$ 2048 pixel). In order to reduce background due to air scattering most of the flight path, including the sample chamber was evacuated. A beam stop was installed for the direct beam. Also a moveable beamstop for shadowing the high intensity specular peak was built in. Moreover, in order to attenuate high intensity, a semi-transparent strip made of steal was fixed to this moveable beamstop. With the semi-transparent set-up allowing higher counting times more information in the out of plane area can be collected, without fully shadowing.

Major goal of the comparison of thin and thick SIS/SI blend films is the separation of bulk and surface structures, which might be difficult from the 2d GISAXS pattern due to the superposition of the bulk and the surface scattering signal. A typical indication of bulk structures with a powder like orientation is the occurrence of ring shaped intensity centered around the direct beam. To illustrate the presence of different scattering contributions from the bulk film and from the film-vacuum surface in figure 2.26 a part of the 2d scattering pattern from the bulk film (right half) is displayed together with the 2d scattering pattern from the thin film (left half). Only the central part close to the Yoneda and the specular peak is displayed for clarity. In the bulk scattering from the solution-cast film two strong ring-segment intensity maxima are present. These are Bragg peaks from the internal ordering of the bulk film. In the scattering from the thin film, these rings are only extremely weak in intensity due to the very limited bulk volume. In contrast, the diffuse scattering from the thin spin-coated film is dominated by the presence of a side maxima close to the Yoneda peak, indicating a highly ordered surface structure. It is also weakly present in the scattering from the thick film.

A detailed data analysis including horizontal cuts at the critical angle of polystyrene is in progress. Furthermore surface sensitive probes such as atomic force microscopy and optical imaging will complement the scattering experiment.

[1] C.C. Honeker, E.L. Thomas; Chem. Mater. 8, 1702 (1996)

[2] Laurer et al., Macromolecules 30, 3938-3941 (1997)

[3] A. Roos, C. Creton, Macromol. Symp. 214, 147-156 (2004)

[4] P. Müller-Buschbaum, Anal. Bioanal. Chem. 376, 3 (2003)

Study of Titania nanodot-arrays

Y. Cheng [1], J. S. Gutmann [1], P. Müller-Buschbaum

[1] Max-Planck Institute for Polymer Research, Mainz

Synthesis and application of anatase nanostructured TiO_2 thin films in dye-sensitized solar cells have attracted both academic and industrial interests because of its exciting performance to convert solar light into electricity [1-3]. The TiO_2 film is used as an electron transport layer in the solar cell device and the efficiency of electron transport is strongly dependent on the morphology of the films because the morphology controls the surface-to-volume ratio, which determines the active-site density on the surface. Furthermore, different morphologies can provide varied charge carrier delocalization routes to influence the electron-hole pair recombination probabilities [4]. Therefore it is very important to prepare TiO_2 thin films with reproducible desired morphologies which are homogeneous over surface areas of cm^2.

In order to prepare TiO_2 films with varied morphologies in a controllable way, we use an amphilic PS-b-PEO as a templating agent and combine it with a so-called good-poor-solvent-pair induced phase separation with inorganic sol-gel chemistry [5, 6]. The block copolymer is first dissolved into a single common solvent, which is good for both hydrophobic and hydrophilic blocks, for example 1,4-dioxane. Afterwards, a sol-gel source of concentrated HCl and Titanium tetraisopropoxide (TTIP) is added into the solution. Because HCl solution and TTIP are poor solvents for the hydrophobic block, a solvent induced phase separation leads to nanoparticle formation upon

film preparation via spin-coating. Nanostructured crystalline TiO_2 films of anatase modification are then obtained through calcination at 400 ^oC in air [7].

To investigate if the nanostructured, ultrathin hybrid titania films exhibit a uniform structure over mm^2 surface areas, we conducted grazing incidence small angle X-ray scattering experiments at the A2 beamline of the HASYLAB. Using a sample detector distance of 1.1 m, a wavelength of 0.15 nm, and a 2D-MarCCD detector, asymmetric surface scattering images were recorded, which exhibited a pronounced structure peak due to inter particle correlations. Figure 2.27 shows a typical AFM image of a vesicular nanodoughnut structure. From the radially averaged power spectral density, the presence of a lateral structure is clearly visible in form of two structure peaks. As the GISAXS image shows similar structure peaks, it is save to conclude that the lateral structure imaged in the AFM experiment, exists over mm^2 sized surface areas as well.

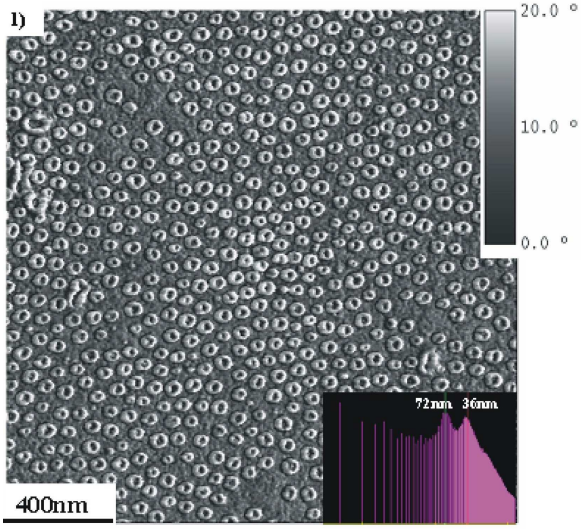

Figure 2.27:
AFM image of the nanodoughnut structure after calcination (inset is the power spectral density profile of the image).

This work was financially supported by the DFG in the framework of the SPP 1181 "Nanoskalige anorganische Materialien durch molekulares Design: neue Werkstoffe für zukunftsweisende Technologien" (Mu1487/5).

[1] Fujishima, A.; Zhang, X. T.; Proc. Japan Acad., 2005, 81, Ser. B, 33-42.

[2] Grätzel, M.; Journal of Photochemistry and Photobiology A: Chemistry, 2004, 164, 3-14.

[3] Coakley, K. M.; McGehee, M. D.; Chem. Mater. 2004, 16, 4533-4542.

[4] Cozolli, P. D.; Kornowski, A; Weller, H.; J. Am. Chem. Soc., 2003, 125, 14539-14548.

[5] Choucair, A.; Eisenberg, A.; Eur. Phys. J. E.; 2003, 10, 37-44.

[6] Soo, P.; Eisenberg, A.; J. Polym. Sci. Part. B: Polym. Phys.; 2004, 42, 923-938.

[7] Y. J. Cheng, J. S. Gutmann, JACS, submitted.

Magnetic nanoparticles in supported diblock copolymer nanostructures: A GISAXS investigation

M. M. Abul Kashem, V. Körstgens, S. Stüber, W. Petry, P. Müller-Buschbaum

Composite materials formed from polymer matrix and metallic or inorganic fillers are of great interest to the scientist since long as the desirable mechanical, electrical and thermal properties can be achieved by using a perfect combination of the type and ratio of matrices and fillers. Nanocomposites, with fillers having dimensions in the nanoscale, are one step ahead. A new class of composite materials can be formed by incorporating magnetic nanoparticles into the template offered by block copolymer nanostructures. These nanostructured templates arise from an interplay of dewetting and micro-phase separation. One very prominent morphology is the lamellar stacking of chemically immiscible polymers by using symmetric diblock copolymers. The nanoparticles distribute themselves inside the layers of the stack due to their selective affinity to one block. This leads to a spatially distributed ordered arrangement of the nanoparticles within the copolymer matrix [1, 2]. Within this investigation, the lateral distribution of nanoparticles in the polymer lamella and the structures formed at the thin polymer film surface coated on a solid silicon substrate were investigated by grazing incidence small angle x-ray scattering (GISAXS). The grazing incidence geometry enhances the surface sensitivity. GISAXS overcomes the limitations of conventional small angle x-ray scattering studies regarding extremely small sample volumes in the thin film geometry [3].

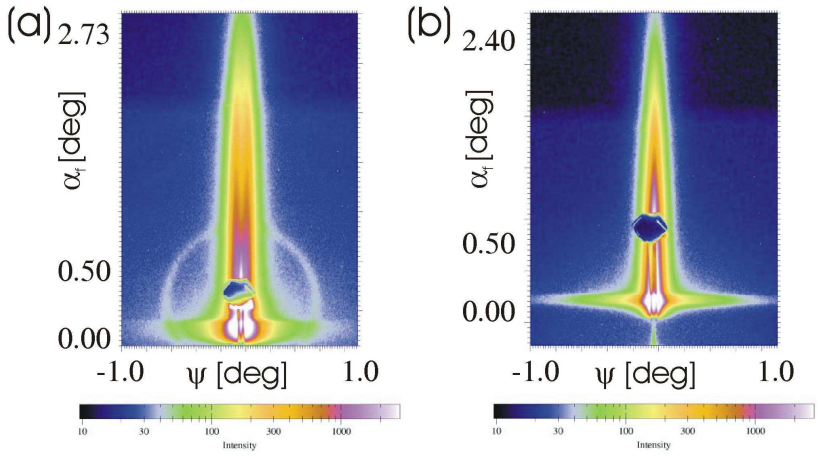

Figure 2.28:
Typical two-dimensional GISAXS scattering pattern measured at BW4: a) Thin and b) thick P(S-b-I) film containing 10 %(wt.) of nanoparticles after annealing. The intensity is shown on a logarithmic scale. The colour coding was chosen to emphasize on the features in the diffuse scattering (blue=low and purple=high intensity).

Magnetic (metal oxide) nanoparticles covered with polystyrene hairs from a-lithium polystyrene sulfonated (LPSS) were used as filler in the di-block copolymer poly(styrene-b-isoprene), denoted

P(S-b-I), matrix. Different solutions of polymer in toluene containing the nanoparticles were used for producing thin film of different thickness on pre-cleaned silicon wafer surface by spin-coating. A total of 24 samples was prepared by varying the film thickness and the amount of the particles. One half of the samples were annealed at 160^{o}C for 12 hours in atmospheric pressure.

GISAXS measurements were carried out at the beamline BW4 of the DORIS III storage ring at HASYLAB (DESY, Hamburg). The selected wavelength was 0.138 nm. The beam divergence in and out of the plane of reflection was set by two entrance cross-slits. The beam was focused to the size of 76 $\times$ 40 μm by using an assembly of refractive beryllium lenses. The sample was placed horizontally on a goniometer. The scattered intensities were recorded by a 2D detector (MARCCD; 2048 $\times$ 2048 pixel) positioned at 1.114 m behind the sample. Most of the flight path of the beam was evacuated to avoid the scattering due to air. A beamstop (a diode) was used to avoid direct beam to the detector. Besides, a moveable beamstop with a semi-transparent tail was also used to decrease the specular peak intensities on detector. At one fixed angle of incident the two-dimensional intensity distribution can be cut in several vertical and horizontal slices with respect to the sample surface. Vertical slices contain mainly scattering information from structures perpendicular to the sample surface, whereas horizontal slices contain only scattering contributions with an in-plane information. Figure 2.28 shows typical two-dimensional GISAXS scattering patterns as measured in case of a samples P(S-b-I) film containing 10 %(wt.) of nanoparticles after annealing. Because an incident angle α_i larger than the critical angle of the polymeric material was chosen, the specular and the diffuse scattering contributions are well separated along the vertical detector direction and thus easily separated. The specular peak is shielded by a beam stop (resulting in a shadow) to protect the array detector, because the specular scattering is orders of magnitude larger compared to the diffuse scattering.

The influences of the film thickness on the 2d scattering pattern is shown in the figure 2.28. At present, it is assumed that the ring of intensity present in figure 2.28a is not produced by the sample. Moreover two different angles of incident were chosen in the experiments related to thin and thick P(S-b-I) films, which results in a shift of the specular peak. Beside these differences in the 2d intensity, clearly several characteristics can be distinguished. The thin film produces a diffuse scattering with relatively broader distribution in the Yoneda peak region and a splitting of the central scattering (observable at exit angles above the specular peak due to the presence of the semi-transparent beamstop). Such a splitting is clear indication of a very well pronounced surface ordering [4]. As the thickness of the film increases the intensity distribution in the Yoneda region becomes narrower and more extended towards larger out-of plane angles Ψ. In addition, the split in the intensity is vanished and thus no highly ordered surface present. It has to be noted, that due to the semi-transparent beamstop, in figure 2.28a the intensity region below the specular peak looks artificially splitted to the left and right as well, which is not present without this special beamstop.

This work was supported by the CompIntnetwork.

[1] V.Lauter-Pasyuk, H.J.Lauter, G.P.Gordeev, P.Müller-Buschbaum, B.P.Toperverg, M.Jernenkov, W.Petry; Langmuir 19, 7783 (2003)

[2] V.Lauter-Pasyuk, H.Lauter, G.Gordeev, P.Müller-Buschbaum, B.P.Toperverg, W.Petry, M.Jernenkov, A.Petrenko, V.Aksenov; Physica B 350, e939 (2004)

[3] P. Müller-Buschbaum; Anal. Bioanal. Chem. (2003) 376, 3

[4] R. Lazzari; Appl. Cryst. (2002) 35, 406

Nanocomposite films: changes of the lamellar period by nanoparticles

V. Lauter-Pasyuk, H. Lauter, M. Jernenkov, P. Müller-Buschbaum, W. Petry

Via the self-organization process we produce nano-composite lamellar films with high volume fraction of nanoparticles. We used symmetric poly(styrene-deuterated-block-butylmethacrylate), denoted P(Sd7-b-BMA) (or A-B copolymer), diblock copolymer films and Fe_3O_4 nano-particles. Nanoparticles, coated with short polystyrene chains, self-assemble during the annealing within the multilayer lamellar structure of the film. The presence of the nanopartcles changes the morphology of the multilayer by changing the interfacial structure and the lamellar period. Considerable effort has been devoted to theoretical and computer simulation studies of the structure of composite films. Previous computational investigations have focused not only on the transitions between the many ordered structures [1], but also on the lamellar structural spacing [2, 3]. Recent model calculations of symmetric block copolymer/nanoparticle composites [4] performed in the frame of discontinuous molecular dynamics showed that neutral nanoparticles decrease the periodic spacing, while nanoparticles with preference for domain A increase the periodic spacing. It was obtained that the increasing period is caused by the swelling of domain A by the nanoparticles but is partially counterbalanced by a contraction of domain B.

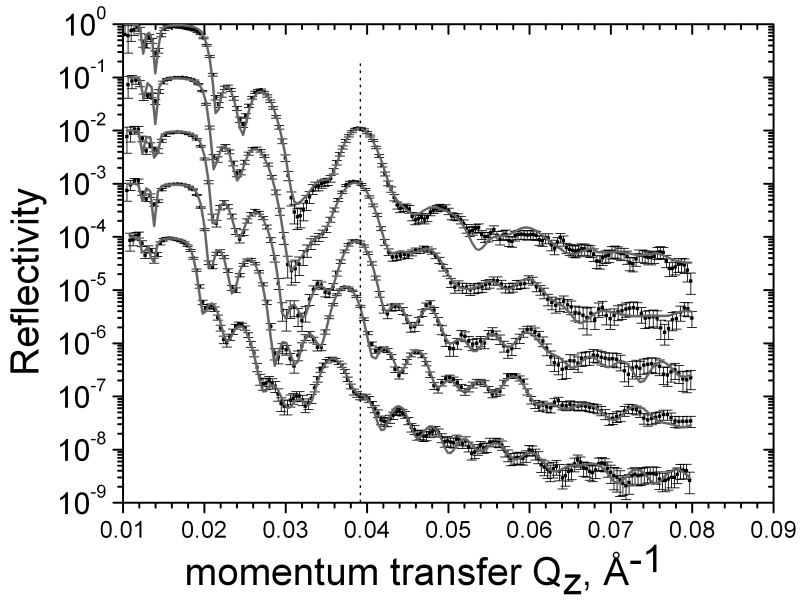

Figure 2.29:
Experimental (filled circles) and fitted (solid lines) reflectivity profiles for samples with different volume fractions of nanoparticles

For the synthesis of highly organized composite materials, it is important to control the modification of the structure of the host matrix due to the presence of nano-particles. We investigated the change in the lamellar period with neutron reflectometry. Deuteration of selected blocks of copolymer chains provides a big contrast and consequently high neutron sensitivity to the modification of buried copolymer interfaces and individual lamellar thickness, lateral and transverse conformity of roughness and distribution of nano-particles within the lamellae. Composite films were obtained

via spin-coating of a toluene solution of the P(Sd7-b-BMA) copolymer with a molecular weight M_w = 187000 g/mol and of PS-coated nano-particles with different volume fractions. During the subsequent annealing the diblock copolymer films spontaneously self-assemble into lamellar multilayers and order the coated nano-particles in a periodic lamellar structure. The evolution of the reflectivity profiles for samples with different volume fraction v_f of nano-particles is shown in figure 2.29. In all reflectivity curves the presence of Bragg reflections indicates the repeating lamellar structure parallel to the film surface. In addition, the Bragg peaks shift to smaller values of momentum transfer with increasing particle volume fraction due to increasing the thickness of the periodic structure L. The transverse structure of the composite films is obtained after the fit to the data. The high contrast in the neutron scattering length densities (NSLD) between deuterated PS and non-deuterated PBMA lamellae allows to quantify the thickness of the individual lamellae. Figure 2.30 shows the lamellar thickness as a function of v_f . We obtained that the period L increases linear with particles volume fraction v_f due to a swelling of the PS layers, while the width of PBMA layers stays unchanged.

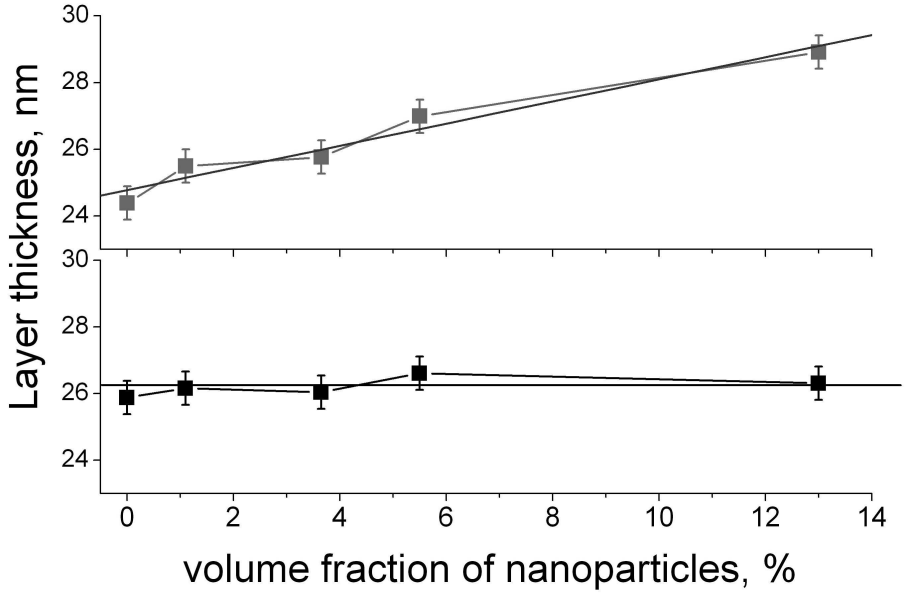

Figure 2.30:
Thickness of PS (upper part) and PBMA (lower part) layers as a function of the volume fraction of nanoparticles.

This work was financially supported by the BMBF (grant 03DU03MU).

[1] G. Besold et al. Comput. Phys. Commun, 122, 542, 1999

[2] R.G.Larson, Macromolecules 27, 4198, 1994

[3] M.Murat et al.,Macromolecules 32, 595, 1999

[4] A.J.Schultz et al., Macromolecules 38, 3007, 2005

3 Dynamics of Melts and Liquids

Inelastic Neutron Scattering on AlNi Melts

S. Stüber, S. Mavila Chathoth and A. Meyer

Continuing the previous work on AlNi melts [1,2], we performed inelastic neutron scattering (INS) measurements on Al_4Ni samples with two isotopic compositions. An alloy with natural Ni isotopic composition was compared to a ^{58}Ni enriched sample. The experiments were performed at the new time-of-flight instrument ToF-ToF at the FRM-II, yielding a high flux and an exceptionally good signal-to-noise ratio.

AlNi melts exhibit a chemical short range order (CSRO) at an intermediate length scale of $q \approx 1.8$ Å^{-1}. They also show a strong non-linear behaviour of the Ni self-diffusion coefficients as a function of composition [1]. In a first step to deriving the partial structure factors S_{nn}, S_{nc}, and S_{cc}, we measured Al_4Ni with two different isotopic compositions for Ni: natural abundance and a ^{58}Ni enriched alloy. The alloys were prepared from a mixture of pure elements by arc melting in Argon atmosphere. For the INS, the alloys were melted into double-walled Al_2O_3 hollow cylindrical cells (wall thickness each 0.5 mm), resulting in a sample with 22 mm outer diameter and 1.2 mm wall thickness. At the time-of-flight spectrometer we used an incident wavelength $\lambda = 5.1$ Å, resulting in an elastic q range from 0.4 to 2.0 Å^{-1}. For the chosen geometry, scattering at the sample is less than 5 %, therefore multiple scattering should be negligible for $q > 0.6$ Å. Each alloy was measured at 1350 K, complemented by measurements of the empty oven, an empty Al_2O_3 cell and a Vanadium standard. Fig. 3.1 shows the intensity signal of the samples compared to empty cell and empty oven, normalized to Vanadium, note the very convincing signal-to-noise ratio.

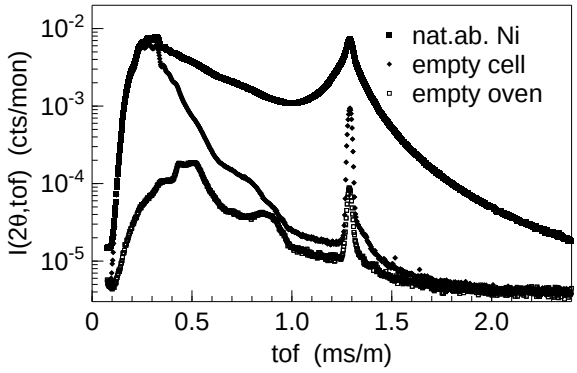

Figure 3.1:
Intensity vs. time of flight for the two samples (natural Ni composition and ^{58}Ni enriched), and the background (empty sample cell and empty oven). Even for large time-of-flights, the signal is more than one order of magnitude above the background.

For data analysis, the scattering of aluminum can be neglected, as our q range was far below its first structure factor maximum, and the incoherent scattering length of Al is reasonably small. Ni in natural isotopic composition scatters strongly incoherently, and with the same argument concerning the q range, we can treat the natural Ni signal as indication of the self-correlation. The ^{58}Ni sample is a coherent scatterer, the signal containing both self and distinct correlation.

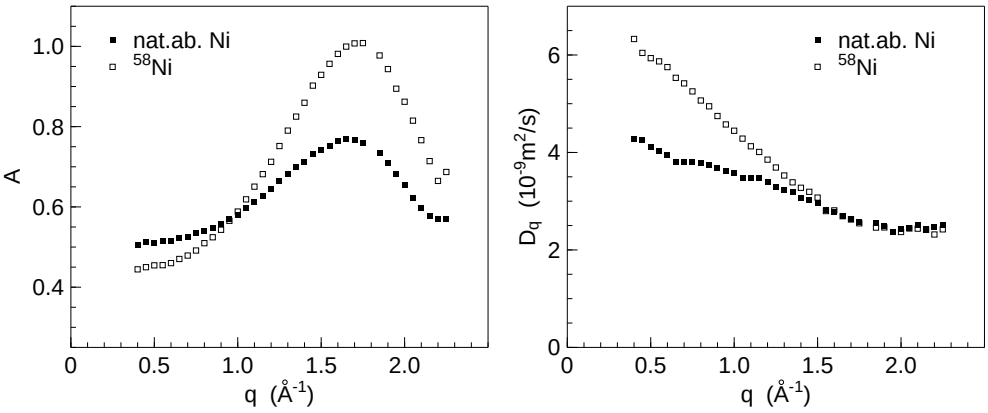

Figure 3.2:
Left: Area of the quasielastic line by scaled Lorentz fit, corresponding to the quasielastic structure factor of the two Ni compositions. Both samples exhibit a prepeak at $q \approx 1.7\text{Å}^{-1}$. Right: q dependent diffusivity coefficient $D(q)$ for Al_4Ni, natural abundance, and $Al_4{}^{58}Ni$.

The focus of data treatment was on the broadening of the quasielastic line. The data were normalized to Vanadium and corrected for self absorption and container scattering, then interpolated to constant q and symmetrized with respect to energy with the detailed balance factor. The resulting $S(q, \omega)$ was fitted with a scaled Lorentzian convoluted with the resolution given by the Vanadium measurement. The scaling factor of the Lorentzian gives the area of the quasielastic line, corresponding to the quasielastic structure factor, shown in fig. 3.2. A prepeak in the structure factor shows up at $q \approx 1.7$ Å^{-1}. For the Al_4Ni alloy with natural Ni isotopic composition, one can discern the contribution from incoherent scattering and the lower intensity of coherent scattering.

The inverse of the FWHM of the Lorentzian in energy and space corresponds to the mean relaxation time τ. For $q \to 0$ (hydrodynamic limit), τ should be indirectly proportional to q^2. Out of this proportionality, we can define the diffusivity $D = 1/(\tau q^2)$, plotted in fig. 3.2. The mainly incoherent signal of the sample with natural Ni isotopic composition should extrapolate to the known value of Ni self diffusion in Al_4Ni with $D = 3.8 \times 10^{-9}\text{m}^2\text{s}^{-1}$[1], the increase in $D(q)$ below $q \approx 0.6$ Å^{-1} is presumably caused by multiple scattering. The equal values for $D(q > 1.5\text{Å}^{-1})$ for Al_4Ni, natural abundance, and $Al_4{}^{58}Ni$ are interesting, because one would expect a behavior in phase with A of fig. 3.1.

In contrast to existing work covering the whole q range [3], our experiments focus on wavenumbers in the range of the structure factor prepeak with unprecedented data quality. Additional measurements on a third Ni isotopic composition, namely $Al_4{}^{60}Ni$, will enable us to determine all three partial structure factors, and to investigate the diffusion mechanism in the Al_4Ni melt in broad detail. The experimental results are also continously compared with Molecular Dynamics computer simulations.

In addition we are preparing container-free measurements using a levitation technique, which will open new q and temperature ranges.

[1] S. K. Das, J. Horbach, M. M. Koza, S. Mavila Chathoth, A. Meyer, Appl. Phys. Lett. **86**, 011918 (2005)

[2] S. Mavila Chathoth, PhD thesis, TU München, 2005

[3] M. Maret, T. Pomme, A. Pasturel and P. Chieux, Phys. Rev. B **42**, 1598 (1990)

Mechanism of Ionic Transport in Viscous Sodium Borate Melts

A. Meyer, F. Kargl, E. Longueteau and T. Unruh[1]

[1] Forschungsneutronenquelle Heinz-Meier-Leibnitz, Garching

We investigate the atomic motion in multicomponent oxidic melts with inelastic neutron scattering and dynamic light scattering in order to clarify the microscopic transport mechanisms. The high-resolution energy and momentum information emerging from inelastic neutron scattering experiments allows to study the interplay between structure, viscous flow and the atomic diffusion of particular components. In this context sodium borates are binary systems in the sense that long range atomic transport of sodium is faster by orders of magnitude as compared to the transport of the boron and oxygen atoms.

In multicomponent hard sphere like viscous metallic melts, where diffusion coefficients of the various components exhibit similar values above T_c, the relaxational dynamics is in quantitative agreement with the universal mode coupling scaling functions [1] and mixing effects only play a minor role for the mass transport [2]. In sodium borates the time scales for the Na α relaxation and the B-O network structural relaxation are separated. We used inelastic neutron scattering and dynamic light scattering to investigate the fast MCT β relaxation regime in sodium diborate and sodium tetra borate in order to address the question how far the relaxational dynamics in such a system can be described with universal mode coupling scaling functions.

In the low q-region incoherent neutron scattering on sodium is the dominant contribution to the signal, whereas around the first sharp diffraction peak at $q \approx 1.5$ Å^{-1} coherent scattering on B and O dominates. Therefore, the q dependence of amplitude and time scale of a fast β relaxation process should display the coupling to the two distinct α relaxation processes. The dynamic susceptibility measured with depolarized light scattering does apparently not couple to the relaxational dynamics of the Na ions and does therefore only contain information on the B-O network relaxations.

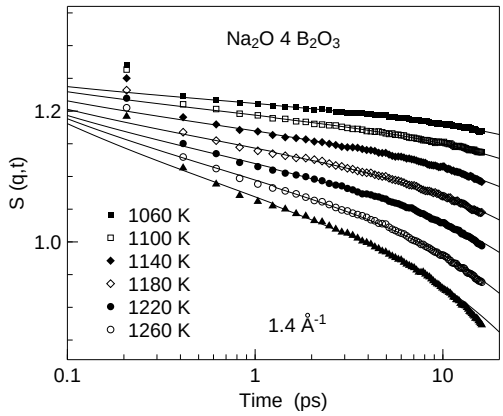

Figure 3.3:
Density correlation function of a viscous sodium tetra borate melt obtained by quasielastic neutron scattering. The lines are fits with the β scaling function of mode coupling theory.

Figure 3.3 shows density correlation functions obtained from quasielastic neutron scattering on the neutron time-of-flight spectrometer ToF-ToF of the new TU neutron source in Munich. The lines

are fits with the mode coupling β scaling law. The full set of data can consistently be described with a temperature and q independent line shape parameter λ and a q independent cross over time t_σ as found in one component viscous liquids. The amplitude h_q of the fast relaxation is found to be in phase with static structure factor for all q. h_q^2 plotted as a function of temperature extrapolates to one T_c value for all q.

Since toward small q the signal is dominated by incoherent scattering on the sodium atoms, the q dependence of the amplitude h_q shows that sodium contributes to the fast relaxation process. Therefore, the Na ion diffusion in sodium borates is prepared by a fast MCT β relaxation process. This conclusion is supported by the light scattering results: The susceptibility spectra do not exhibit a strong signal around the susceptibility minimum. As found in pure boron oxide [3] the contribution of the B-O network to the fast β relaxation as compared to the signal of the Boson peak is rather weak.

[1] A. Meyer, Phys. Rev. B **66**, 134205 (2002).

[2] S. Mavila Chathoth, A. Meyer, H. Schober, F. Juranyi, Appl. Phys. Lett. **85**, 4881 (2004).

[3] A. Brodin et al, Phys. Rev. B **53**, 11511 (1996).

Spin-Spin correlations and Fe-Fe structure factor in x Na_2O: y Fe_2O_3:z SiO_2

F. Kargl, A. Meyer, and M. M. Koza[1]

[1] Institut Laue-Langevin, Grenoble, Frankreich

In recent years we investigated the dynamics and structure of binary alkali silicates. We contributed to the solution of outstanding questions as the microscopic mechanism of fast ion diffusion and the non linear dependence of viscosity on alkali concentration.

Extensive analysis was performed on silicate melts varying the modifier species and concentration. A prepeak was revealed in the elastic structure factor that is a signature of alkali diffusion channels embedded in the static structure [1,2]. This finding is supported by the results on the microscopic dynamics. Only the self correlation of the alkali ions leads to a decay in the density correlation function on a 10 picosecond timescale. The coherent correlators of the alkali modifier ions and the Si-O network decay on longer timescales. The latter was already proposed by molecular dynamics (MD) simulations performed on a sodium disilicate melt [4] and confirmed by our neutron scattering experiments.

An important question was always to reveal partial structure factors of the various components that can be compared to MD simulation data. However, the full set of the six partial structure factors for the binary alkali silicate melts cannot be provided by experiments up to now.

To provide a more general picture of the dynamics and structure in silicate melts the influence of a second network forming component Al_2O_3 on melt structure and Na motion was investigated [3]. The results showed a disruption of the network of Na diffusion channels by adding Al_2O_3 to a binary sodium silicate melt.

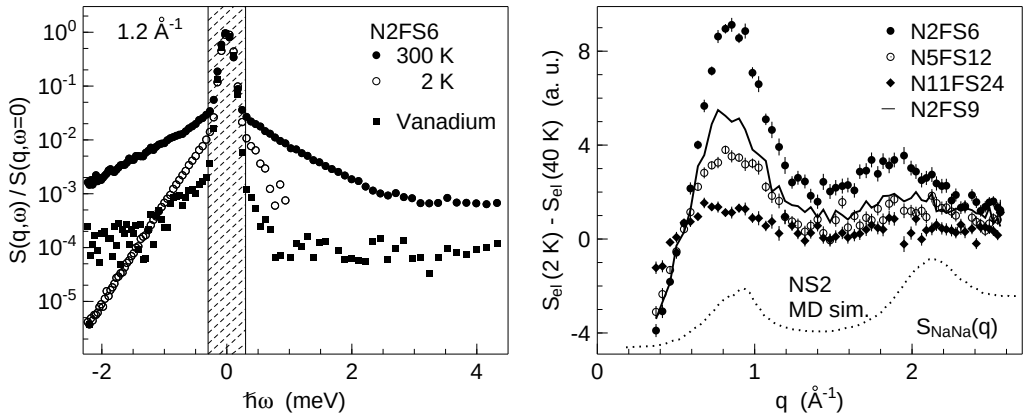

Figure 3.4:
Left: Scattering law of N2FS6 and Vanadium normalized to unity for $\hbar\omega = 0$ meV. Diffuse scattering contributes to scattering on N2FS6. Right: Difference structure factor. Fe-Fe correlation shows a peak around 0.9 Å^{-1} at the position of the prepeak in binary sodium silicate melts independent on total Fe concentration. The partial MD structure factor of $Na_2O\,2\,SiO_2$ is shown for comparison.

The aim was to gain access to the structure factor of the network forming ions. Magnetic scattering turns out to be a highly valuable method in deriving a partial structure factor for the ions of the additional network former. For that purpose Fe_2O_3 was added to a binary sodium silicate melt yielding four samples $2\,Na_2O$-Fe_2O_3-$6\,SiO_2$ (N2FS6), $5\,Na_2O$-Fe_2O_3-$12\,SiO_2$ (N5FS12), $11\,Na_2O$-Fe_2O_3-$24\,SiO_2$ (N11FS24), and $2\,Na_2O$-Fe_2O_3-$9\,SiO_2$ (N2FS9).

The samples were synthesized under air leading to iron predominantly built into the glass structure as Fe^{3+}. Mößbauer investigations on the synthesized glasses revealed a Fe^{3+} fraction larger than 95%.

Fe belongs to the group of elements with 3-d electron shells. Fe^{3+} has electron spin $S = 5/2$. At room temperature and down to about 40 K paramagnetic behavior is observed by means of magnetic susceptibility measurements. A Curie Weiss fit to the data results in a negative Curie temperature indicating predominantely anti-ferromagnetic exchange of the electron spins. Below 40 K a strong increase in the susceptibility is observed characteristic for ferrimagnetic behavior.

The scattering law accessed by means of time-of-flight spectroscopy using the instrument IN6 of the ILL features a broad diffuse magnetic scattering contribution (s. Figure 3.4 left). The measurements were performed on glass disks using the 4.1 Å incoming wavelength setup of the IN6. Measurements were performed at ambient temperature, 40 K and 2 K by using a standard Orange Cryostat. Data correction consisted of standard procedures as normalization to Vanadium, correction for background and self absorption, interpolation to constant wavenumbers and correction for detailed balance.

Below about 20 K spin dynamics is slowing down. Elastic structure factors were derived for the different temperatures integrating the scattering law in the range of the instrumental energy resolution (s. shaded area in Figure 3.4 left). Lowering the temperature from 40 K to 2 K additional intensity is observed in the obtained elastic structure factors around 0.9 Å^{-1} indicating the emergence of correlations that reflect ordering of the magnetic moments.

To separate nuclear from magnetic contributions the difference of the 2 K and the 40 K elastic structure factors was calculated. Between 40 K and 2 K changes in the Debye-Waller factor accounting for vibrational motion of the nuclei can be safely neglected.

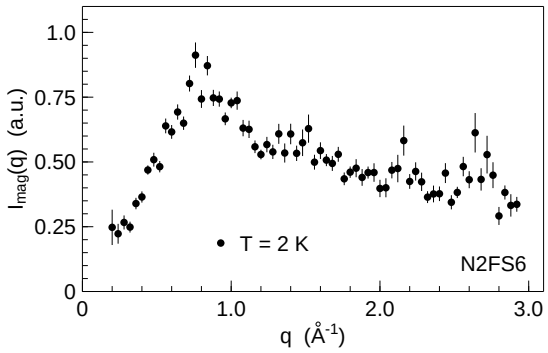

Figure 3.5:
Magnetic contribution to the structure factor measured on D7. The data was obtained by means of polarization analysis.

The difference data features a peak in the Fe-Fe correlation around 0.9 Å^{-1} that is at the position of the prepeak in the binary silicate melts. The position of this Fe-Fe correlation peak is independent of the total Fe concentration, whereas its height scales with the total Fe^{3+} content. The latter is similar to the behaviour of the prepeak in the binary sodium silicate melts. Consequently Fe^{3+} is inhomogeneously distributed in the iron bearing silicate glasses.

In order to justify the analysis of the data determining the Fe-Fe correlation by means of subtraction of elastic structure factors of a time-of-flight experiment a neutron diffraction experiment using polarization analysis was performed on the D7 spectrometer of the ILL on N2FS6 (see Figure 3.5). Polarization analysis allows to only determine the magnetic contribution to the scattering. The obtained magnetic structure factor compares well to the time-of-flight data. However, the statistical data quality is worse owing to the lower neutron flux.

[1] A. Meyer, J. Horbach, W. Kob, F. Kargl, H. Schober, Phys. Rev. Lett. **93**, 027801 (2004).

[2] F. Kargl, A. Meyer, M.M. Koza, H. Schober, Phys. Rev. B, (submitted).

[3] F. Kargl, A. Meyer, Chem. Geol. **213**, 163 (2004).

[4] J. Horbach, W. Kob, K. Binder, Phys. Rev. Lett. **88**, 125502 (2002).

Mixed alkali silicate melts: structure and microscopic dynamics

F. Kargl, A. Meyer, and M. M. Koza[1]

[1] Institut Laue-Langevin, Grenoble, Frankreich

Ion dynamics and microscopic structure of binary silicate melts was investigated by means of quasielastic neutron scattering. The fast alkali ion conduction decoupled even in the melt by orders of magnitude of the network relaxation was explained by a network of alkali diffusion channels embedded in the static structure [1,2].

Here we report on the impact of the addition of a second network modifier potassium oxide to a binary sodium silicate melt on structure and ion dynamics. The investigations were performed on two ternary melts comprising equal amounts of Na_2O and K_2O at 66 mol% and 75 mol% total SiO_2 content, respectively. For the measurements on $Na_2O\,K_2O\,4SiO_2$ (NKS4) and $Na_2O\,K_2O\,6SiO_2$ (NKS6) the time-of-flight spectrometer IN6 with an incoming neutron wavelength of 5.9 Å was used. The data was normalized to a Vanadium standard, corrected for background, empty can

scattering and self absorption. The scattering law was obtained by means of interpolation to constant wavenumbers q. Elastic structure factors $S_{el}(q)$ are yielded by integration of the scattering law over the instrumental energy resolution function. $S_{el}(q)$ is to a good approximation the static structure factor times the Debye-Waller factor. In order to evaluate the quasielastic contribution to the scattering law the data was energy Fourier transformed and deconvoluted by dividing with the energy Fourier transform of the measured resolution function. We note that Si and O scatter almost only coherent. Na and K contribute both to the coherent and the incoherent scattering with incoherent scattering of Na a factor 6 larger than incoherent scattering on K at comparable coherent scattering.

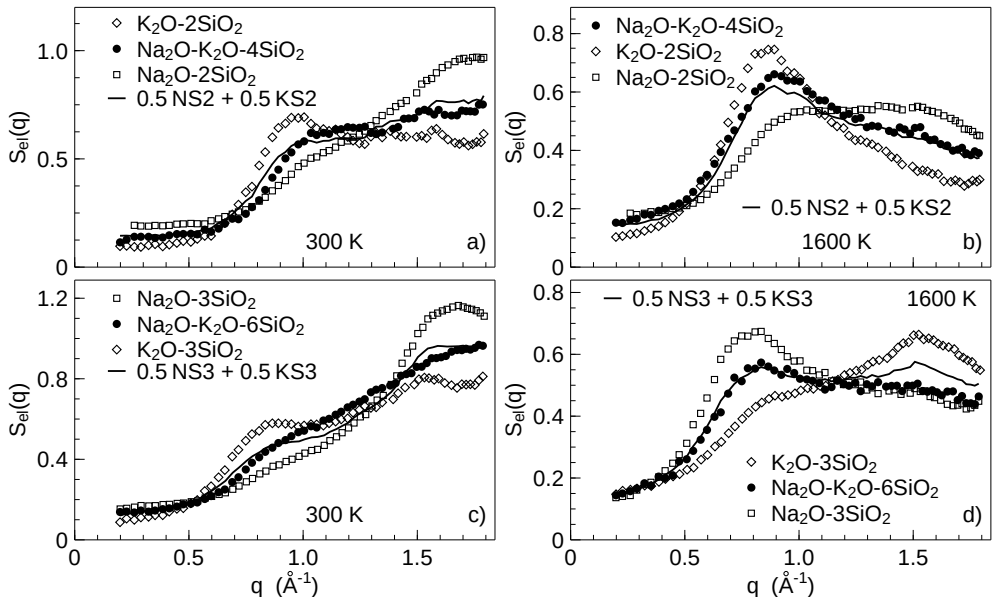

Figure 3.6:
Elastic structure factors of NKS4 ((a) and (b)) and NKS6 ((c) and (d)) at 300 K in the glass and at 1600 K in the melt (closed and open symbols) compared to their corresponding binary endmembers NS2, KS2, NS3, and KS3. For comparison a structure factor calculated by summation of the binary entities is shown as solid line. For a detailed discussion see the text.

Comparing our neutron scattering experiments on binary silicate melts with literature data it is well accepted that the alkali ion motion is separated by orders of magnitude of the network relaxation. The latter tends to be on a nanosecond timescale whereas the self diffusion of the alkali ions leads to a decay of the relaxation on a picosecond timescale. Ternary alkali silicates comprising two different alkali ions feature the so called mixed alkali effect which is a reduction of the alkali ion diffusivity upon alkali mixing compared to the corresponding binary endmembers [3]. The effect is less pronounced at higher temperatures and almost vanishes at typical temperatures in the melt being subject to this study. To explain for the non-linear dependence of modifier ion diffusivity upon mixing different scenarios are discussed for the glassy state. Recently based on reverse Monte-Carlo simulations on sodium phosphates a random distribution of the alkali ions in percolation pathways was postulated with ion transport reduced due to blockage of site incompatible alkalis [4].

The elastic structure factors at 1600 K in the melt and at 300 K in the glass are presented in Figure 3.6 for NKS4 and NKS6. A prepeak is observed similar to the binary endmembers. Different to the binary silicates the prepeak in the ternary systems changes its position and height gradually with

increasing temperature and composition. We note that we can not determine the partial structure factors. Thus in the following one possible explanation for the behavior of the data is presented which also allows for the observed dynamical behavior. We note that NKS4 and NKS6 compared to NS2, KS2 and NS3, KS3 comprises additional contributions to the scattering law e. g. the coherent Na-K scattering contributions.

A linear superposition of the binary structure factors was assumed for calculating a mixed structure factor represented by the solid lines. It is based on two assumptions: Firstly, Na-K correlations give only a minor contribution. Secondly, the molar volume of Na and K silicates is not strongly different being itself a linear superposition of the molar volume of the binary silicates. Consequently, we assume that two distinct percolation channels and no random distribution of the alkali ions in the channels exists. Hence the different partial structure factors of the binary systems though not accessible in our experiments shall respect with only minor changes their positions and intensities.

The measured elastic structure factor for NKS4 at room temperature and a structure factor represented by the solid line that was calculated from NS2 and KS2 data agree qualitatively. The first sharp diffraction peak (FSDP) and the plateau at small q dominated by incoherent scattering on Na are reproduced. Only the prepeak intensity (at $q \simeq 1.2$ Å^{-1}) of the measured curve exceeds the calculated curve. In glassy NKS6 the calculated curve features distinct oscillations whereas the measured curve shows a broad intensity distribution with no clearly pronounced prepeak. At 1600 K the data agrees qualitatively with the measured curve in NKS4 slightly exceeding the calculated curve around the prepeak position and additional intensity around the FSDP in NKS6. The latter might be explained either though rather unlikely by a stronger influence of the Debye-Waller factor or by a pronounced shift in the partial structure factors between the glass and the melt.

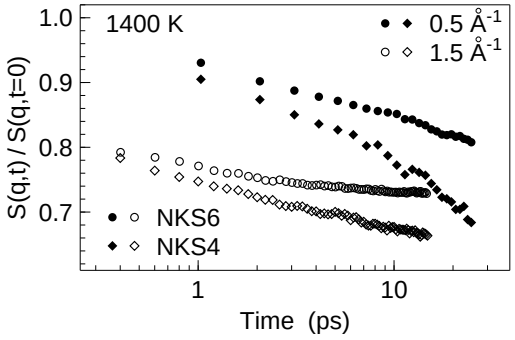

Figure 3.7:
Intermeadiate scattering function $S(q,t)$ of NKS4 and NKS6 at two different wavenumbers at 1400 K in the melt. Data is normalized by means of $S(q,t=0)$ as obtained from the Fourier transformation. No fit was performed on the data since there are at least two processes at the larger wavenumber that correspond to the decay in $S(q,t)$.

In the binary silicates it was observed that the intensity of the FSDP decreases with increasing alkali content, but that the positions of the prepeak and the FSDP are unchanged. Only replacing the modifier ion species leads to a pronounced change of the prepeak. In both samples we observe the intensity around 1.6 Å^{-1} overestimated in the calculation compared to the measured data. We also observe additional intensity roughly around 1.2 Å^{-1}. It is less in the system containing more alkali atoms. The findings are in agreement with our proposed explanation, that will enhance lengthscales reflecting inter alkali-alkali channel distances.

In order to clarify whether only the incoherent Na correlator decays on the 10 ps timescale or whether also the coherent Na-K correlator contributes to relaxation on this timescales we investigated the intermediate scattering function $S(q,t)$ (see Figure 3.7). $S(q,t)$ of NKS4 and NKS6 at 1400 K and two different wavenumbers normalized for clarity reasons by means of the measured $S(q,t=0)$ are shown. We note that in the mixed-alkali silicate glasses as seen in the elastic

structure factors at small wavenumbers incoherent scattering on Na mostly contributes to a decay in the density correlation function. With the number of Na ions in NKS4 reduced by a factor of two compared to NS2 and in NKS6 by almost a factor of three compared to NS2 and relaxation times expected to be up to a factor of two larger in the mixed system an analysis of the data with respect to relaxation processes becomes a difficult task.

At 0.5 Å^{-1} at which only incoherent scattering on Na contributes to the decay in the density correlation function on this 10 ps timescale a faster relaxation of Na in NKS4 compared to NKS6 is suggested by the data. The relaxation process is slower compared to the equivalent binary sodium silicates. Assuming that a q^2 scaling holds to a first approximation in the mixed alkali silicates we expect at 1.5 Å^{-1} the intermediate scattering function to decay owing to Na relaxation on timescales of approximately 2 ps. At this wavenumber already coherent scattering dominates the total scattering signal. Hence contributions of the decay of the coherent Na-K correlator cannot be excluded. In NKS4 we observe the onset of a second structural relaxation process at timescales of 5 ps, whereas in NKS6 only a single decay is observed. The onset of this second relaxation process can be a signature for the decay of the coherent Na-K correlator, since the network relaxation according to viscosity data is on a nanosecond timescale. To analyse the data in terms of the determination of relaxation amplitudes and relaxation times over the entire wavenumber range demands for measurements that yield density correlation functions up to 60 ps in time.

Also in the mixed alkali silicates the prepeak and its dependence on composition and temperature reflects the non-homogeneous distribution of the alkali ions in percolation pathways embedded in the SiO_2 matrix. Our detailed temperature and composition dependent measurements will allow for a comparison with molecular dynamics simulations. The Na self motion is still decoupled of the network in the mixed alkali systems by orders of magnitude. However, the relaxation amplitudes were not resolved by our experiments. Consequently, the interpretation of the dependence of the prepeak on the alkali ratio as formation of two interpenetrating alkali networks is only one possibility to explain the data.

[1] A. Meyer, J. Horbach, W. Kob, F. Kargl, H. Schober, Phys. Rev. Lett. **93**, 027801 (2004).

[2] F. Kargl, A. Meyer, M.M. Koza, H. Schober, Phys. Rev. B, (submitted).

[3] R. E. Tickle, Phys. Chem. Glasses **8**, 101 (1967).

[4] J. Swenson, S. Adams, Phys. Rev. Lett. **90**, 155507 (2003); J. Swenson, A. Matic, C. Karlsson, L. Börjesson, C. Meneghini, W. S. Howells, Phys. Rev. B **63**, 132202 (2001).

Nuclear resonant scattering from ^{57}Fe bearing sodium silicate glasses and melts.

C. Strohm[1], U. van Bürck, F. Kargl, I. Sergueev[2], A. Meyer, W. Petry

[1] TUM, E13; ESRF, Grenoble

[2] ESRF, Grenoble

Silicate glasses and melts have great relevance both in earth science and technology: The physical properties of magma (molten silicate rock) dominate many geological processes, and technological glasses are synthesized from the molten state. Considerable effort has been made to investigate a wide range of silicate melts with the general aim of linking structural with physical properties and to develop an atomic level understanding of their structure and dynamics [1]. Nuclear forward

scattering has proven to be a powerful technique for the investigation of the hyperfine interactions and dynamics of ^{57}Fe bearing glasses and melts. The aim of the study was to probe the iron dynamics as a function of temperature on the intrinsic iron in ironoxide bearing alkali silicate melts. The mobility of the Si-O network and the Na atoms is decoupled by about five orders of magnitude in the temperature range considered [2]. What is the iron relaxation in these systems?

Samples of ironoxide bearing sodium silicate glass of $2Na_2OFe_2O_36SiO_2$ and $5Na_2OFe_2O_312SiO_2$, enriched in ^{57}Fe, were prepared from powder in two steps, in order to avoid foaming. In a first step the compositions Na_2O3SiO_2 and Na_2O5SiO_2 were prepared from Sodium Carbonate and Silicon Dioxide. They are subsequently mixed and molten with Fe_2O_3 in a laboratory furnace at 1350 C.

For the nuclear resonant scattering experiments, the samples are held in a platinum wire loop (dia. 2mm thickness 0.5mm) by surface tension. The loop is mounted inside an Al_2O_3 tube by capillaries of the same material, equipped with radiation baffles and a thermocouple thermometer. The fully sealed Al_2O_3 tube is heated indirectly by a resistive heater of a Pt:10Rh wire, which is wound in a longitudinal meander pattern to achieve homogeneous temperatures up to 1600 K in about 1 cm^3. The housing is water-cooled and the cold entrance and exit windows are made from Capton foil.

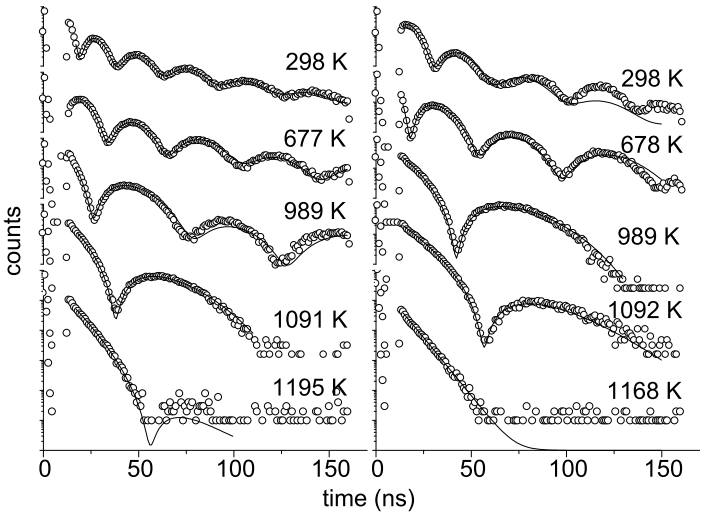

Figure 3.8:
Nuclear forward scattering. Left: $2Na_2OFe_2O_36SiO_2$, right: $5Na_2OFe_2O_312SiO_2$. The solid lines are fits to the data. The differences in the beat structure are mainly due to different effective thicknesses.

In nuclear forward scattering NFS, a Mössbauer transition (^{57}Fe: E = 14.413 keV) is excited with synchrotron radiation, using the time structure of the ESRF synchrotron in 16-bunch mode: flashes of 100 ps separated by empty buckets for 176 ns. Electronic scattering decays on a scale of 10^{-15}s leaving 176 ns in which the decay of the nuclear transition with a lifetime of 141 ns can be observed practically without background. The excitation of the nuclei is coherent over all nuclei in the sample (multiple scattering) and over the levels of the nuclear transition, which may be split by hyperfine interactions. The characteristic beat pattern (Fig 2) in the NFS time spectrum arises from optical interference in the sample and from interference between the levels of the nuclear transition. The hyperfine interactions (Fig. 3.9 b)) obtained by fitting the spectra,

allow to draw conclusions on the valence, co-ordination and magnetism of the ^{57}Fe within the sample. The observation and damping (Fig. 3.8) of the beat pattern depend on the square of the recoilless fraction (Fig. 3.9 a)) of scattered γ-quanta as well as on the change of the relative positions of the nuclei in during the observation time (17ns $<$ t $<$ 176ns). This allows in addition the study of dynamics on two different time scales: On the scale of atomic vibrations (Fig. 3.9 a)) (Lamb-Mössbauer-factor) and the self-diffusion of the iron atoms (Fig. 3.9 c), d)) [3].

We studied the dynamics and hyperfine interactions of two compositions of ^{57}Fe bearing silicate glasses of geological relevance from ambient temperature to 1200 K. In both compositions, the iron is predominantly trivalent in tetrahedral co-ordination. The Lamb-Mössbauer factor follows a Debye-law up to the calorimetric glass temperature and decreases by two orders of magnitude with respect to an ideal Debye solid at the highest observed temperatures Fig.3.9 a). The self-diffusion of iron becomes observable above the glass temperature and does not differ significantly for both compositions Fig. 3.9 c), d).

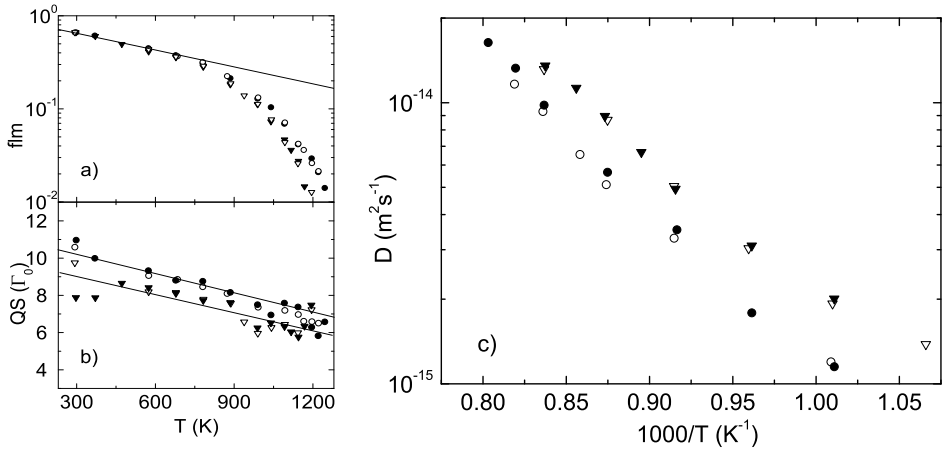

Figure 3.9:
a) Lamb-Mössbauer-factor: circles: $2Na_2OFe_2O_36SiO_2$, triangles: $5Na_2OFe_2O_312SiO_2$. Line: Lamb-Mössbauer factor for a Debye solid with Θ_D = 312 K. b) quadrupole splitting: circles: $2Na_2OFe_2O_36SiO_2$, triangles: $5Na_2OFe_2O_312SiO_2$. The lines are guides to the eye. c) self diffusion coefficient D: circles: $2Na_2OFe_2O_36SiO_2$, triangles: $5Na_2OFe_2O_312SiO_2$.

The measurements presented above are currently limited by the vanishing of the Lamb-Mössbauer factor at high temperatures. In ongoing work we hope to extend the range of observation through the detection of perturbed angular correlations (SR-PAC) excited with synchrotron radiation. The latter being independent of the Lamb-Mössbauer factor, has recently been demonstrated as a tool for the study of dynamics in molecular glass formers using ^{57}Fe bearing probe molecules [4]. In order to further understand the role of ironoxide for the viscosity of volcano melts we plan to study the same compositions under reducing conditions, forcing the iron in its two-valent state and octahedral co-ordination. This offers the unique possibility to study the dynamical properties of one constituent in the same composition in different structural environments. Other interesting systems are the Albeite and Jadeite compositions, in which the iron is partly present in the reduced state. A point of particular interest is the redox kinetics itself. The progress of the reaction directly reflects the interplay between the dynamics and co-ordination of the different iron species. It is

worth to point out, that studies of the dynamics and hyperfine interactions of Mössbauer nuclei of geological importance (e.g. Fe, Ni, Sm, Eu, Sn) can be performed on samples down to 100 μm^3 in volume. This allows the investigation of larger samples with high spatial resolution or the study of earth core and mantle compositions under extreme conditions like for example in laser heated diamond anvil high pressure cells.

[1] For an overview see: Rev. Mineralogy **32**, Structure, Dynamics and Properties of Silicate Melts, (1995) edts: J. F. Stebbins, P. F. McMillan, D. B. Dingwell.

[2] A. Meyer, J. Horbach, W. Kob, F. Kargl, H. Schober. Channel Formation and Intermediate Range Order in Sodium Silicate Melts and Glasses. Phys. Rev. Lett. **93**, 027801 (2004)

[3] A. Meyer et al. Z. Phys. B **103**, 479 (1997) Nuclear resonant scattering of synchrotron radiation for the study of glass dynamics around the glass transition.

[4] I. Sergueev et al. Synchrotron-radiation-based perturbed angular correlations used in the investigation of rotational dynamics in soft matter. Phys. Rev. B **73**, 024203 (2006).

Rotational glass dynamics investigated by SRPAC on different nuclear probes

I. Sergueev[1], A. I. Chumakov[1,2], U. van Bürck, T. Asthalter[3], H. Franz[4], R. Rüffer[1], W. Petry

[1] ESRF, Grenoble
[2] Russian Research Center 'Kurchatov Institute', Moscow
[3] Institut für Physikalische Chemie, Universität Stuttgart
[4] Hasylab, Hamburg

The dynamics of glass formers can be investigated by nuclear resonant scattering of synchrotron radiation (SR) provided that small quantities of nuclear probes can be dissolved in the glass matrix. However, above a critical temperature the Lamb-Mössbauer factor breaks down and makes the coherent nuclear scattering of SR to vanish. At higher temperatures only spatially incoherent scattering can be observed by SRPAC (SR based Perturbed Angular Correlations) [1,2]. SRPAC requires that the nuclear probes exhibit some hyperfine splitting of the intermediate excited state. Interference of indistinguishable scattering paths via different intermediate substates leads to a quantum beat in the time evolution of the scattering. Rotational dynamics of the probe is then observed as a damping of this quantum beat.

For the glass former dibutyl phthalate (DBP) (unit volume V ~ 443Å^3, glass transition temperature $\sim$ 179 K, critical temperature $\sim$ 202 K) a convenient probe has been found with ferrocene (Fc) (V ~ 203Å^3) [3]. Ferrocene contains one iron atom sandwiched between two C_5H_5 rings, which cause a strong field gradient at the iron site. The dynamics of DBP has been investigated via SRPAC on Fc probes enriched in ^{57}Fe in the temperature range 180 - 330 K [4], i.e. far up into the liquid state. In this range the rotational relaxation rate λ was found to vary between $1 \cdot 10^6$/s (lower limit of sensitivity) and $3 \cdot 10^{10}$/s (see Fig. 3.10). The temperature dependence of λ can be described at lower temperatures (< 210 K) by an Arrhenius law, and at higher temperatures ($>$ 220 K) e.g. by a Vogel-Fulcher-Tammann law [4].

In order to corroborate these findings, the question had to be solved to which extent the obtained results reflect the properties of the solvent or those of the probe. For this purpose the same glass

former DBP was now studied using another nuclear probe. We used a ferrocene derivative, decamethylferrocene (DMFc) (V $\sim 450 Å^3$), where the H atoms of the two C_5H_5 rings are replaced by CH_3 groups. Thus the sandwich structure and therefore also the nuclear properties were almost the same as for Fc, but the size of the probe was about twice as large. The probes were synthesized using ^{57}Fe [5].

The dynamics of DBP was investigated by SRPAC on DMFc probes in the temperature range 185 - 310 K. The experiments were performed at the beamline ID18 of the ESRF Grenoble. The results for the rotational relaxation rates for DMFc probes are displayed in Fig. 3.10: The rates exactly follow the corresponding rates measured on the Fc probes, however they are reduced by a factor of about three. Closer inspection shows that the two temperature dependences λ(T) can nicely be brought to coincidence over the large range of 200 - 310 K by a vertical shift (in scale), but not by a horizontal shift (in temperature). Below 200 K, the values for DMFc are at the sensitivity limit.

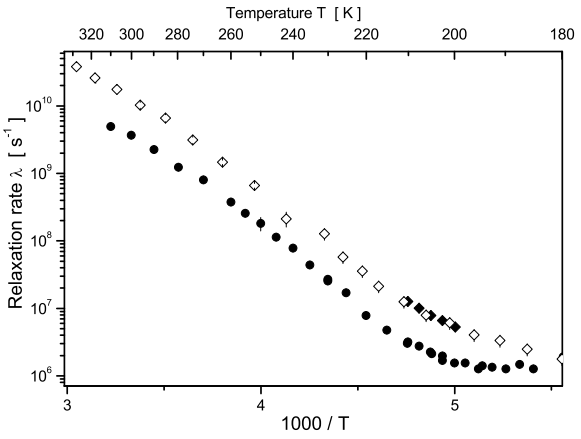

Figure 3.10:
Rotational relaxation rates in DBP measured on Fc probes (◊ , ⧫) and DMFc probes (●).

It is surprising that the reduction factor is the same for the liquid (e.g. at $\sim$ 300 K) and the glassy regimes (e.g. at $\sim$ 200 K). In the liquid, we can understand the reduced rotational relaxation from free diffusion, which is a kinematical process where the Stokes-Einstein equation gives for spheres $\lambda \sim 1/V$. The aspherical shapes of the probes will play an additional role. In the glass, rotational hopping is a thermally activated process with an energy barrier mainly defined by steric hindrance.

The fact, that after scaling the temperature dependences λ(T) for different probes coincide both in the liquid and in the glassy regimes, proves that indeed the probe dynamics reflects well the dynamics of the solvent glass former DBP. On the other hand, the different results for the two kinds of probes evidence that the absolute values of the relaxation rates are a feature of the respective probe.

In summary, different rotational relaxation rates have been measured for different nuclear probes dissolved in a glass former. However, when appropriately scaled, the rates surprisingly well coincide over the entire temperature range indicating that SRPAC on these probes reveals the dynamics of the solvent glass former.

[1] I. Sergueev et al., Ann. Report TUM Physik-Dep. E13, 39 (2001) and 7 (2002); ESRF Highlights 2002, p.61 (2003)

[2] I. Sergueev et al., Phys. Rev. B, **73**, 024203 (2006)

[3] S. L. Ruby et al., J. Physique **37**, C6-745 (1976)

[4] I. Sergueev, PhD-thesis, TU-München (2004)
[5] H. Schottenberger, Univ. Innsbruck, Austria

Dynamics of Simple Liquids as Described by Mode-Coupling Theory

H. Sinn[1], W. Schirmacher

[1] Argonne National Laboratory, 9700 S. Cass Avenue, Argonne, IL 60439, USA

By comparison to experimental and simulation data it is shown that mode-coupling theory, which is known to give a good description of the relaxational dynamics of viscous liquids in the liquid-glass transformation regime, does also describe the non-viscous regime at higher temperatures fairly well.

It is by now well known that mode-coupling theory (MCT) gives a good and detailed account of the sophisticated and non-trivial dynamic blocking phenomena which occur in the vicinity of the liquid-glass transformation regime [1].

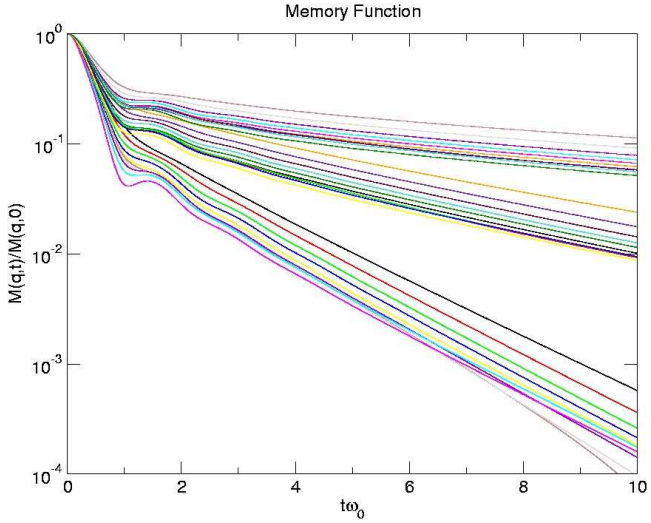

Figure 3.11:
Memory functions for the hard-sphere like model for packing fractions $\eta = 0.40$ (bottom curves), $\eta = 0.45$ (intermediate curves) and $\eta = 0.49$ (top curves). The q values are (essentially from bottom to top) $\sigma q = 0.9, 0.18, \cdots, 8.1, 9.0$, where σ is the hard-sphere diameter, $\eta = (\pi/6)\rho\sigma^3$ and ρ is the number density.

The key role in the description of the so-called cage effect is played by the memory function $M(q,t)$ in the generalized Langevin equation for the density fluctuation correlator $\phi(q,t)$. Precursors of this theory were versions of MCT in which memory functions corresponding to current fluctuations were considered and which have been applied successfully for describing the microscopic density and current fluctuations of simple liquids [2]. However, the implementation of this theory is rather cumbersome, as it involves detailed knowledge of the interatomic potentials. In contrast, the only input to the present MCT version is the static structure factor $S(q)$ and known parameters like temperature, mass and density. As in all versions of MCT, there are no adjustable parameters.

We therefore became interested in the question as to whether the liquid dynamics in the less viscous regime away from the glass transition can also be described in terms of the "glass MCT". In fact, using the measured static structure factor as input, we found in the case of liquid titanium

that the dynamical structure factor predicted by MCT shows almost perfect agreement to recent inelastic X-Ray diffraction data obtained at the Advanced Photon Source at the Argonne National Laboratory [3].

As the the static structure factor of simple liquids can be well described in terms of hard spheres the effective packing fraction η is the relevant density parameter of simple liquids. If the hard-sphere diameter σ is used as length scale and the isothermal sound velocity, divided by σ, i. e. $\omega_0 = \frac{v_{iso}}{\sigma} = \sqrt{\frac{k_B T}{mS(q=0)}}/\sigma$ as frequency scale, η remains as the only parameter of the theory.

In Fig. 3.11 we have plotted the memory function as calculated by MCT for different values of η. It is remarkable that it shows a two-step decay as, in fact, found in experimental and simulation data of several liquid metals [4]. It can be seen that the slow part of the decay gradually approaches the regime where, eventually at a critical value of η the non-ergodic plateau appears.

[1] W. Götze, in *Liquids, Freezing and the Glass Transition*, J.-P. Hansen, D. Levesque, J. Zinn-Justin, Eds., North-Holland, Amsterdam 1991.

[2] J. Bosse, W. Götze and M. Lücke, Phys. Rev. A **17**, 434 (1978); *ibid.*, **17**, 447 (1978); *ibid.*, **18**, 1176 (1978).

[3] A. Said *et al.*, to be published

[4] T. Scopigno, G. Ruocco, F. Sette, Rev. Mod. Phys. **77**, 881 (2005).

4 Dynamics of ordered and disordered solids

Single crystal growth and anomalous phonon softening in NiAlMn shape memory alloys

T. Mehaddene, J. Neuhaus, W. Petry

NiAlMn is one of the promising high-temperature shape memory alloys. In a first step, measurements of the martensitic transformation in NiAlMn alloys using differential scanning calorimetry have been performed. Alloys with several compositions of both compounds have been prepared by arc-melting starting from pure metals. The effects of the composition as well as the thermal treatment have been investigated. The martensite start temperature was found to be highly dependent on concentration. It ranges from 300 K up to 800 K in NiAlMn depending on the Al and Mn content. To get more insight on the martensitic transition that is well known triggered by phonons, lattice dynamics investigation and information on interatomic potentials are a necessary step for any extensive research on this system. For this purpose, Bridgmann, Floating-zone and Czocharlski techniques have been used to grow single crystals of Ni_2AlMn. It turned out that the surface tension was too low for holding the molten charge during the floating-zone experiments. Different rod diameters and growing rates have been unsuccessfully tried. Brigdmann technique has been used first with commercially available Al_2O_3 crucibles. It lead to a handful of relatively long crystals (8–10 mm) along the rod but of limited size along the cross section. Polishing of the inner surface of the Alumina crucible with a diamond paste of 5 μm particle size lead to crystals with a volume of 50 mm^3. Only the Czocharlski technique in which the solid-liquid interface is contact free lead to single crystals of reasonable size (300 mm^3). Two single crystal have been up to now grown. The chemical composition has been determined by Elastic Recoil Detection: $Ni_{54}Al_{28}Mn_{18}$ and $Ni_{53}Al_{24}Mn_{23}$. The single crystals have been oriented by a Laue-back reflexion technique and tested with neutrons. The mosaic spread is 0.8^o and 1^o respectively.

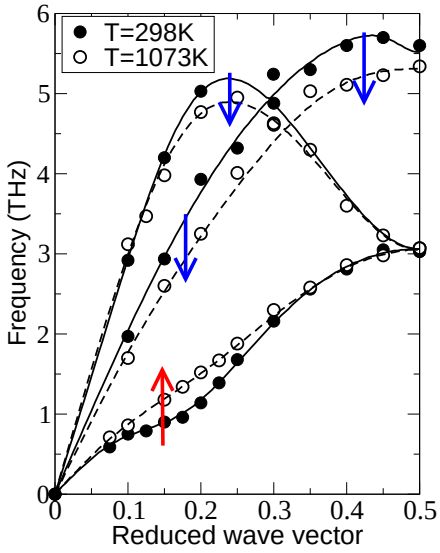

Figure 4.1:
Acoustic normal modes of vibration in of $Ni_{54}Al_{28}Mn_{18}$ in [110] direction measured at room temperature (open circles) and at 1073K (filled circles). The arrows show the frequencies variation when increasing temperature.

Normal modes of vibration in $Ni_{54}Al_{28}Mn_{18}$ have been measured by inelastic neutron scattering on the triple-axis spectrometer PUMA in the new research reactor FRM II and the spectrometer 2T

at the Laboratoire Léon Brillouin. The sample, which consisted in a piece of a cylinder with a volume of 250 mm^3 has been aligned to have the (001) plane coincide with the scattering plane. We focused during the measurements on the phonon dispersion in the particular high-symmetry direction [110]. To get more insight on the temperature dependence of the normal modes of vibration, phonons have been measured in a wide range of temperature, from 1073 K down to 4 K. Low-lying phonon frequencies of the TA2[110] phonon branch have been observed indicating low-restoring forces against the sliding of the (110) atomic planes in the [1-10] direction. Such displacements associated with atomic shuffles in the (110) planes constitute basal planes of the close-packed martensite low-temperature phase. The measured phonons showed a slight decrease in the frequencies when increasing temperature because of the increasing anharmonicity at high temperatures expect the TA2[110] phonon modes with the polarisation $\{1\text{-}10\}$ where an anomalous softening has been observed in the reduced Q-range ξ=0.1-0.25 (Fig. 1). At room temperature a wiggle is observed in the TA2[110] branch in the same Q-range as the anomalous softening. The same behavior has been observed in other Ni-based alloys. An anomalous softening of the TA2[110] phonons has been measured in Heusler Ni_2MnGa [1] along with a wiggle which deepens with decreasing temperature, resulting in a distinct minimum at 260 K for ξ=0.33. Shapiro et al. [2] have studied this anomaly in Ni_xAl_{1-x} for x=0.5,0.58 and 0.63. The position of the minimum has been found to shift linearly to lower wave vectors with increasing Ni content but remains roughly the same in magnitude. Along with this anomaly, elastic diffuse scattering has been also measured in NiAl as well as in Nii_2MnGa. The appearance of the elastic peak is known as the precursor effect of the martensitic transformation, it is related to the occurrence of a premartensitic phase which has been attributed to a strong magnetoelastic coupling in Ni_2MnGa [3]. It is worth to compare the lattice dynamics in Ni_2MnAl to other Ni-based systems with the same B2 atomic ordering. We report in Fig. 2 the measured frequencies with the fitting using axially-symmetric forces based on Born von Karman model. The optical phonons have been included in the fit when available. The most striking feature is the weak dependence of the LA[110] and the TA1[100] with the composition in contrast to the TA2[110]. The NiAlMn sample being stable down to 2 K A, a further step is the check the evolution of the kink in the TA2[110] branch on cooling down. Does it develop to a distinct minimum? if yes, for which Q-value?. Are there any precursor effects? Phonon measurements have been performed and the data analysis is in progress.

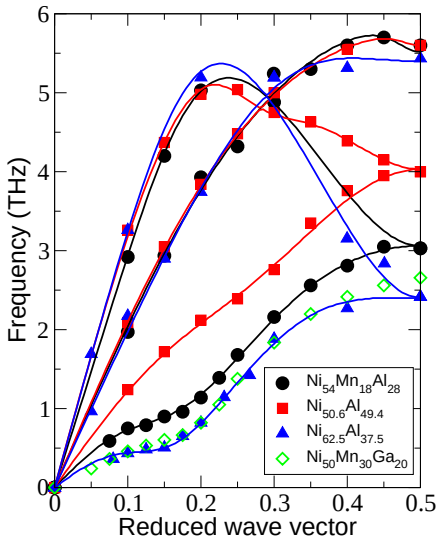

Figure 4.2:
Acoustic normal modes of vibration of $Ni_{54}Al_{28}Mn_{18}$ in [110] direction at room temperature compared to those of other Ni–based alloys with the same B2 atomic order. Note the dependence of the low frequency branch [110] on composition in comparison to the LA[110] and TA1[110]. Note: $Ni_{50}Mn_{30}Ga_{20}$ orders in the Heusler $L2_1$ structure.

[1] A. Zheludev, S.M. Shapiro, P. Wochner, A. Scwartz, M. Wall and L.E. Tanner, Phys. Rev. B **51**, 11 310 (1995).

[2] S.M. Shapiro, B.X. Yang, Y. Noda, L.E. Tanner and D. Schryvers, Phys. Rev. B **44**, 9301 (1991).

[3] A. Planes, E. Obradó, A. Gonzàlez, and L. Mañosa, Phys. Rev. Lett. **79**, 39263929 (1997).

Hysteresis of rotational dynamics in two plastic crystals as studied by SRPAC

T. Asthalter [1], I. Sergueev[2], U. van Bürck

[1] Institut für Physikalische Chemie, Universität Stuttgart

[2] ESRF Grenoble

In several studies, we have proven that Synchrotron Radiation based Perturbed Angular Correlations (SRPAC) [1] yield valuable information on molecular rotations, e.g. in glassy systems [2,3] and in plastic crystals [4,5]. In the case of the plastic crystal octamethyl-ethinyl-ferrocene (OMFA) [4,5], we observed a dynamical precursor effect, i.e. an onset of rotation some 10 K below T_{pc}, the transition temperature from the ordered crystalline to the plastically crystalline mesophase. Furthermore, OMFA exhibits a clear deviation from Arrhenius behaviour (reduced activation energy) on cooling, which indicates that the rotation can not be described in terms of a simple activated rotational jump.

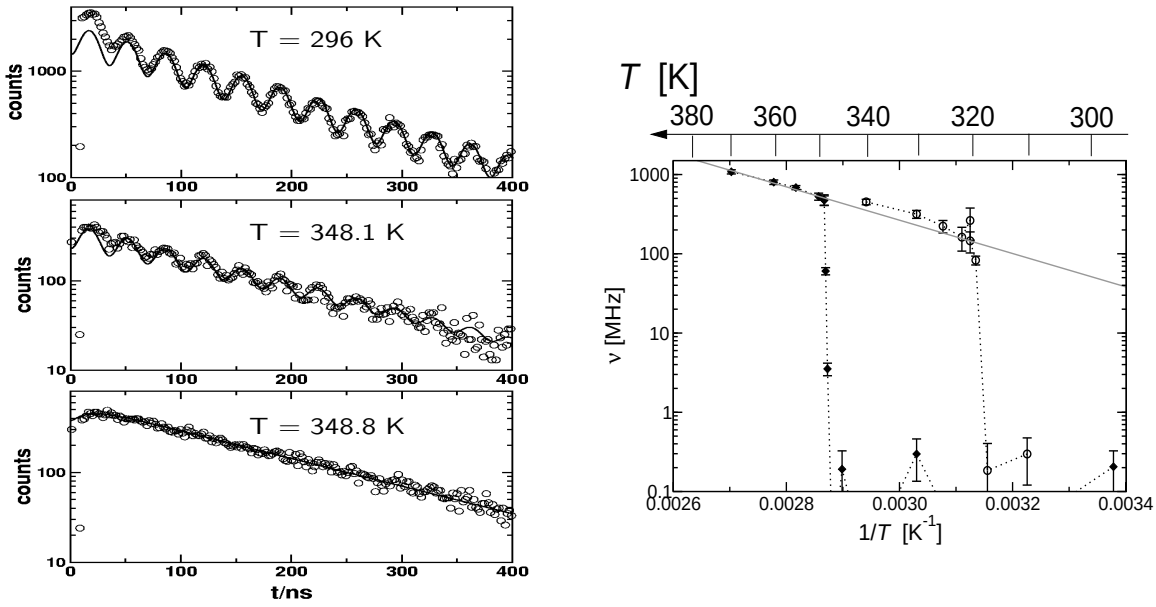

Figure 4.3:
SRPAC time spectra of OMF for three temperatures (left, fits are based on the strong-collision model); rotation rate of the electric field gradient in OMF (right).

In this report, we present new SRPAC data on an analogous but simpler molecule, octamethyl ferrocene (OMF), which carries no ethinyl substituent [6]. OMFA and OMF exhibit transitions to the plastic state at temperatures of about 240 K (348 K), which in both cases are far below the

melting temperatures of 436 K (431 K), respectively. The SRPAC experiment was carried out at the Nuclear Resonance beamline ID18 at the ESRF in 4-bunch mode. A nested high-resolution monochromator yielding an overall energy resolution of 6 meV was employed.

Using SRPAC, time spectra were obtained as shown in Fig. 4.3 (left). The damping of the QB pattern increases abruptly above T_{pc}, and the QB pattern has completely disappeared already a few tenths of a degree above T_{pc}, much in contrast to OMFA where a gradual onset of rotation (at lower temperatures and hence with lower rates) had been observed [4,5].

From these time spectra, we calculated the rotational relaxation frequency ν of OMF versus temperature through a full hysteresis cycle, as shown in Fig. 4.3 (right). The hysteresis loop exhibits sharp steps at T_{pc}= 348.5 K on heating and around T' = 320 K on cooling. Above the transition temperature T_{pc}, ν follows an Arrhenius behaviour (dotted line), with an activation energy of (40.3$\pm$3.3) kJ mol^{-1} and a frequency factor of 5.4$\cdot 10^{14}$ s^{-1}. Much like the transition entropy, these parameters are higher than in OMFA, and in particular the activation energy is much higher than the energy necessary to activate mutual ring rotation in ferrocene.

We can therefore conclude that

- SRPAC has provided us with direct evidence of nearly free rotation in the high-temperature phase of OMF,
- in OMF, no dynamical precursor effect on heating and no deviation from Arrhenius behaviour on cooling are observed,
- the differences observed in the rotational dynamics between OMF and OMFA are mainly due to the absence vs. presence of the protruding ethinyl substituent.

[1] I. Sergueev et al.: Ann. Report TUM Physik-Dep. E13, 39 (2001) and 7 (2002);
ESRF Highlights 2002, p.61 (2003)

[2] I. Sergueev, PhD-thesis, TU-München (2004)

[3] I. Sergueev, U. van Bürck, A.I. Chumakov, T. Asthalter, G.V. Smirnov, H. Franz, R. Rüffer, W. Petry, Phys. Rev. B **73**, 024203 (2006)

[4] T. Asthalter, U. van Bürck, I. Sergueev, Ann. Report TUM Physik-Dep. E13, 69 (2004)

[5] T. Asthalter, I. Sergueev, U. van Bürck, J. Phys. Chem. Solids **66**, 2271 (2005)

[6] T. Asthalter, I. Sergueev, U. van Bürck, R. Dinnebier, J. Phys. Chem. Solids, in press (2006)

5 Biomolecular Complexes, Stability and Dynamics

Displacement Distributions in Proteins

W. Doster, M. Settles, R. Gebhardt and A. Gaspar

Globular proteins are close-packed structures with densities approaching those of molecular crystals. However, biological function is closely connected with conformational changes and considerable structural plasticity is required to enable the exchange of small ligands between a dense protein interior and the solvent. The general plasticiser is liquid water interacting with the protein surface. To characterize the spatial and time properties of conformational distributions using dynamic neutron scattering is thus of considerable interest. This project aims to reconstruct the displacement distribution from the experimental scattering functions using a moment expansion (Doster & Settles, 2005).

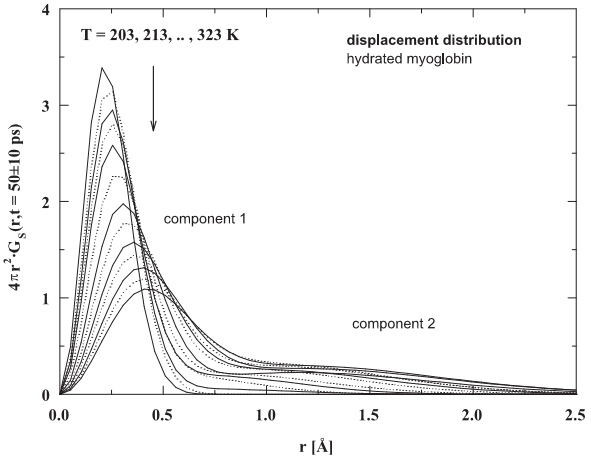

Figure 5.1:
Displacement distribution of D_2O-hydrated myoglobin at a fixed time of 80 ps with temperature, derived from IN13 (ILL) elastic scans covering a wide Q-range).

Fig. 5.1 displays an example of a displacement distribution function at various temperatures for hydrated myoglobin. A change in temperature shifts the effective time scale of molecular motions at fixed intrumental time window. At low temperature only vibrational motions are resolved which leads to a Gaussian distribution of displacements. The corresponding maximum (component 1) broadens with increase in temperature. The distinct shift and broadening of the maximum above 200 K reveals small scale diffusive displacements, which are absent in the dry and vitrified sample. Component 1 thus represents the liquid aspect of protein motions. In contrast component 2 is observed in all three environments above about 160 K. It reflects hydrogen motions on a larger scale due to rotational jumps, essentially of methyl groups and other dihedral transitions. This result suggests that rotational transitions of side chains in the protein interior are not strongly coupled to the properties of the environment. Torsional motions of methyls occur also in molecular crystals. Component 2 thus represents the solid aspect of structural fluctuations.

[1] W. Doster, M. Settles, Biochim.Biophys. Acta **1749**, 173-186 (2005)

Quasi-elastic and low-frequency inelastic neutron scattering from proteins with different secondary structure

A.M. Gaspar, W. Doster, R. Gebhardt and T. Unruh

Proteins: structure, dynamics and function

Proteins are polymers formed by a given sequence of a high number of amino acids, linearly connected (primary structure) by a common central part , but constituted by side chains which are different for the twenty types of amino acids. Generally the formation of additional, weaker, bonds between the side chains gives raise to a folding of the main chain into well defined secondary structures (β-sheets, α-helices, turns) as well as a tertiary structure (the three dimensional arrangement of the secondary structure). It is generally believed that the function of the proteins is, to a large extent, determined by this three dimensional structure that results from the specific folding of the main chain (the structure-function paradigm). The majority of proteins (such as myoglobin and lysozyme) is, in fact, characterized, in its native state, by a specific three dimensional structure. There are, however, proteins (such as the casein proteins) which are characterized, in their native state, by the absence of secondary and tertiary structure (which, in a certain way, questions the function-structure paradigm). Little is known about this type of proteins, but it is generally believed that their "unstructured" character is related to the need of a high structural flexibility for their functioning [1,2].

With these investigations we intend to analyze this interplay between structure, function and dynamics. In particular, we are interested in the repercussions that the differences in the bonds between the side chains of the amino acids may have on the rotational motions of those side-chains, as well as on the fluctuations of the main chain. Such motions occur, respectively, in time scales of the order of the pico- and the nano-seconds, easily accessible by quasielastic neutron scattering of cold neutrons (since such neutrons are characterized by wavelengths and energies comparable to the atomic distances and excitations characteristic of condensed and soft matter) [3,4].

Results obtained

First experiments were performed in August 2005, using the time-of-flight spectrometer TOF-TOF at FRMII. This type of spectrometer is adequate for the investigation of the rotational motions of side chains, with characteristic times of the order of pico-seconds, as well as of low frequency vibrational motions of proteins [3].

We studied, at three different temperatures, proteins with different secondary structures (myoglobin, lysozyme, β-casein), in their states of dry powder ($<$0.05g D_2O/g protein) and hydrated powder (with one hydration shell completed: $\sim$ 0.4 g D_2O/g protein). The use of D_2O, instead of H_2O, as solvent allowed to isolate the motions of the protein hydrogens, taking advantage of the fact that the scattering power of the H atom is much higher than that of the other atoms.

The spectra obtained at 115K show practically no quasielastic broadening of the elastic line and a well-resolved low-frequency inelastic band, around 2-4 meV of similar characteristics in the spectra of the different proteins (for the same hydration state). As temperature increases, this inelastic maximum becomes less distinct due to the overlapping with a broad quasielastic component of increasing intensity (which is accompanied by a decrease in the elastic intensity). Noteworthy is the fact that, for the same hydration state, these temperature changes appear much more pronounced in the β-casein spectra than in the spectra of myoglobin or lysozyme, suggesting shorter

correlation times and/or higher quadratic mean square displacements for the rotational motions of the side chains of this protein, in agreement with the hypotheses of less rigidity of this molecule.

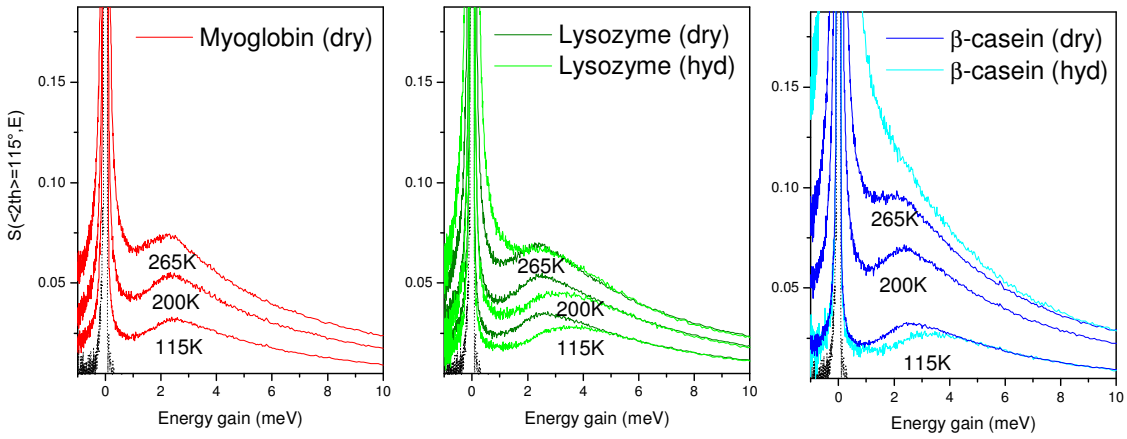

Figure 5.2:
Neutron scattering spectra obtained for Myoglobin, Lysozyme and β-casein powder samples, at TOFTOF spectrometer (λ=6 Å, Elastic Resolution FWHM= 60μeV).

When comparing the spectra obtained for the hydrated and the dry lysozyme and β-casein samples, one finds, in agreement of the results of previous investigations on myoglobin [5-7], that the solvent appears to restrict the vibrational modes contributing around 2meV to the inelastic maximum observed (possibly due to the strong hydrogen bonds that are formed between the protein with the solvent molecules [5,6]). Conversely, at temperatures higher than 200K, the hydrated samples exhibit a more pronounced quasielastic spectrum than the dry samples, in agreement with the hypothesis that proteins, when hydrated, exhibit a higher variety and complexity of diffusive motions (plasticizing effect of water) [7].

A more thorough,quantitative, analysis of these results is underway. In addition, further neutron scattering experiments are already planned, which will extend the investigations to the study of proteins in concentrated solution (closer to the physiological conditions), as well as to the analysis of dynamical processes characterized by time scales of the order of nano-seconds (fluctuations and diffusion of the main chain), by means of the use of both TOFTOF spectrometer and the spin-echo neutron spectrometer RESEDA at FRMII.

A.M. Gaspar acknowledges the Portuguese Science and Technology Foundation (FCT) for support in the form of a pos-doc grant SFRH / BDP / 17571 / 2004

[1] P. E. Wright, H. J. Dyson, J. Mol. Biol. **293**, 321-331 (1999)

[2] V. N. Uversky, J. R. Gillespie, A. L. Fink, Proteins **41**, 415-427 (2000)

[3] M. Bee: Quasielastic Neutron Scattering, Adam Hilger (1988)

[4] J. Fitter, T. Gutberlet, J. Katsaras (Eds.): Neutron Scattering in Biology: Techniques and Applications, Springer Biological Physics Series (2006)

[5] S. Cusack, W. Doster,Biophys. J. **58**, 243-251 (1990)

[6] M. Diehl, W. Doster, W. Petry, H. Schober, Biophys. J. **73**, 2726-2732 (1997)

[7] W. Doster, M. Settles, Biochim. Biophys. Acta **1749**, 173-186 (2005)

β-casein dynamics and association: quasi-elastic scattering studies

A.M. Gaspar, W. Doster, R. Gebhardt

Native proteins with non-regular structure include casein proteins, which constitute a family of four different phospho-proteins (α_1-, α_2-, β- and κ-casein), representing about 80% of the total milk proteins [1,2]. These proteins are believed to exhibit extreme structural flexibility, being also highly surface active and exhibiting strong tendencies to associate. As an approximation the caseins can be thought of as block copolymers consisting of blocks with high levels of hydrophobic and hydrophilic amino acid residues [3]. In the milk, they exist in colloidal particles known as the "casein micelle" whose shape is generally accepted as that of a roughly spherical, fairly swollen particle of 100-300 nm in diameter (Fig. 5.3). Its function is that of binding and transporting a large proportion of the minerals that the newborn requires (mainly in the form of calcium phosphate nanoparticles). These casein complexes are the result of the ensemble of multiple competing equilibria arising from the interactions of individual caseins with themselves and with Ca-Phosphate [1-3].

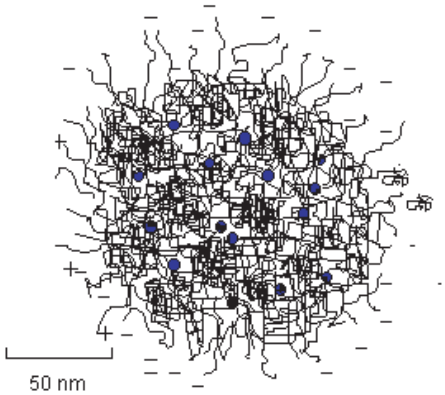

Figure 5.3:
Schematic representation of a casein micelle. Blue circles represent the calcium phosphate nanoclusters.

By using dynamic neutron scattering techniques, together with light scattering methods, we intend to characterize the structural flexibility (and mobility) of the different casein proteins, in their different association forms (ranging from the monomer to the whole micelle), by exploring a wide range of thermodynamic (pressure and temperature) conditions. The combined analysis of the results of such studies will certainly contribute to a better understanding of this structure-stability-function interplay in casein systems (and of the interactions leading to association).

The results obtained so far concern the β-casein dynamics and association. The outstanding characteristic of the self-association of β-casein, is its strong dependence on temperature, in both

the presence and absence of calcium ions [4,5]. Results from previous studies on β-casein self-association and micellisation indicate that at low temperature (T<4°C) the β-casein is predominantely in its monomeric state, with the onset temperature for self-association being generally between 15°C and 35°C, for a neutral pH solution, depending on the protein concentration as well as on the presence/absence (and concentration) of calcium or Na phosphate [4,5]. Dynamic light scattering studies performed at our laboratory, on neutral pH β-casein solutions, confirm such observations, indicating that at temperatures higher than 60°C all the protein content exists in the form of micelles of hydrodynamic radius 14 nm (Fig. 5.4).

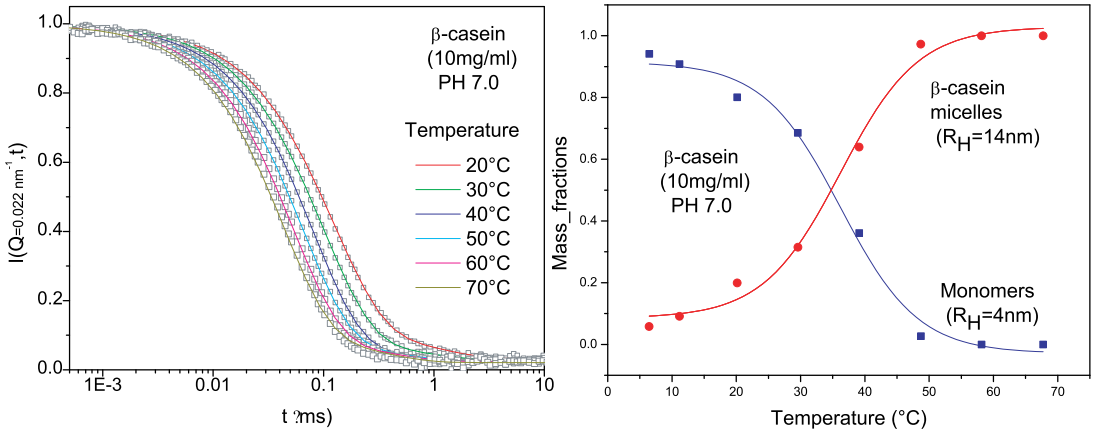

Figure 5.4:
Photon correlation functions obtained for a neutral pH β-casein solution at different temperatures (left) and mass fractions of the monomer and micelle populations (right) extracted from the fits to the photon correlation function. These studies were performed also as function of concentration.

The dynamical information that can be obtained by light scattering reflects, however, only the mobility of the entire macromolecular entities (either monomers or micelles) and not the internal protein motions, nor even, in the case of the micelle, the intra-micelle diffusive motions of its constituent proteins. The use of neutron scattering methods allows us to overcome these difficulties by providing dynamical information on the length scale of atomic distances. In particular, we are interested to evaluate how the dynamics of this protein in solution is affected by an increase in confinement when going from the monomers, at T≈0°C, to the micelles, at T=60°C.

Neutron beamtime has been requested (and granted) for both the time-of-flight spectrometer TOF-TOF and at the spin-echo spectrometer RESEDA at FRMII, the corresponding experiments being planned to be undertaken during the course of next year. The experiments at TOFTOF will mainly provide us information concerning the rotational motions of the protein side-chains (occurring on a pico-second time scale), while the experiments at RESEDA will provide us information concerning fluctuations of the protein main chain (occurring on a nano-second time scale) [6,7].

As further steps, we intend to compare the results of these experiments with similar neutron scattering results to be obtained on the other individual casein proteins and on the complete “casein micelle”. Once again, the results from past [8,9], and future, static and dynamic light scattering investigations will play an important role in the characterization of the different aggregation states that exist in solution under different thermodynamic conditions and in providing an independent means of obtaining the corresponding diffusion coefficients (an important parameter for an unbiased interpretation of the neutron scattering results to be obtained on solution samples [10]).

A.M. Gaspar acknowledges the Portuguese Science and Technology Foundation (FCT) for support in the form of a post-doc grant SFRH / BDP / 17571 / 2004

[1] P. Walstra, R. Jennes: Dairy Chemistry Physics, New York: Willey (1984)

[2] E. Smyth, R. A. Clegg, C. Holt, Int. J. Dairy Tech. **57**, 121-126 (2004)

[3] D. S. Horne, Curr. Op. in Colloid and Inteface Sci. **7**, 456-461 (2002)

[4] C. C. Kruif and V. Y. Grinberg, Colloids and Surfaces A: Physicochem. Eng. Aspects **210**,183-190 (2002), and references

[5] M. S. Sood and C. W. Slattery, J. Dairy Sci. **80**,1554-1560 (1997)

[6] A. M. Gaspar, W. Doster, R. Gebhardt, T. Unruh, Prop n 268, awarded 4 days of beamtime

[7] A. M. Gaspar, W. Doster, R. Gebhardt, W. Haeussler, Prop n 344, awarded 7 days of beamtime

[8] R. Gebhardt, W. Doster, U. Kulozik, Brazil. J. Med. and Biol. Res. **38**,1209-1214 (2005)

[9] R. Gebhardt, PhD Dissertation, Technischen Universitaet Muenchen (2005)

[10] J. Perez, J.-M. Zanotti, D. Durand, Biophys. J. **77**, 454-569, (1999)

Pressure-induced aggregation of β-lactoglobulin, a dynamic light scattering study

K. Song[1], A. Baars [1], R. Gebhardt and W. Doster

[1] TU München, Lehrstuhl für Prozessautomation, Freising-Weihenstefan

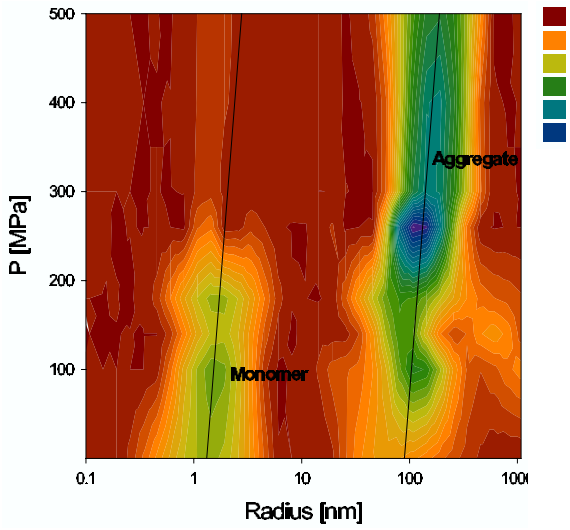

Figure 5.5:
Pressure-size diagram of lactoglobulin, derived from time-resolved aggregation plots (PCS), colour code: red low, blue high species concentration.

Hydrostatic pressure generally induces dissociation and unfolding of protein complexes. With β-lactoglobulin, however, an increase of the solution viscosity with pressure was observed suggesting association. K. Song investigated the pressure effects on this protein using dynamic light

scattering as a central part of his diplom thesis at E 13. He could confirm that lactoglobulin dissociates at low pressures, but forms high molecular complexes at high pressure. The figure shows the size distribution versus pressure, revealing the monomer-dimer equilibrium and the strongly associated state.

Protein-unfolding in bacterial cells, an FTIR study

G. Gröhnke [1], W. Doster, K. Kilimann[1], R.F. Vogel [1] and M.Gänzle [1]

[1] TU München, Lehrstuhl für Mikrobiologie, Freising-Weihenstefan

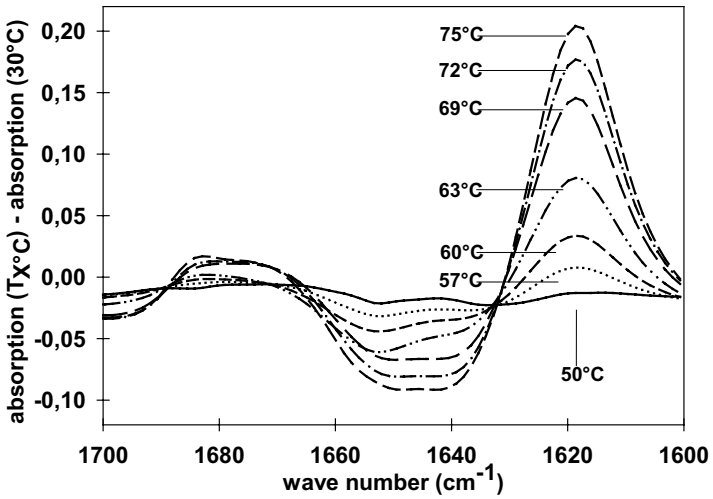

Figure 5.6:
FTIR difference spectra of bacterial cells in the amide I region versus the temperature relative to a spectrum taken at 30 C.

Gesa Gröhnke investigated the protection by sucrose against heat-induced lethal and sublethal injury of Lactococcus lactis using FTIR spectroscopy in E 13 as part of her Studienarbeit. The bacterial cells were also studied at high pressure. From the C-H stretching frequency versus temperature a transition of the bacterial membrane from a crystalline to the liquid phase was observed. The amide bands revealed structural changes of bacterial proteins versus temperature, which could be correlated with biological activity. Fig. 5.6 shows the unfolding of cell proteins, loss of helical structures, and the formation of new anti-parallel β-sheets in the amide I region of the FTIR spectrum.

6 Teaching and conferences

Lectures, seminars and lab courses

Spring semester 2005

Prof. Dr. Winfried Petry, *Physik mit Neutronen 2*

Prof. Dr. Andreas Meyer, *Experimentalphysik 2, Elektrodynamik u. Relativ. Dynamik*

Prof. Dr. Christine Papadakis, *Angewandte Physik: Polymerphysik 2*

Prof. Dr. Christine Papadakis, PD Dr. Peter Müller-Buschbaum, *Seminar über spezielle Probleme der weichen Materie*

PD Dr. Wolfgang Doster, *Experimentalphysik für Bauingenieure*

PD Dr. Peter Müller-Buschbaum, *Experimentalphysik 2 für LB (BT, ET, MT)*

Fall semester 2005/2006

Prof. Dr. Winfried Petry, *Physik mit Neutronen 1*

Prof. Dr. Andreas Meyer, *Experimentalphysik 1, Mechanik u. Thermodynamik*

Prof. Dr. Christine Papadakis, *Angewandte Physik: Polymerphysik 1*

Prof. Dr. Christine Papadakis, PD Dr. Peter Müller-Buschbaum, *Seminar über spezielle Probleme der weichen Materie*

PD Dr. Wolfgang Doster, *Experimentalphysik I für Lehramt*

PD Dr. Peter Müller-Buschbaum, *Experimentalphysik 1 für LB (BT, ET, MT)*

PD Dr. Walter Schirmacher, *Mathematische Ergänzungen zur Experimentalphysik 1*

Lab courses 2005

Statische und dynamische Lichtstreuung (Biophysikalisches Praktikum)

Theoretische und praktische Einführung in AFM (Fortgeschrittenenpraktikum)

Thermische Analyse (Fortgeschrittenenpraktikum)

Conferences

EDGAR–LÜSCHER–LECTURES DILLINGEN/DONAU 2005
Thema: Physik im Nanometerbereich

Datum: Dienstag, 4. Oktober bis Freitag, 7. Oktober 2005
Tagungsort: Akademie für Lehrerfortbildung und Personalführung Dillingen, Kardinal-von-Waldburg-Str. 6-7, 89704 Dillingen/Donau
Veranstalter: Akademie Dillingen und TU München
Wissenschaftliche Leitung: Priv. Doz. Dr. W. Schirmacher, Technische Universität München.

PROGRAMM

Dienstag, 4. 10. 2005	
15.30 – 17.00	Dr. Markus Dilger, Infineon München *Strukturierung von Kleinst-Bauelementen*
18.30 – 20.00	Prof. Dr. W. Wegscheider, Univ. Regensburg *Molekularstrahlepitaxie*
Mittwoch, 5. 10. 2005	
8.30 – 10.00	Prof. Dr. J. Zweck, Univ. Regensburg *Nano-Magnetismus*
10.15 – 11.45	Prof. Dr. P. Böni, TU München *Magnetismus in dünnen Filmen und Multischichten*
15:30 – 17.00	Prof. Dr. Chr. Pfleiderer, TU München *Exotische magnetische Strukturen*
18.30 – 20.00	Prof. Dr. Christine Papadakis, TU München *Funktionelle Polymersysteme*
Donnerstag, 6. 10. 2005	
8.30 – 10.00	Dr. Th. Franosch, LMU München *Kolloid-Kristalle*
10.15 – 11.45	Dr. Tanja Schilling, Univ. Mainz *Computersimulationen von kolloidalen Flüssigkristallen*
15:30 – 17.00	Dr. Th. Hugel, ZIMT, TU München *Nanophysik mit Polymeren und Viren an Oberflächen*
18.30 – 20.00	Dr. U. Gerland, LMU München *Molekulare Motoren und Translokation von DNA und RNA*
Freitag, 7. 10. 2005	
8.30 – 10.00	Prof. Dr. J. Rädler, LMU München *Nanopartikel in der Physik und der Medizin*
10.15 – 11.45	Prof. Dr. A. Wixforth, Univ. Augsburg *„lab-on-a-chip“ : Akustisch getriebene programmierbare Biochips*

GISAXS – an advanced scattering method

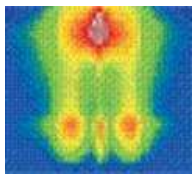

Section 1 - Lectures
Tuesday, May 10

12:15-12:30	R. Gehrke:	Brilliance at the present and future Synchrotron Radiation Light Sources at DESY
12:30-13:00	M. Rauscher:	Distorted-Wave Born Approximation
13:00-13:45	R. Lazzari :	Simulation of Grazing Incidence Small-Angle X-ray Scattering from nanostructures
14:15-14:45	M. Schmidbauer :	Self-organized nanostructures: What can be learned from GISAXS and GID
14:45-15:15	P. Müller-Buschbaum:	High-resolution GISAXS
15:15-15:45	C. M. Papadakis:	Grazing-incidence small-angle X-ray scattering - structure and kinetics of thin block copolymer films
16:00-18:00	Poster Session	(contributed presentations)
18:30	Workshop Dinner	

Wednesday, May 11

08:30-09:15	U. Pietsch:	White beam SAXS ate the EDR Beamline at ESSYII
09:15-09:45	A. Meyer:	Preparation of highly ordered nanostructures on surfaces using diblock copolymers as templates
10:15-10:45	J.S. Gutmann:	Nanoparticles (embedded in a plymer matrix)
10:45-11:15	A. Gibaud:	In-situ GISAXSstudies of self-assembled surfactant templated silica thin films
11:15-11:45	G. Artus:	Superhydrophobic surfaces
13:30-14:00		30 min safety course
14:00-15:00	S. V. Roth:	Introduction into BW4
15:00-17:30	Practical training	

(1) Measurement @ BW4 : S. V. Roth / P. Müller-Buschbaum
(2) Data treatment : C. M. Papadakis / J.S. Gutmann
(3) Simulation : R. Lazzari / R. Gehrke

Thursday , May, 12

09:00-12:00	Practical Training Part 2
13:00-16:00	Practical Training Part 3

Lehrerfortbildung an der TU München 2005

Thema:

Physik bei tiefen Temperaturen

Datum: Samstag, 25. Juni 2005

Tagungsort: Wissenschaftszentrum Weihenstephan der TU München, HS 1

(direkt neben dem „Bräustüberl“)

Veranstalter: Physik-Department und Zentralinstitut für Lehrerbildung und Lehrerfortbildung der TU München

Wissenschaftliche Leitung: Priv. Doz. Dr. W. Schirmacher, Physik-Department E13, TU München, Prof. Dr. R. Gross, Walther-Meissner-Institut für Tieftemperaturforschung der Bayerischen Akademie der Wissenschaften (WMI)

Anmeldung: wschirma@ph.tum.de

Programm

9.00 – 10.15	Prof. Dr. K. Lüders, FU Berlin:
	Erzeugung von tiefen Temperaturen I.
10.15 – 10.30	*Diskussion*
10.30 – 11.45	Prof. Dr. E. A. Schuberth, WMI:
	Erzeugung von tiefen Temperaturen II.
11.45 – 12.00	*Diskussion*
12.00 – 13.30	*Mittagspause*
13.30 – 14.45	Dr. R. Hackl, WMI:
	Supraleitung
14.45 – 15.00	*Diskussion*
15.00 – 15.30	*Kaffeepause*
15.30 – 16.45	Priv.-Doz. Dr Dietrich Einzel, WMI:
	Supraflüssigkeit
16.45 – 17.00	*Diskussion*
17.00 – 18.15	Dipl.-Ing. K. Löhlein, Linde AG Pfungen:
	Kryotechnik
18.15 – 18.30	*Diskussion*

RLFB-Tagungsprogramm

29. Edgar-Lüscher-Physikseminar am Gymnasium Zwiesel
Thema: Optik und Quantenoptik
Freitag, 8. April bis Sonntag, 10. April 2005

Veranstalter: Der Ministerialbeauftragte für die Gymnasien in Niederbayern, OStD Klaus Drauschke

Wissenschaftliche Leitung: Prof. Dr. Gerhard Rempe, Max-Planck-Institut für Quantenoptik, Garching und Privatdozent Dr. Walter Schirmacher, Technische Universität München

Org. am Gymnasium Zwiesel: OStD Günther Kratzer, OStR Günther Haller, OStR Wolfgang Achatz

Freitag, 8. April 2005

15.30 – 16.00	Begrüßung, Organisatorisches	MB Drauschke, OStD Kratzer, OStR Haller
16.00 – 17.15	Einführung	Prof. Dr. Gerd Leuchs, Universität Erlangen
17.15 – 18.00	Diskussion und Kaffeepause	
18.00	Kleine Feierstunde	Studienrat Stefan Urlbauer mit der Big-Band des Gymnasiums Zwiesel

Samstag, 9. April 2005

9.00 – 10.15	Bose-Einstein-Kondensation	Prof. Dr. Gerhard Rempe, Max-Planck-Institut für Quantenoptik, Garching
10.15 – 11.00	Diskussion und Kaffeepause	
11.00 – 12.15	Entwicklung von Quanten-Radierern	Dr. Schenker, Phywe AG, Göttingen
12.15 – 12.30	Diskussion	
14.00 – 15.15	Quanten-Kryptographie und Erzeugung von einzelnen Photonen	Prof. Harald Weinfurter, Universität München
15.15 – 16.00	Diskussion und Kaffeepause	
16.00 – 17.15	Optische Uhren	Prof. Joachim von Zanthier, Universität Erlangen
17.15 – 17.30	Diskussion	
17.30 – 18.45	Hochauflösende optische Mikroskopie	PD Dr. Stefan W. Hell, Max-Planck-Institut für biophysikalische Chemie, Göttingen
18.45 – 19.00	Diskussion	

Sonntag, 10. April 2005

9.00 – 10.15	Nichtabbildende Optik	Dr. Ralf Leutz, Universität Marburg
10.15 – 11.00	Diskussion und Kaffeepause	
11.00 – 12.15	Optische Nahfelder von Nanostrukturen	Prof. Dr. Paul Leiderer, Universität Konstanz
12.15 – 13.00	Diskussion; Neues Thema	

Der Ministerialbeauftragte für die Gymnasien in Niederbayern und das Gymnasium Zwiesel danken für finanzielle Unterstützung durch:

RLFB-Tagungsprogramm

Bayerisches Staatsministerium für Unterricht und Kultus, Technische Universität München, E.on Bayern

2nd FRM-II Workshop on Neutron Scattering - Advanced materials Burg Rothenfels am Main - 25. - 28.7.2005 organized by A. Meyer, W. Petry, P. Böni, C. Pfleiderer, C. Papadakis and Georgii				
	25.07.2005	26.07.2005	27.07.2005	28.07.2005
08:45 - 10:45		**Applied science** H. G. Brokmeier (GKSS) M. Hölzel K. Lorenz T. Bücherl K. Pranzas (GKSS) V. Koerstgens	**Magnetism 2** C. Pfleiderer A. Schreyer (GKSS) A. Ioffe (FZJ) D. Lamago	**Polymers** C. Papadakis A. Radulescu (FZJ) P. Müller-Buschbaum H. Frielinghaus (FZJ) O. Holderer (FZJ) G. Rother (FZJ)
11:15 - 13:00		**Magnetism 1** Y. Shu (FZJ) J. Voigt (FZJ) U. Rücker (FZJ) S. Bayrakci	**Methods** A. Rühm (MPI) N. Wieschalla N. Arend F.-M. Wagner X. Li V. Hutanu	**Magnetic Layers** E. Kentzinger (FZJ] S. Mattauch (FZJ) A. Paul (FZJ)
14:30 - 16:15	**Applied Science** C. Hugenschmidt M. Stadlbauer S. Krimmel P. Staron (GKSS) R. Gilles	**13:45 Excursion: Boat trip to Lohr am** Main	**Biophysics** R. Willumeit (GKSS) A. Gaspar A. Ostermann W. Doster C. Reich (LMU)	
16:45 - 18:30	**Viscous Melts** F. Kargl C. Strohm W. Häußler **Fundamental Physics** H. F. Wirth D. Rich P. Kudejova		**Structure** F. Frey (LMU) H. Boysen (LMU) B. Pedersen T. Mehaddene	
19:30	F. v. Feilitzsch			

7 Other activities

Publications

T. Asthalter, I. Sergueev, U. van Bürck
Molecular rotations studied by nuclear resonant scattering
J. Phys. Chem. Solids, **66**, 2271 (2005)

P. Braun, R. Gebhardt, L. Kwa and W. Doster
High Pressure Near Infrared Study of Mutated Light Harvesting Complex LH2
Bras.J. Med. Biol. Res.**38(8)** 1273 (2005)

P. Busch, M. Rauscher, D.-M. Smilgies, D. Posselt, C. M. Papadakis
Grazing-incidence small-angle X-ray scattering (GISAXS) from thin, nanostructured block copolymer films - The scattering cross-section in the distorted-wave Born approximation
J. Appl. Crystallography, eingereicht (2005)

S.K. Das, J. Horbach, M.M. Koza, S. Mavila Chathoth, A. Meyer
The Influence of Chemical Short Range Order on Atomic Diffusion in Al-Ni Melts
Appl. Phys. Lett. **86**, 011918 (2005)

W. Doster and M. Settles
Protein-water displacement distributions (invited and refereed review)
BBA Proteins, Proteomics, **1749**, 173-186 (2005).

W. Doster
Brownian Oscillator Analysis of Protein Dynamics
in 'Neutrons for Biology', Ed. R. Gutberlet and J. Fitter, Springer Verlag (2006), 461-483

W. Doster
Dynamical structural distributions in proteins
Physica B (2005) in press

R. Gebhardt, W. Doster and U. Kulozik
Pressure-induced dissociation of casein micelles, size distribution and effect of temperature
Brazilian Journal of Medical and Biological Research **38(8)**,1209 (2005).

R. Gebhardt, W. Doster and J. Friedrich
Size distribution of pressure-decomposed casein micelles studied by dynamic dynamic light scattering and AFM
Eur. Biophys. J. (2005) in press

E. Gutsmiedl, W. Petry, K. Schreckenbach
Status of the new research reactor FRM-II
Proceedings of the International Symposium on Research Reactor and Neutron Science- In Commemoration of the 10th Anniversary of HANARO - Daejeon, Korea, April (2005)

N. Hermsdorf, M. Stamm, S. Förster, S. Cunis, S. S. Funari, R. Gehrke, P. Müller-Buschbaum
Self Supported Particle Track Etched Polycarbonate Membranes as Templates for Cylindrical Polypyrrole Nanotubes and Nanowires: An X-Ray Scattering and Scanning Force

Microscopy Investigation
Langmuir **21**, 11987 (2005)

M. Jernenkov, H. Lauter, V. Lauter-Pasyuk, B. P. Toperverg, S. Klimko, R. Gähler
Angular encoding with Larmor precession
Physica B **357**, 94 (2005)

F. Kargl, A. Meyer, M.M. Koza, H. Schober
Alkali Silicate Melts: Formation of Channels for Fast Ion Diffusion
Phys. Rev. B, eingereicht (2005)

F. Kargl, A. Meyer, M.M. Koza
Cage Effect as Origin of Fast Ion Transport in Sodium Borate Melts
Phys. Rev. Lett., eingereicht (2005)

K. Kilimann, W. Doster, R.F. Vogel, C. Hartmann, M.G. Gänzle
Protection by sucrose against heat-induced lethal and sublethal injury of Lactococcus lactis: an FT-IR study
Bioch. Biophys. Acta, Proteins and Proteomics (2005) submitted

I. Köper, M. Bellissent-Funel, W. Petry
Dynamics from picoseconds to nanoseconds of trehalose in aqueous solutions as seen by quasielastic neutron scattering
J. Chem. Phys. **122**, 014514-1-6 (2005)

E. Maurer, S. Loi, D. Wulff, N. Willenbacher, P. Müller-Buschbaum
Microscopic structure in pressure sensitve adhesives: An ultra small angle x-ray study
Physica B **357**, 144 (2005)

E. Maurer, S. Loi, P. Müller-Buschbaum
Debonding of pressure sensitive adhesives: A combined tack and ultra-small angle X-ray scattering study
in 'Adhesion - Current Research and Applications', edt. W. Possart, Wiley-VCH, 421-434 (2005)

P. Müller-Buschbaum, S. V. Roth, M. Burghammer, E. Bauer, S. Pfister, C. David, C. Riekel
Local defects in thin polymer films: A scanning sub-microbeam grazing incidence small angle scattering investigation
Physica B **357**, 148 (2005)

P. Müller-Buschbaum, E. Bauer, O. Wunnicke, M. Stamm
Control of thin film morphology by an interplay of dewetting, phase separation and microphase separation
J.Phys.Condens.Matter **17**, S363 (2005)

P. Müller-Buschbaum, O. Wunnicke, M. Stamm, Y. C. Lin, M. Müller
Stability-instability transition by tuning the effective interface potential in polymeric bilayer films
Macromolecules **38**, 3406 (2005)

C.M. Papadakis, F. Rittig
Influence of the morphology on the translational and collective dynamics in ordered diblock

copolymer melts (invited and refereed review)
J. Phys.: Condens. Matter **17**, R551 (2005).

M. Pöhlmann, A. Meyer, A. Müller, H. Schober, T. Hanssen
Structural and Dynamical Properties of Hydrous Amorphous Silicates as seen by Neutron Scattering
Phys. Rev. B, submitted (2005)

K. Rätzke, V. Zöllmer, A. Bartsch, A. Meyer, F. Faupel
Diffusion in bulk-metallic glass-forming PdCuNiP alloys: From the glass to the equilibrium melt
J. Non. Cryst. Solids, in press (2005)

A. Röhrmoser, W. Petry, N. Wieschalla
Reduced Enrichment Program for the FRM -II, Status 2004/05
Proceedings 9th International Meeting on Reduced Enrichment for Research and Test Reactors (RERTR) Budapest 10.-13.03. (2005)

S. V. Roth, M. Rankl, G. R. J. Artus, S. Seeger, M. Burghammer, C. Riekel, P. Müller-Buschbaum
Domain nano-structure of thin cellulose layers investigated by microbeam grazing incidence small-angle x-ray scattering
Physica B **357**, 190 (2005)

I. Sergueev, U. van Bürck, A. I. Chumakov, T. Asthalter, G. V. Smirnov, H. Franz, R. Rüffer, W. Petry
Synchrotron-radiation-based perturbed angular correlations used in the investigation of rotational dynamics in soft matter
Physical Review B **73** 024203 (2006)

G.V. Smirnov, U. van Bürck, W. Potzel, P. Schindelmann, S.L. Popov, E. Gerdau, Yu.V. Shvyd'ko, H.D. Rüter, O. Leupold
Propagation of nuclear polaritons through a two-target system: Effect of inversion of targets
Phys. Rev. A **71**, 023804 (2005).

B. P. Toperverg, V. Lauter-Pasyuk, H. J. Lauter
Larmor pseudo-precession of neutron polarization in reflection
Physica B **356**, 1 (2005)

B. P. Toperverg, V. Lauter-Pasyuk, H. J. Lauter, A. Vorobiev
Grazing incidence neutron diffraction from ferromagnetic films in multidomail state
Physica B **356**, 51 (2005)

T. Unruh, A. Meyer, J. Neuhaus, W. Petry
The Time-of-Flight Spectrometer TOFTOF
Neutron News, submitted (2005)

K. Zeitelhack, C. Schanzer, A. Kastenmüller, A. Röhrmoser, C. Daniel, J. Franke, E. Gutsmiedl, V. Kudyrashov, D. Maier, D. Päthe, W. Petry, T. Schöffel, K. Schreckenbach, A. Urban, U. Wildgruber

Measurement of neutron flux and beam divergence at the cold neutron guide system of the new Munich research reactor FRM-II
Nuclear Instruments and Methods in Physics Research A, accepted (2005)

Talks given by members of E13

T. Bonné
Frühjahrstagung der Deutschen Physikalischen Gesellschaft, Berlin
Fluorescence Correlation Spectroscopy Investigations of Water Soluble Polymers
09.03.2005

W. Doster
International Conference of Neutron Scattering, Sydney, invited talk
Protein-Water Displacement Distributions
02.10.05

W. Doster
SFB 533 Kolloqium, Munich
The effect of volume changes on protein dynamics
29.09.05

W. Doster
Statusseminar FRM2, Rothenfels
Protein-Water Displacement Distributions
25.07.05

R. Gebhardt and W. Doster
Statusseminar der Hochdruck-Forschergruppe, Freising
Pressure Dissociation of Protein Complexes
20.10.05

F. Kargl
Nuclear Resonant Group Seminar, ESRF, Grenoble
Inelastic neutron scattering on silicate melts: the interplay of microscopic dynamics and structure
22.02.2005

F. Kargl
Abschlusskolloquium des DFG Schwerpunktprogramms SPP 1055: Bildung, Transport und Differenzierung von Silikatschmelzen, München
Interplay of structure and atomic transport in sodium aluminosilicate investigated by means of inelastic neutron scattering
04.04.2005

F. Kargl
5th International Discussion Meeting on Relaxations in Complex Systems, Lille, France
Ion dynamics in oxidic melts as observed by inelastic neutron scattering
11.07.2005

F. Kargl
2nd FRM-II Workshop on Neutron Scattering - Advanced Materials, Burg Rothenfels
Ion dynamics in oxidic melts as observed by inelastic neutron scattering
25.07.2005

F. Kargl
Scandinavian Neutron Scattering Meeting, Göteborg, Schweden
QUENS investigations on ion transport and structure in oxidic melts
07.10.2005

V. Körstgens, P. Müller-Buschbaum
Diskussionstreffen 'Haftklebstoffe' in München
Blends of triblock and diblock copolymers used as PSA materials
06.10.2005

V. Lauter-Pasyuk
PSI, Villigen (Schweiz)
Tailoring nanoparticles structure via self-assembling copolymer matrix
04.2005

V. Lauter-Pasyuk
Ecole de neutrons, Anglet (Frankreich)
Neutron grazing incidence techniques for nanoscience
06.2005

V. Lauter-Pasyuk
Russian-German meeting, Potsdam
Specular reflection, off-specular scattering and GISANS from novel self-organized nanomaterials
09.2005

V. Lauter-Pasyuk
Workshop 'Reflectometry, Off-specular scattering and GISANS - ROG2005' in Villigen (Schweiz)
New frontiers of reflectometry: 3D characterization of nano-object materials
24.-27.10.2005

V. Lauter-Pasyuk
RSNE Nano2005, Moscow (Russland)
Grazing incidence techniques for nanoscience
11.2005

V. Lauter-Pasyuk
ICNS 2005, Sydney (Australien)
Highly ordered copolymer-nanoparticle composite films: monitoring of self-organized structure
27.11.-2.12.2005

V. Lauter-Pasyuk
ANSTO, Sydney (Australien)
Off-specular scattering in reflectometry experiment
12.2005

T. Mehaddene
2nd FRM-II Workshop on Neutron Scattering, Rothenfels
Single crystal growth and phonon measurements in NiAlMn shape memory alloys.
25.-28.7.2005

A. Meyer
DPG Frühjahrstagung, Berlin
Atomic Transport in Metallic Melts
04.03.2005

A. Meyer
Evaluierung der Verbundforschung des BMBF, TU München
Liquids and Glass Transitions
15.04.2005

A. Meyer
European Geoscience Union Meeting, Wien
The Interplay of Microscopic Dynamics and Structure with Mass Transport in Silicate Melts
25.04.2005

A. Meyer
Berichtskolloquium im DFG Schwerpunkt 1120, Bad Honnef
Phasenumwandlungen in mehrkomponentigen Schmelzen, Atomic Transport in Metallic Melts
19.05.2005

A. Meyer
Universität Konstanz
Sillikatschmelzen unterm Neutronenmikroskop
24.05.2005

A. Meyer
V. International Discussion Meeting on Relaxation in Complex Matter, Lille
Atomic Motions in Metallic Melts: A Prime Example of Viscous Liquid Dynamics
08.07.2005

A. Meyer
Deutsches Zentrum für Luft und Raumfahrt, Köln
Structure and Dynamics of Viscous Liquids
08.12.2005

P. Müller-Buschbaum
Satellite meeting - status and perspectives of SAXS/WAXS, Hamburg
Bio-polymeric nano-structures: A GISAXS investigation
27.01.2005

P. Müller-Buschbaum
Seminar der Technischen Fakultät am Lehrstuhl für Materialverbunde, Kiel
The morphology of thin polymer films with metal nano-particles
31.01.2005

P. Müller-Buschbaum
ESRF Usermeeting '10 years of ESRF', Grenoble
Sub-Microbeam grazing incidence small angle x-ray scattering: A new technique for the detection of local structures in thin polymer films
07.-09.02.2005

P. Müller-Buschbaum
Projektreffen 'Haftklebstoffe', Ludwigshafen
Probing thin surface layers with x-ray specular reflection
21.02.2005

P. Müller-Buschbaum
Tagung '10th Dresden Polymer Discussion: Characterization of polymer surfaces and thin films' in Meissen
Grazing Incidence Small Angle Scattering - An Advanced Characterization Technique for Structured Polymer Films
10.-13.04.2005

P. Müller-Buschbaum
Kolloquium HU Berlin
Nano-structured polymer films - relation between structure and function
14.04.2005

P. Müller-Buschbaum
Tagung 'Evaluierung der Verbundforschung an der TU München durch das BMBF', München
Oberflächen
15.04.2005

P. Müller-Buschbaum
'1st International GISAXS workshop', Hamburg
High-resolution GISAXS
10.-12.05.2005

P. Müller-Buschbaum
Kolloquium der Physikalischen Chemie, Konstanz
Nano-structured polymer films - relation between structure and function
23.06.2005

P. Müller-Buschbaum
Kolloquium der Technischen Physik, Ilmenau
Nano-structured polymer films - relation between structure and function
04.07.2005

P. Müller-Buschbaum
Workshop 'Future perspectives in polymer science', Borkum
Microbeam experiments - probing local surface structures
04.-09.07.2005

P. Müller-Buschbaum
Workshop 'Neutron Scattering - advanced materials', Rothenfels
Grazing incidence- SANS
25.-28.07.2005

P. Müller-Buschbaum, E. Bauer, V. Körstgens, J. Wiedersich, S.V. Roth, V. Lauter-Pasyuk, W. Petry
Workshop 'Polymer/Metal Nanocomposites', Geesthacht

Magnetic particles in supported polymer nano-structures
26.-28.09.2005

P. Müller-Buschbaum, E. Bauer, E. Maurer, R. Cubitt
Workshop 'Reflectometry, Off-specular scattering and GISANS - ROG2005', Villigen (Switzerland)
Free- surface induced morphology transition in triblock copolymer films: A GISANS investigation
24.-27.10.2005

P. Müller-Buschbaum
Konferenz '2te WING Konferenz', Aachen
Enthaftung unter die Lupe genommen
09.-11.11.2005

P. Müller-Buschbaum
Projektreffen 'Haftklebstoffe', München
Probing thin surface layers with x-ray specular reflection - recent results
14.11.2005

P. Müller-Buschbaum
Kunststoff-Kolloquium des DKI, Darmstadt
Nano-structured polymer films - relation between structure and function
17.11.2005

P. Müller-Buschbaum, E.Bauer, E.Maurer, R.Cubitt
ICNS 2005, Sydney (Australien)
Fast swelling kinetics of thin polymer films
27.11.-02.12.2005

P. Müller-Buschbaum
Projektreffen 'Haftklebstoffe', Düsseldorf
Tack measurements at PSA
19.12.2005

P. Müller-Buschbaum
Projektreffen 'Industrieklebstoffe', Düsseldorf
Probe-tack measurements - an introduction
20.12.2005

C.M. Papadakis
Kolloquium des Instituts für Festkörperphysik, Technische Universität Darmstadt
Kleinwinkelstreuung unter streifendem Einfall: Die innere Struktur dünner Blockcopolymerfilme
31.01.2005

C.M. Papadakis
Freiburger Makromolekulares Kolloquium
Unter die Oberfläche schauen - die innere Struktur dünner Polymerfilme
25.02.2005

C.M. Papadakis
Frühjahrstagung der Deutschen Physikalischen Gesellschaft, Berlin
Slow dynamics in block copolymer melts in the ordered morphologies
04.03.2005

C.M. Papadakis
Bunsentagung 2005, Frankfurt am Main
Fluorescence correlation spectroscopy: The aggregation behavior of amphiphilic block copolymers in aqueous solution
07.05.2005

C.M. Papadakis
Workshop 'GISAXS - an advanced scattering method', Hasylab at DESY, Hamburg
Grazing-incidence small-angle X-ray scattering - Structure and kinetics of thin block copolymer films
10.05.2005

C.M. Papadakis
Seminar of the Lehrstuhl für Biomolekulare Optik, Fakultät für Physik, Ludwig-Maximilians-Universität München
Block copolymers - Aggregation behavior in solution and in thin films
12.07.2005

C.M. Papadakis
Edgar-Lüscher-Lectures Dillingen/Donau 2005: 'Physik im Nanometerbereich'
Nanostrukturierte Blockcopolymerfilme:Matrizen fr die Nanotechnologie
05.10.2005

W. Petry
Kerntechnisches Kolloquium der RWTH Aachen
Neutronen für Wissenschaft, Technik und Medizin, der FRM-II in München
11.01.2005

W. Petry
Physikalisches Kolloquium, Lst. für Experimentalphysik II der Universität Bayreuth
FRM II - Neutronen für Wissenschaft, Technik und Medizin
18.01.2005

W. Petry
Workshop des Centre for Nanotechnology and Nanomaterials der TU München - nanotum
Metals go Nano
15.02.2005

W. Petry
TOP Management Programm der Bayerischen Staatsregierung in St. Quirin/Tegernsee
Benötigen wir Kerntechnik?
26.02.2005

W. Petry
MPI für Plasmaphysik, Bereich Materialforschung, Garching bei München
Materials Science with Neutrons
12.05.2005

W. Petry
Rencontres Rossat-Mignod im Rahmen der 13èmes Journées de la Diffusion Neutronique, Anglet/Frankreich
First routine operations of the new neutron source FRM-II
09.06.2005

W. Petry
Reactor Institute, Delft University of Technology, The Netherlands
Light in the dark, the German new neutron source for science, medicine and industry
15.06.2005

W. Petry
'caesarianum spezial' - Stiftung 'caesar', Bonn
Licht ins Dunkel - Neutronen für Wissenschaft, Medizin und Industrie
27.06.2005

W. Petry
Physikalisches Kolloquium, Ruhr-Universität Bochum
Neutronen bringen Licht ins Dunkel
04.07.2005

W. Petry
Jahrestagung der Société Francaise de la Physique, Lille
Teilnahme am Round Table Gespräch: Rôle des grands instruments
01.09.2005

W. Petry
NIST (National Institute of Standard and Technology), Gaithersburg, USA
Light in the dark, the German neutron source FRM-II for science and industry
08.09.2005

W. Petry
Oak Ridge National Laboratory, USA
Innovative Neutron Instrumentation at FRM-II - First Results
12.09.2005

W. Petry
TRTR-IGORR10, Gaithersburg, USA
Performance of the new high flux neutron source FRM-II
13.09.2005

W. Petry
Tagung Neutronenstreuung für Kristallographen, LMU und TUM
Flugzeitmethoden - weiche Materie
30.09.2005

W. Petry
7th Baltic Development Forum, Stockholm, Schweden
Innovation and cooperation between industry and academia at ESS, the new neutron source FRM-II at Munich
17.10.2005

W. Petry
Universität Wuppertal
Neutronen bringen Licht ins Dunkel - Physik am Forschungsreaktor München (FRM-II)
31.10.2005

S.V. Roth, H. Walter, R. Gehrke, P. Müller-Buschbaum
Frühjahrstagung der Deutschen Physikalischen Gesellschaft, Regensburg
Morphology of tempered gold nanoparticle thin films as a function of film thickness
03.-09.03.2005

C. Strohm
2^{nd} FRM-II Workshop, Burg Rothenfels
Nuclear resonant scattering of synchrotron radiation from ^{57}Fe bearing sodium silicate glasses and melts
25.07.2005

P. Uhlmann, P. Müller-Buschbaum, P. Truman, M. Stamm
DFG Schwerpunktbegutachtung, Bad Honnef
Non-equilibrium flow on confined geometries
11.-13.12.2005

Posters

T. Asthalter, I. Sergueev, H. Franz, U. van Bürck
Nuclear Resonance Scattering Symposium, ESRF Grenoble (France) and
ICAME 2005, Montpellier (France)
Hysteresis of rotational dynamics in two plastic crystals as studied by SRPAC
02. and 05.-09.09.2005

T. Asthalter, J. Villanueva-Garibay, V. Olszowka, J. Kornatowski, I. Sergueev, U. van Bürck
Nuclear Resonance Scattering Symposium, ESRF Grenoble (France) and
ICAME 2005, Montpellier (France)
The dynamics of ferrocene in one-dimensional channels as studied by nuclear forward scattering
02. and 05.-09.09.2005

E. Bauer, P. Müller-Buschbaum, E. Maurer, T. Mehaddene, S. Cunis, R.Gehrke
'HASYLAB User Meeting' in Hamburg
Dewetting of confined polystyrene films as a function of the applied surface clean
January 2005

E. Bauer, P. Müller-Buschbaum
Frühjahrstagung der Deutschen Physikalischen Gesellschaft in Berlin
Dewetting of confined polymer films
March 2005

U. van Bürck
Nuclear Resonance Scattering Symposium, ESRF Grenoble (France)
Features of nuclear forward scattering
02.09.2005

U. van Bürck, C. Strohm
APD Detector Workshop, ESRF Grenoble (France)
Interest in APD-development lines
03.09.2005

A.I. Chumakov, I. Sergueev, U. van Bürck, W. Schirmacher, T. Asthalter, R. Rüffer, O. Leupold, W. Petry
ICAME 2005, Montpellier (France)
Dynamics of glasses studied with nuclear inelastic scattering
07.09.2005

A.I. Chumakov, I. Sergueev, U. van Bürck, T. Asthalter, W. Schirmacher, R. Rüffer, G.V. Smirnov, H. Franz, O. Leupold, W. Petry
5th International Discussion Meeting on Relaxation in Complex Systems, Lille (France)
Boson peak and slow β-relaxation studied by nuclear resonant scattering of synchrotron radiation
10.07.2005

W. Doster, A. Gaspar, M. Settles
European Biophysical Conference 2005, Montpellier (France)
Protein-water displacement distributions
28.09.2005

W. Doster, A. Gaspar, M. Settles
International Neutron Scattering Conference 2005, Sydney (Australia)
Protein-water displacement distributions from dynamic neutron scattering
28.10.2005

W. Doster, R. Gebhardt and A. Soper
European Biophysical Conference 2005, Satellite Meeting: Neutrons in Biology, Grenoble (France)
Pressure unfolding of myoglobin, neutron diffraction and dynamic scattering experiments
02.10.2005

W. Doster, S. Naydenova, A. Ogrodnik, J. Wachtveitl, R. Huber, X. Cai
SFB 533 'Light induced reactions in biopolymers Meeting, Munich
Pressure Effects on the Kinetics of Ligand Binding to Myoglobin
29.09.2005

R. Gebhardt and W. Doster,
Workshop of the DFG Research Group 'High Pressure Treatment of Food', Freising
Pressure-induced dissociation of casein
19.10.2005

R. Ivanova, T. B. Bonné, T. Komenda, K. Lüdtke, R. Jordan, C. M. Papadakis
Frühjahrstagung der Deutschen Physikalischen Gesellschaft, Berlin
Multi-compartment micellar networks formed by lipophilic-hydrophilic- fluorophilic triblock copolymers in aqueous solution
05.03.2005

F. Kargl and A. Meyer
European Geoscience Union General Assembly 2005, Union Symposium 1, Neutrons at the Frontier of Earth Sciences & Environment
The impact of Al_2O_3 and Fe_2O_3 on relaxation and structure in sodium silicates disclosed by inelastic neutron scattering
25./26.04.2005

E. Maurer, S. Loi, P. Müller-Buschbaum
'HASYLAB User Meeting', Hamburg
Structure creation in pressure sensitive adhesives
January 2005

E. Maurer, S. Loi, P. Müller-Buschbaum
Frühjahrstagung der Deutschen Physikalischen Gesellschaft, Berlin
In situ ultra small angle x-ray scattering on pressure sensitive adhesives
March 2005

T. Mehaddene
'Neutron Scattering for Crystallographers', LMU Munich

Phonon-driven martensitic transitions in CuAlMn and NiAlMn
September 29-30, 2005

A. Meyer
Workshop on Correlated Electrons and Glassy Matter, Augsburg
Silicate Melts: A Microscopic View on Mass Transport
15.07.2005

A. Monaco, A.I. Chumakov, Y. Z. Yue, W. Crichton, A. Meyer, U. van Bürck, F. Kargl, R. Rüffer, G. Monaco, U. Ponkratz, S. Roitsch, G. Wortmann
Nuclear Resonance Scattering Symposium, ESRF Grenoble (France) and
ICAME 2005, Montpellier (France)
Nuclear inelastic scattering in densified and hyperquenched glasses
02. and 05.-09.09.2005

P. Müller-Buschbaum, E. Bauer, E. Maurer, S.V. Roth, R. Gehrke
'HASYLAB User Meeting', Hamburg
High-resolution grazing incidence small angle x-ray scattering
January 2005

P. Müller-Buschbaum, E. Bauer, S. Pfister, S.V. Roth, M. Burghammer, C. Riekel, U. Thiele, C. David
Frühjahrstagung der Deutschen Physikalischen Gesellschaft, Berlin
Phase-separation by evaporating polymer blend solution sub-jected to flow
March 2005

P. Panagiotou, E. Maurer, R. Cubitt, P. Müller-Buschbaum
Frühjahrstagung der Deutschen Physikalischen Gesellschaft, Berlin
Kinetics of ternary polymer blend films investigated with neutron re ectometry and AFM
March 2005

C.M. Papadakis, C. Vasilev, G. Reiter
Hasylab User Meeting, Hamburg
Thin films of crystalline diblock copolymers
28.01.2005

C.M. Papadakis, C. Vasilev, G. Reiter
Hasylab User Meeting, Hamburg
Thin films of poly(styrene-b-butadiene) diblock copolymers
28.01.2005

C.M. Papadakis, P. Busch, D.-M. Smilgies, M. Rauscher, D. Posselt
Frühjahrstagung der Deutschen Physikalischen Gesellschaft, Sektion Chemische und Polymerphysik, Berlin
In-situ time-resolved grazing-incidence small-angle X-ray scattering: A tool to study reorientational processes in thin diblock copolymer films
08.03.2005

S.V. Roth, H. Walter, R. Döhrmann, M. Dommach, R. Gehrke, P. Müller-Buschbaum
'HASYLAB User Meeting' in Hamburg

Morphology of annealed gold nanopartcile thin films: Influence of film thickness and annealing time
January 2005

S.V. Roth, H. Walter, G. Bauer, O. Rankl, G. Artus, S. Seeck, M. Burghammer, C. Riekel, P. Müller-Buschbaum
'ESRF user meeting' in Grenoble
Advances in microbeam GISAXS
February 2005

W. Schirmacher
Workshop on Correlated Electrons and Glassy Matter, Augsburg
Thermal conductivity and the "boson peak"
16.-17.07.2005

K.M. Schlögl, E. Maurer, S. Loi, P. Müller-Buschbaum
Frühjahrstagung der Deutschen Physikalischen Gesellschaft in Berlin
Surface morphology of pressure sensitive adhesive blend films as probed by atomic force microscopy
March 2005

I. Sergueev, A.I. Chumakov, U. van Bürck, T. Asthalter, H. Franz, R. Rüffer, W. Petry
Nuclear Resonance Scattering Symposium, ESRF Grenoble (France) and
ICAME 2005, Montpellier (France)
Rotational glass dynamics investigated by SRPAC on different nuclear probes
02. and 05.-09.09.2005

I. Sergueev, U. van Bürck, A.I. Chumakov, T. Asthalter, G.V. Smirnov, H. Franz, R. Rüffer, W. Petry
ICAME 2005, Montpellier (France)
Rotational and translational glass dynamics studied by nuclear resonant scattering
07.09.2005

C. Strohm, I. Sergueev, U. van Bürck, F. Kargl, F.E. Wagner, A. Meyer, W. Petry
Nuclear Resonance Scattering Symposium, ESRF Grenoble (France) and
ICAME 2005, Montpellier (France)
Nuclear resonant scattering from iron bearing sodium silicate glasses and melts
02. and 05.-09.09.2005

G. Wellenreuther, H. Franz, U. van Bürck, I. Sergueev
ICAME 2005, Montpellier (France)
Rotational dynamics in anisotropic confinement
05.-09.09.2005

Invited talks at E13

Dr. Jürgen Horbach, Johannes-Gutenberg-Universität Mainz
Multicomponent viscous liquids and their peculiarities: computer simulation studies
20.01.2005

Dr. Bernard Hehlen, Université Montpellier II
Recent developments in hyper-Raman spectroscopy: new prospects in liquid and glass physics
27.01.2005

Dr. Stephan Roth, HASYLAB, Hamburg
Thin noble metal films - novel samples investigated with advanced x-ray scattering methods
04.02.2005

Dr. Tanja Asthalter, Universität Stuttgart
Synthesis and characterization of coated metal oxide nanoparticles
11.02.2005

Jacques Fleck, Bayerisch-französisches Hochschulzentrum
Bayerisch - französisches Hochschulzentrum
25.02.2005

Dr. Alexander Brodin, Universität Bayreuth
Temperature evolution of the dynamic susceptibility in supercooled liquids: light scattering and dielectric results
14.04.2005

Dr. Michael Koza, ILL, Grenoble
Glasübergang in Wasser: Mythos und Wirklichkeit
21.04.2005

Prof. Dr. Jochen S. Gutmann, Universität Mainz
Titania nanoparticle formation in bulk block-copolymers and ultrathin films
22.04.2005

Prof. Igor Potemkin, Phys. Dept. Moscow State University
Block copolymer for functional substrates: from thin films to single molecules
29.04.2005

Dr. Dan Neumann, NIST, Gaithersburg
Backscattering spectroscpoy at the NCNR and the tunneling of confined tops
02.05.2005

Sreenath Bolisetty, MPI Mainz
Thin free standing films of self organised polymers
20.05.2005

Prof. Volker Abetz, Institut für Chemie, GKSS
Morphologies of Block Copolymers in the Bulk and in Blends
03.06.2005

Prof. Dorthe Posselt, Universität Roskilde
Mesoscale structure and adaptability of photosynthetic thylakoid membranes
10.06.2005

Elisabeth Wasner
Inelastische Neutronenstreuung an DMPC-Cholesterol Modellmembranen
17.06.2005

Prof. D. Habs, LMU
Proposal for high-brilliance micro-beam of low-energy polarized neutrons
04.07.2005

Dr. Jun Fu, MPI Mainz
Instability of Crystalline-coil PLLA-b-PS Thin Films
08.07.2005

Severin Kampfer, FRM-II
Bestimmung der Strahlqualität des Spaltneutronenstrahls am SR 10
15.07.2005

Mottakin M. Abul Kashem, IPF Dresden
Studies of the effect of surface finish
21.07.2005

Gesa Gröhnke, TUM
Inaktivierung von Lactococcus untersucht mit FTIR-Spektroskopie
22.07.2005

Felix Höfling, HMI Berlin
The Localisation Transition of the 3D Lorentz Model and Continuum Percolation
25.08.2005

Dr. Roland Steitz, HMI Berlin
Boundary Layers of Water at Polymer-Liquid Interface
21.10.2005

Dr. Marie-Sousai Appavou, LLB Paris
Neutron scattering on proteins at high pressure
28.10.2005

Kwonsul Song, TUM
Pressure induced aggregation of beta-globulin
04.11.2005

Dr. Christina Scharnagl, TUM
High Pressure Simulations of Proteins
11.11.2005

Dr. Dag W. Breiby, RisøNational Laboratory, Denmark
Novel Application of X-rays in Material Science
18.11.2005

Prof. Thomas Thurn-Albrecht, Universität Halle
Structure Formation in Polymers under External Contraints
09.12.2005

Funding

Deutsche Forschungsgemeinschaft

Dynamics of supramolecular aggregates of amphiphilic polymers studied by fluorescence correlation spectroscopy
Pa 771/2-1 (Prof. Christine Papadakis)

In the SFB 563 'Bioorganische Funktionssysteme auf Festkörperoberflächen':
Untersuchung der Struktur und des Wachstums von Proteinfibrillen immobilisiert auf Festkörperoberflächen
SFB 563 TP A10 (Prof. Christine Papadakis)

In the SFB 533 'Lichtinduzierte Dynamik von Biopolymeren':
Zeitaufgelöste Kalorimetrie an lichtinduzierten Prozessen in Proteinen
SFB533 - 3001748 (PD Wolfgang Doster)

In the DFG priority program: 'Phasenumwandlungen in mehrkomponentigen Schmelzen'
SPP 1120
Untersuchung des Einflusses der atomaren Dynamik auf Materietransport, Segregation und Erstarrung mehrkomponentiger Schmelzen
ME 1958/2-3 (Prof. Andreas Meyer)

In the DFG priority program SPP 1164:
Non-equilibrium flow in nanoscale geometrics: Influence of confinement and surface functionality
MU 1487/2-1 (PD Peter Müller-Buschbaum)

Inelastische Neutronenstreuung bei hohen Temperaturen und Drücken zur Aufklärung der Lösungs- und Transportmechanismen von Wasser in wasserhaltigen Silikatschmelzen
ME 1958/8-2 (Prof. Andreas Meyer)

Quellverhalten von dünnen Polymerfilmen: Struktur, Kinetik und Dynamik
MU 1487/4-2 (PD Peter Müller-Buschbaum)

Nanostrukturierte Filme aus selbstkapselnden anorganisch-organischen Hybridmaterialien
MU 1487/5-1 (PD Peter Müller-Buschbaum)

Bundesministerium für Bildung und Forschung

ESRF: Methodische Entwicklungen zum SRPAC Spektrometer: Gestörte Winkelkorrelation mit Synchrotronstrahlung
05KS4WOC/3 (Dr. Uwe van Bürck, Prof. Andreas Meyer)

Wechselwirkung von Polymermatrizen mit magnetischen Nanostrukturen und Studium der magnetischen Eigenschaften
03DU03MU (PD Peter Müller-Buschbaum)

Abhängigkeit des Haftvermögens dünner Polymerfilme von der Oberflächenmorphologie
03CO333 (PD Peter Müller-Buschbaum)

Bau eines thermischen Dreiachsenspektrometers am FRM-II
03EC5SRM/1 (Dr. Claudia Hradil)

Others

NATO Collaborative Linkage Grant:
Structure formation in thin block copolymer films
PST.CLG.978046 (Prof. Christine Papadakis)

FuE-Vertrag mit der Henkel KGaA:
Konstruktion einer Messaparatur und Entwicklung einer Methode zur Bestimmung spezifischer Haftklebeeigenschaften von Klebebändern (PD Peter Müller-Buschbaum)

8 The chair

Diploma and PhD theses

Accomplished diploma theses

Gesa Gröhnke
Vergleich von temperaturinduzierten Inaktivierungskinetiken zu Lactococcus lactis ssp. cremoris MG1363 mit Daten der FTIR-Spektroskopie

Kwonyul Song
Aggregation phenomena of β-Lactoglobulin under high pressure

Accomplished PhD theses

Estelle Bauer
Statik und Kinetik der Entnetzung ultradünner Polymerfilme
December 2005

Tune Bonné
Aggregation behavior of water-soluble amphiphilic block copolymers
November 2005

Ronald Gebhardt
Pressure Stability of Protein Complexes: Light Scattering and Thermodynamic Analysis on the Example of Arthropod-Hemocyanins and Casein-Micelles
March 2005

Florian Kargl
The interplay of structure and microscopic dynamics in oxidic melts observed by means of inelastic neutron scattering
November 2005

Edith Maurer
Strukturuntersuchungen an Haftklebstoffen beim mechanischen Tack-Test auf makroskopischer und mikroskopischer Längenskala
December 2005

Suresh Mavila-Chathoth
Structure and Dynamics of Al and Ni Based Melts Studied by Inelastic Neutron Scattering
May 2005

Staff and guests

Chair: Prof. Dr. Winfried Petry (FRM-II)

Head: Prof. Dr. Andreas Meyer

Fellows

Dr. Ezzeldin Metwalli Ali
PD Dr. Wolfgang Doster
Dr. Ana Gaspar (FRM-II)
Dr. Ruzha Ivanova
Dr. Volker Körstgens
Dr. Valeria Lauter-Pasyuk (ILL)
Dr. Emmanuel Longueteau
PD Dr. Peter Müller-Buschbaum
Dr. Jürgen Neuhaus (FRM II)
Prof. Dr. Christine Papadakis
PD Dr. Walter Schirmacher
Dr. Kerstin Schlögl (until January 2005)
Dr. Cornelius Strohm (ESRF)
Dr. Alexander Roth (March - April 2005)
Dr. Tobias Unruh (FRM-II)
Dr. Uwe van Bürck

PhD students

Mottakin Abul Kashem
Estelle Bauer
Tune Bonné
Charles Darko
Ronald Gebhardt
Florian Kargl
Edith Maurer
Suresh Mavila Chathoth
Tarik Mehaddene
Andreas Meier-Koll
Panteleimon Panagiotou
Cornelius Strohm
Sebastian Stüber
Fan Yang

Diploma students

Gesa Gröhnke
Leander Schulz
Kwonyul Song

Student assistants

Max Eickenscheidt
Rosemarie Hengstler
Patrick Michelberger
Suleman Qureshi

Technical/administrative staff

Ricarda Baumhoer
Joachim Dörbecker
Elke Fehsenfeld
Reinhold Funer
Josef Kaplonski
Dieter Müller
Jandal Ringe (FRM-II)
Cornelia Simon
Max Wittich

Guests

Prof. Dr. Dorthe Posselt, Roskilde University, Danmark (1 week in June)
Prof. Dr. Gennadi Smirnov, Russian Research Center “Kurchatov Institute” (June and July 2005)
Prof. Dr. Alfons Schulte, University of Central Florida (June 2005)

A few impressions from E13's excursion to Garmisch-Partenkirchen June 2005